UNIVERSITÀ DEGLI STUDI DI NAPOLI
PARTHENOPE

Lectio Magistralis

Oceano, clima, modelli, sistemi dinamici: 40 anni di ricerca e di didattica

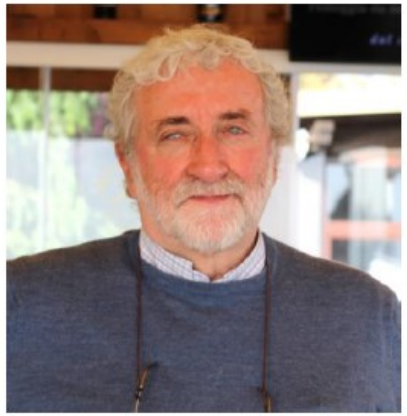

Prof. Stefano Pierini

DiST
Dipartimento di Scienze e Tecnologie

5 dicembre 2024 – ore 11:00

oceanografia meteorologia

Aula Magna – Università degli Studi di Napoli "Parthenope"
Dipartimento di Scienze e Tecnologie - Centro Direzionale, Isola C4, Napoli

In questa lezione ripercorro le principali tappe della mia attività di ricerca e di didattica universitaria. Dopo la laurea in Fisica conseguita presso l'Università La Sapienza di Roma e un'attività di ricerca post-laurea svolta presso la stessa università e, per un biennio, all'Università di Cambridge, inizio la mia carriera accademica nel 1984 presso l'allora Istituto Universitario Navale. Proseguo all'Università dell'Aquila, tornando poi definitivamente all'Università di Napoli Parthenope. Durante questo lungo periodo ho avuto occasione di visitare vari altri atenei e centri di ricerca in giro per l'Europa e gli USA per una serie di progetti e collaborazioni internazionali. Nella presentazione farò riferimento ad alcuni dei principali risultati della mia attività di ricerca scientifica, che hanno riguardato la fisica dell'oceano e del clima, la fluidodinamica, la modellistica di processi oceanografici e varie applicazioni della teoria dei sistemi dinamici nonlineari alla climatologia.

Website: http://stefanopierini.it

stefano.pierini@collaboratore.uniparthenope.it
pierini.uniparthenope@gmail.com

Sono nato a Roma nel 1954

Mi sono Laureato in Fisica “con Lode” presso l’Università degli Studi di Roma “La Sapienza” nel Dicembre 1977

Ho svolto attività di ricerca post-laurea presso la stessa università (1978-80) e all’Università di Cambridge (1981-82 col supporto del CNR)

Ho ricoperto i seguenti ruoli universitari:

1984-1997: **Ricercatore Universitario** presso l’Istituto Universitario Navale di Napoli
(Istituto di Oceanologia / Meteorologia e Oceanografia)

1997-2002: **Professore Associato** presso l’Università degli Studi dell’Aquila
(Dipartimento di Fisica)

2002-2006: **Professore Associato** presso l’Università degli Studi di Napoli “Parthenope”
(Dipartimento di Scienze per l’Ambiente)

2006-2024: **Professore Ordinario** presso l’Università degli Studi di Napoli “Parthenope”
(Dipartimento di Scienze e Tecnologie)

RICERCA

DIDATTICA

RICERCA

DIDATTICA

Rotture di simmetria,
Stabilità di flussi

Modellistica di
onde nonlineari

Aspetti lineari della circolazione
indotta dal vento (Rossby waves)

Applicazioni della teoria
dei sistemi dinamici nonlineari:
modelli alle equazioni primitive

Applicazioni della teoria
dei sistemi dinamici nonlineari:
modelli di bassa dimensionalità

Predicibilità dei processi di
transizione dell'Estensione
del Kuroshio

Modellistica di circolazione
del Mar Mediterraneo

Modellistica Antartica

Simulazioni di laboratorio di
flussi oceanografici

Rotture di simmetria,
Stabilità di flussi

Modellistica di
onde nonlineari

Aspetti lineari della circolazione
indotta dal vento (Rossby waves)

Applicazioni della teoria
dei sistemi dinamici nonlineari:
modelli alle equazioni primitive

Applicazioni della teoria
dei sistemi dinamici nonlineari:
modelli di bassa dimensionalità

Predicibilità dei processi di
transizione dell'Estensione
del Kuroshio

Modellistica di circolazione
del Mar Mediterraneo

Modellistica Antartica

Simulazioni di laboratorio di
flussi oceanografici

Rotture di simmetria, Stabilità di flussi

Jona Lasinio, G., Pierini, S., Vulpiani, A., 1978: Absence of breakdown of a continuous symmetry in more than two dimensions.
Lettere al Nuovo Cimento, **23**, 353-356.

Pierini, S., Vulpiani, A., 1981: Nonlinear stability analysis in multilayer quasigeostrophic systems.
Journal of Physics A, **14**, L203-L207.

Benzi, R., Pierini, S., Salusti, E., Vulpiani, A., 1982: On nonlinear hydrodynamic stability of planetary vortices.
Geophysical Astrophysical Fluid Dynamics, **20**, 293-306.

Pierini, S., Salusti, E., 1982: Nonlinear hydrodynamic stability of some simple rotational flows.
Nuovo Cimento, **71B**, 282-294.

Pierini, S., 1985: On the stability of equivalent modons.
Dynamics of Atmospheres and Oceans, **9**, 273-280.

Petroni, R., Pierini, S., Vulpiani, A., 1987: The double cascade as a necessary mechanism for the instability of steady equivalent-barotropic flows. *Nuovo Cimento,* **10C**, 27-36.

Pierini, S., 1987: Stable equivalent-barotropic oceanic boundary currents.
Nuovo Cimento, **10C**, 323-335.

Prof. Giovanni Jona-Lasinio

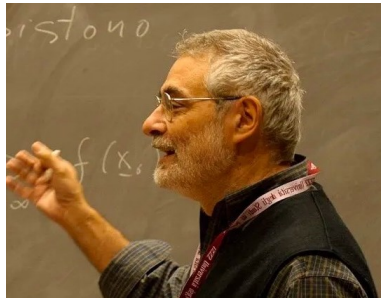

Prof. Angelo Vulpiani

SAPIENZA
UNIVERSITÀ DI ROMA

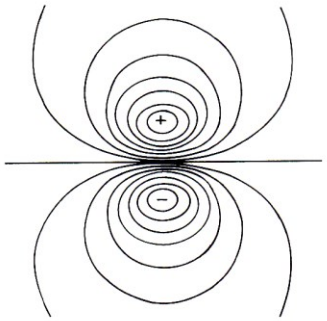

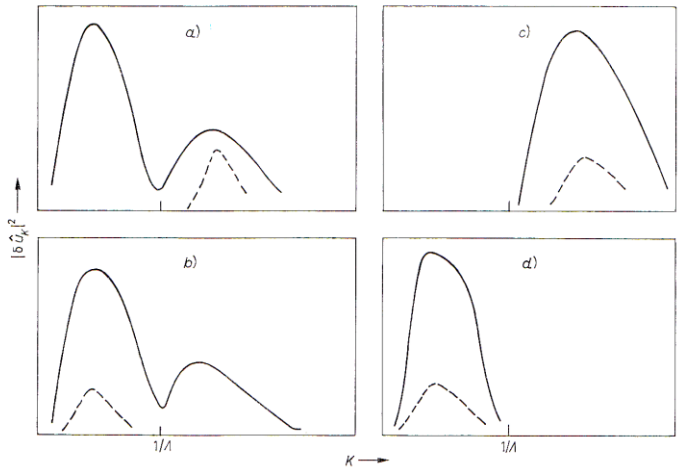

Fig. 1. – Schematic pictures of possible $(a), b))$ and impossible $(c), d))$ instability mechanisms, dashed lines denote the perturbation at $t = 0$, the full lines at $t > 0$.

Rotture di simmetria,
Stabilità di flussi

Modellistica di
onde nonlineari

Aspetti lineari della circolazione
indotta dal vento (Rossby waves)

Applicazioni della teoria
dei sistemi dinamici nonlineari:
modelli alle equazioni primitive

Applicazioni della teoria
dei sistemi dinamici nonlineari:
modelli di bassa dimensionalità

Predicibilità dei processi di
transizione dell'Estensione
del Kuroshio

Modellistica di circolazione
del Mar Mediterraneo

Modellistica Antartica

Simulazioni di laboratorio di
flussi oceanografici

Modellistica di onde nonlineari

Pierini, S., 1984: A weakly nonlinear theory of continental shelf waves.
Journal of Fluid Mechanics, **138**, 197-208.

Pierini, S., 1986: Solitons in a channel emerging from a three-dimensional initial wave.
Nuovo Cimento, **9C**, 1045-1061.

UF | UNIVERSITY of FLORIDA

Korteweg-de Vries (KdV) equation:

$$\eta_t + c\eta_x + \gamma\eta_{xxx} + \delta\eta\eta_x = 0$$

Kadomtsev-Petviashvili (KP) equation:

$$(\eta_t + c\eta_x + \gamma\eta_{xxx} + \delta\eta\eta_x)_x + \frac{c}{2}\eta_{yy} = 0$$

of the initial wave is left in the radiation field. This evolution behaviour is not surprising having in mind what RUSSELL (11) tells on his famous first encounter with the KdV soliton:

« ..., when the boat suddenly stopped—not so the mass of water in the channel, which it had put in motion; it accumulated round the prow of the vessel in a state of violet agitation, then suddenly leaving it behind, rolled forward with great velocity, assuming the form of a large solitary elevation, ... »

The initial « mass of water » observed by RUSSELL was very likely three-dimensional and still evolved a wave that was essentially two-dimensional.

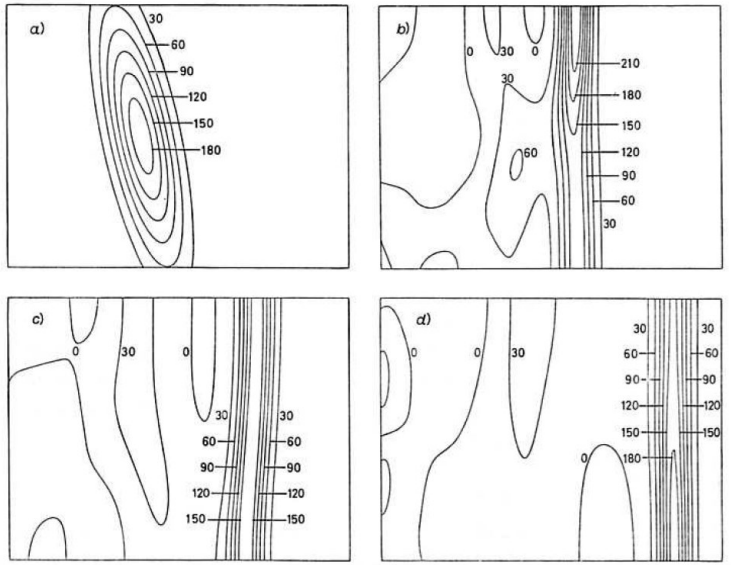

Fig. 3. – Contour lines of $\tilde{E}$ in case B) (see text; $n_{tig} = 250$).

$$\begin{cases} (E^{s+1}_{i,j} - E^{s-1}_{i,j})/(2DT) + (1 + \frac{3}{2}E^{s}_{i,j})(E^{s}_{i+1,j} - E^{s}_{i-1,j})/(2DX) - \\ \quad - (E^{s+1}_{i+1,j} - 2E^{s+1}_{i,j} + E^{s+1}_{i-1,j} - E^{s-1}_{i+1,j} + 2E^{s-1}_{i,j} - E^{s-1}_{i-1,j})/(12DTDX^2) - \\ \quad - \frac{1}{2}\mathrm{INT}_i[(E^{s}_{m,j+1} - 2E^{s}_{m,j} + E^{s}_{m,j-1})/DY^2] = 0\,, \qquad i = 2, \ldots, N-1\,, \\ E^{s+1}_{1,j} = a\,, \\ E^{s+1}_{N,j} = 0\,, \end{cases}$$

$$\mathrm{INT}_i[A_m] = \int_{iDX}^{NDX} A(X')\,\mathrm{d}X'\,, \qquad X' = mDX\,,$$

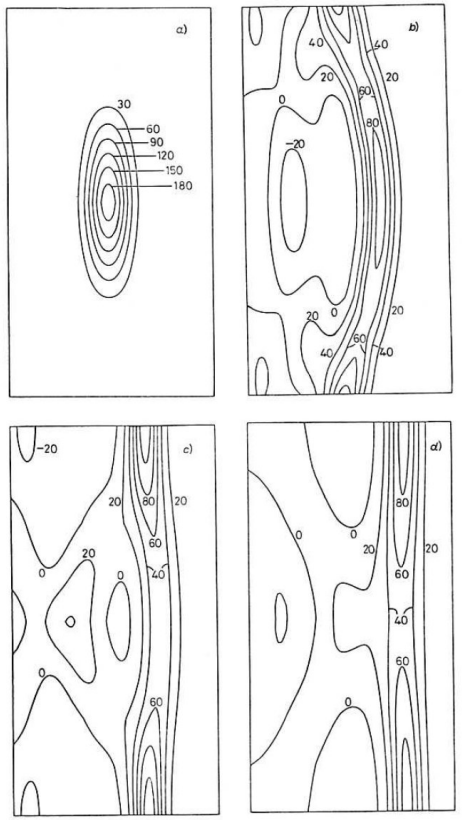

Fig. 4. – Contour lines of $\tilde{E}$ in case C) (see text; $n_{tig} = 200$).

Modellistica di onde nonlineari

Pierini, S., 1989: A model for the Alboran Sea internal solitary waves.
Journal of Physical Oceanography, **19**, 755-772.

Massachusetts Institute of Technology

Prof.ssa Paola Malanotte

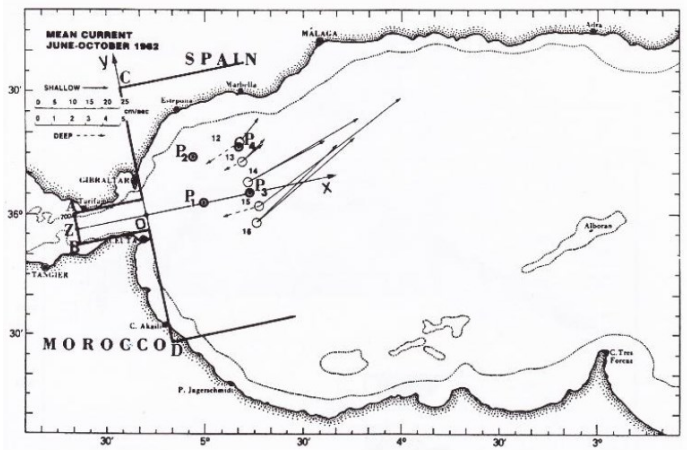

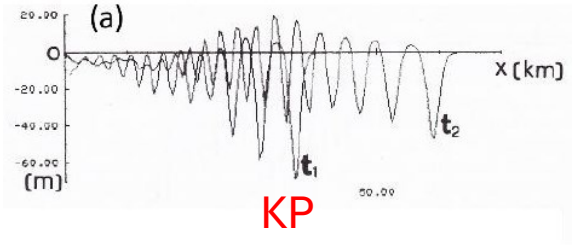

KP

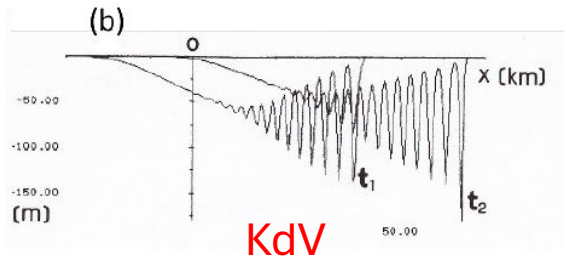

KdV

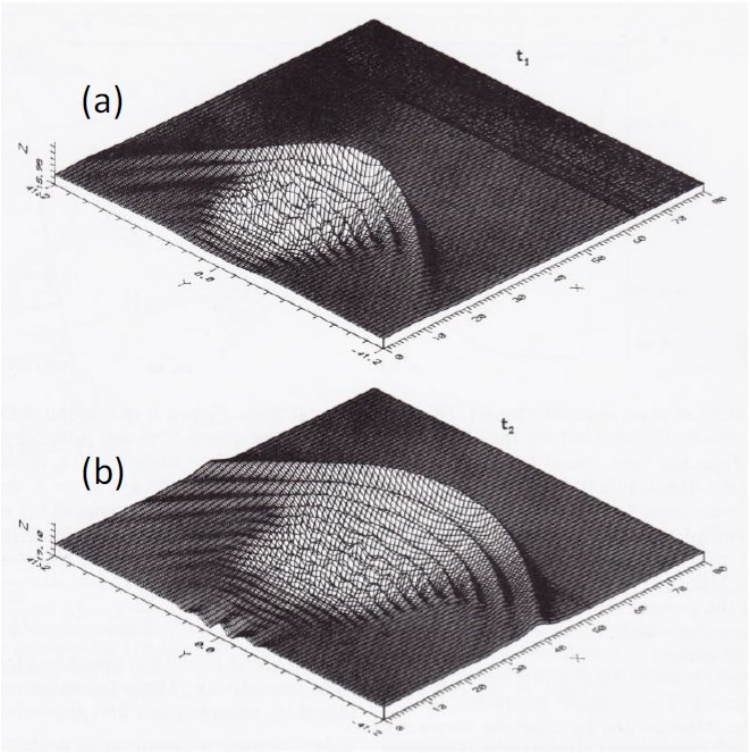

Modellistica di onde nonlineari

Modello SW nonlineare idrostatico (Rubino 1994)

Modello KP (Pierini 1986)

Rubino, A., Pierini, S., Backhaus, J.O., 1998: Dispersive mud-slide induced tsunamis.
Nonlinear Processes in Geophysics, **5**, 127-136.

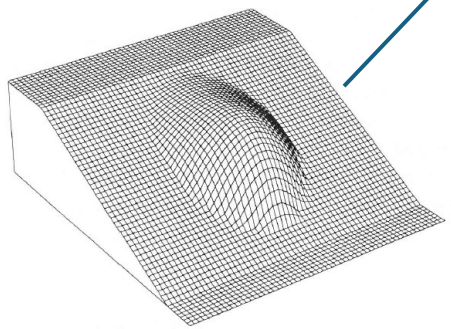

Fig. 3. The initial form of the sediments generating underwater slide.

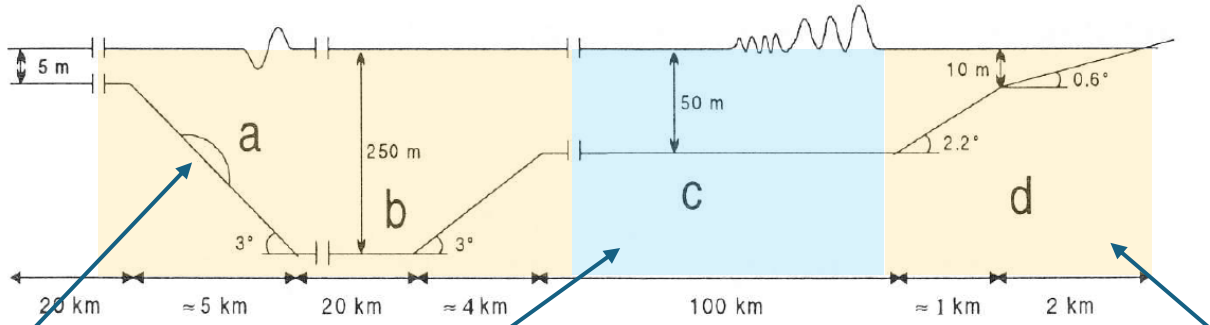

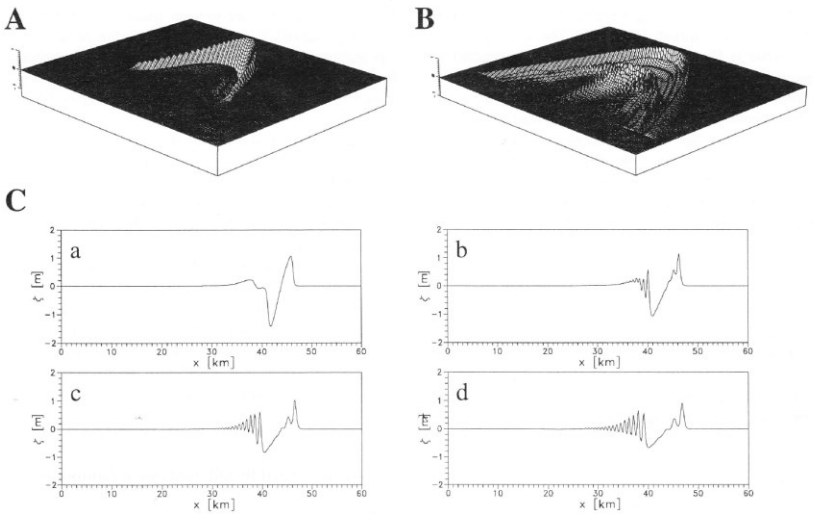

Fig 4. A: Form of the tsunami for experiment I at $t=t_m$. The wave is located at the beginning of sector c. B: Tsunami evolution for Exp. I, 92 min after the coupling with the non-hydrostatic model (3). The wave is still located in sector c. C: Axial sections of the tsunami for Exp. I at the matching time t_m (a) and after 23 (b), 46 (c) and 69 (d) min. In all cases the wave is located in sector c.

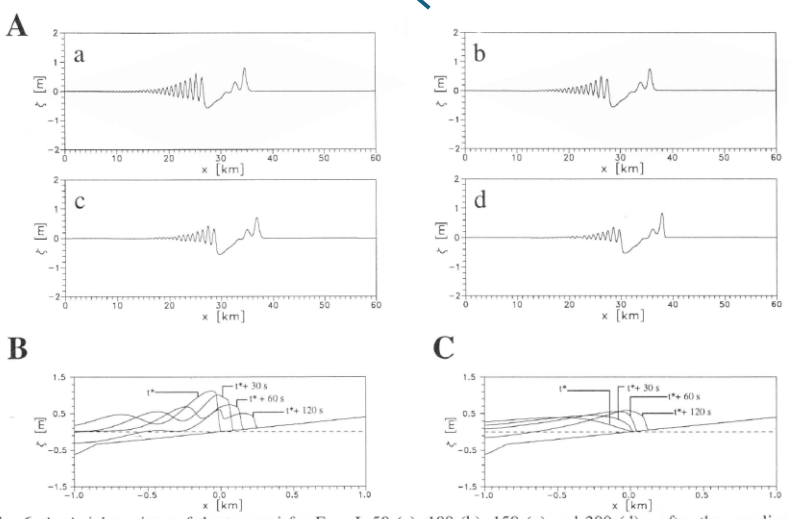

Fig. 6. A: Axial sections of the tsunami for Exp. I, 50 (a), 100 (b), 150 (c) and 200 (d) s after the coupling between the dispersive model (3) and the run-up model (1,2). In all cases the wave is located in the sloping sector d. Axial sections of the tsunami for Exp. I (B) and for Exp. II (C) in the final part of the sloping sector d. At $t=t^*$ the first landpoint has just been flooded.

Rotture di simmetria,
Stabilità di flussi

Modellistica di
onde nonlineari

Aspetti lineari della circolazione
indotta dal vento (Rossby waves)

Applicazioni della teoria
dei sistemi dinamici nonlineari:
modelli alle equazioni primitive

Applicazioni della teoria
dei sistemi dinamici nonlineari:
modelli di bassa dimensionalità

Predicibilità dei processi di
transizione dell'Estensione
del Kuroshio

Modellistica di circolazione
del Mar Mediterraneo

Modellistica Antartica

Simulazioni di laboratorio di
flussi oceanografici

Aspetti lineari della circolazione indotta dal vento (Rossby waves)

Pierini, S., 1990: A divergent quasi-geostrophic model for wind-driven oceanic fluctuations in a closed basin.
Dynamics of Atmospheres and Oceans, **14**, 259-277

Pierini, S., 1997: Westward intensified and topographically modified planetary modes.
Journal of Physical Oceanography, **27**, 1459-1471.

Pierini, S., 1998: Wind-driven fluctuating western boundary currents.
Journal of Physical Oceanography, **28**, 2185-2198.

Pierini, S., Zambianchi, E., 2003: Eulerian and Lagrangian aspects of oceanic Rossby dynamics. In: "*Chaos in Geophysical Flows*", G. Boffetta, G. Lacorata, G. Visconti and A. Vulpiani (Editors). Otto Editore, 279-299.

Pierini, S., 2003: A model of the wind-driven seasonal variability in the tropical North Pacific, with validation through altimeter data.
Journal of Physical Oceanography, **33**, 2156-2172.

Pierini, S., 2005: A model study of the spectral structure of boundary-driven Rossby waves, and related altimetric implications.
Journal of Physical Oceanography, **35**, 218-231.

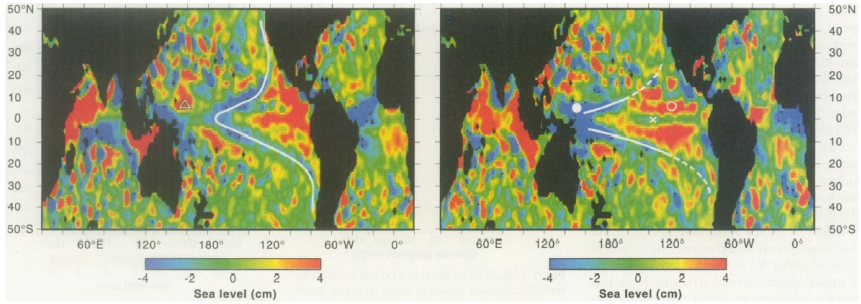

Chelton e Schlax (1996)

Rifrazione-beta di onde di Rossby

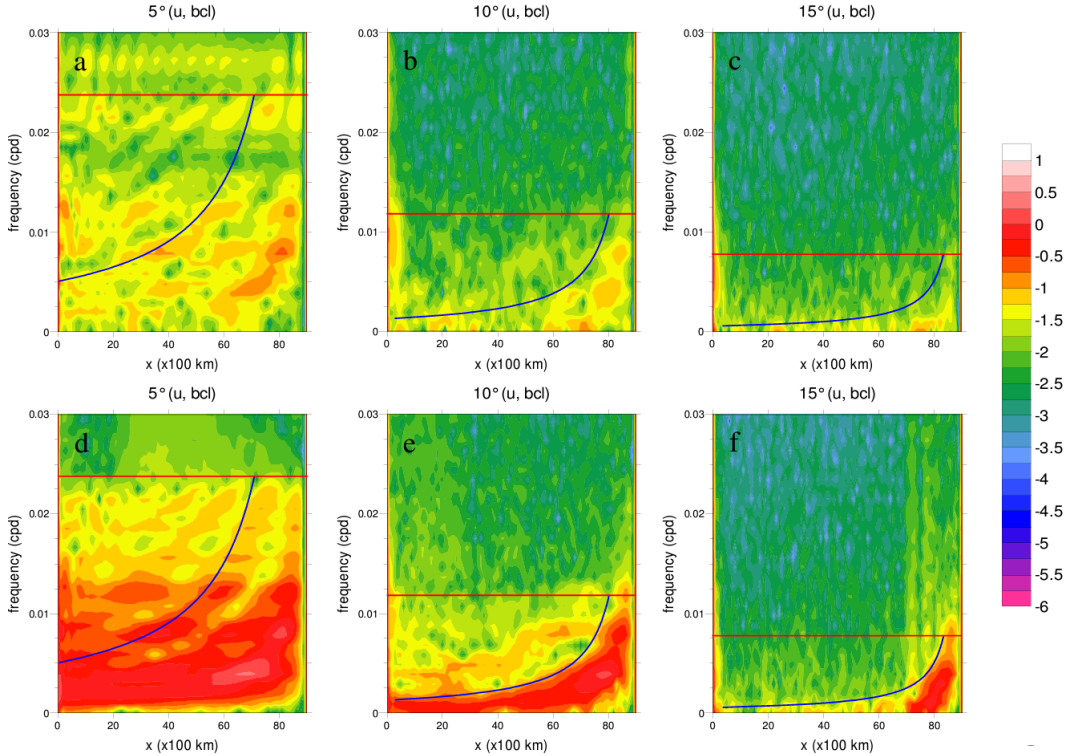

FIG. 6. Longitude–frequency maps of $\log_{10}$ of the spectral density of the zonal component of the upper-layer baroclinic velocity at 5°, 10°, and 15°N for (a)–(c) expt 2 and for (d)–(f) expt 3.

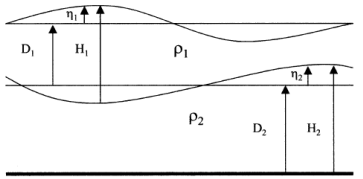

FIG. 1. The two-layer shallow water model setup.

$$u_{1t} + u_1 u_{1x} + v_1 u_{1y} - f v_1 = -g\eta_{1x} + \frac{\tau_x}{\rho_1 H_1} + A_H \nabla^2 u_1$$

$$v_{1t} + u_1 v_{1x} + v_1 v_{1y} + f u_1 = -g\eta_{1y} + \frac{\tau_y}{\rho_1 H_1} + A_H \nabla^2 v_1$$

$$H_{1t} + (H_1 u_1)_x + (H_1 v_1)_y = 0, \quad (1)$$

$$u_{2t} + u_2 u_{2x} + v_2 u_{2y} - f v_2 = -\alpha\eta_{1x} - g'\eta_{2x} + A_H \nabla^2 u_2$$

$$v_{2t} + u_2 v_{2x} + v_2 v_{2y} + f u_2 = -\alpha\eta_{1y} - g'\eta_{2y} + A_H \nabla^2 v_2$$

$$H_{2t} + (H_2 u_2)_x + (H_2 v_2)_y = 0, \quad (2)$$

$$u_{\rm btp} = (u_1 H_1 + u_2 H_2)/(H_1 + H_2) \quad \text{and}$$

$$v_{\rm btp} = (v_1 H_1 - q_{\rm Ekman} + v_2 H_2)/(H_1 + H_2)$$

$$u_{\rm bcl} = u_1 - u_{\rm btp} \quad \text{and}$$

$$v_{\rm bcl} = v_1 - \frac{q_{\rm Ekman}}{H_1} - v_{\rm btp}$$

Rotture di simmetria,
Stabilità di flussi

Modellistica di
onde nonlineari

Aspetti lineari della circolazione
indotta dal vento (Rossby waves)

Applicazioni della teoria
dei sistemi dinamici nonlineari:
modelli alle equazioni primitive

Applicazioni della teoria
dei sistemi dinamici nonlineari:
modelli di bassa dimensionalità

Predicibilità dei processi di
transizione dell'Estensione
del Kuroshio

Modellistica di circolazione
del Mar Mediterraneo

Modellistica Antartica

Simulazioni di laboratorio di
flussi oceanografici

Applicazioni della teoria dei sistemi dinamici nonlineari: **modelli alle equazioni primitive**

Pierini S., 2006: A Kuroshio Extension System model study: decadal chaotic self-sustained oscillations. *Journal of Physical Oceanography*, **36**, 1605-1625.

Pierini S., 2008: On the crucial role of basin geometry in double-gyre models of the Kuroshio Extension. *Journal of Physical Oceanography*, **38**, 1327-1333.

Pierini S., 2010: Coherence resonance in a double-gyre model of the Kuroshio Extension. *Journal of Physical Oceanography*, **40**, 238-248.

$$\begin{cases} \dfrac{d\mathbf{u}_1}{dt} + f\mathbf{k}\times\mathbf{u}_1 = -g'\nabla_H\tilde{\eta} + \dfrac{\boldsymbol{\tau}^{(s)}}{\rho_1 H} + K_H\nabla_H^2\mathbf{u}_1 \\ \dfrac{\partial H}{\partial t} + \nabla_H\cdot(H\mathbf{u}_1) = 0 \end{cases}$$

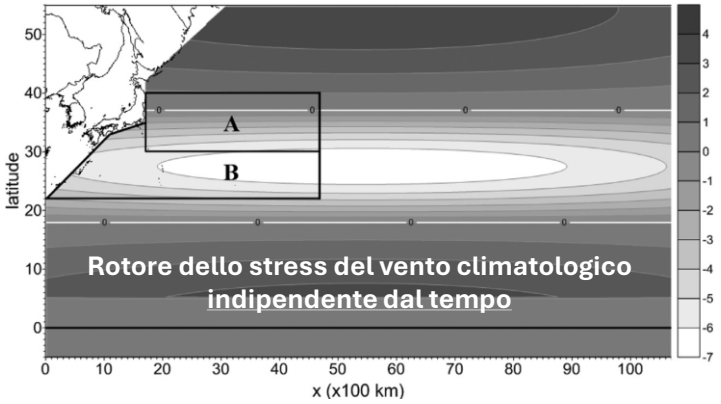

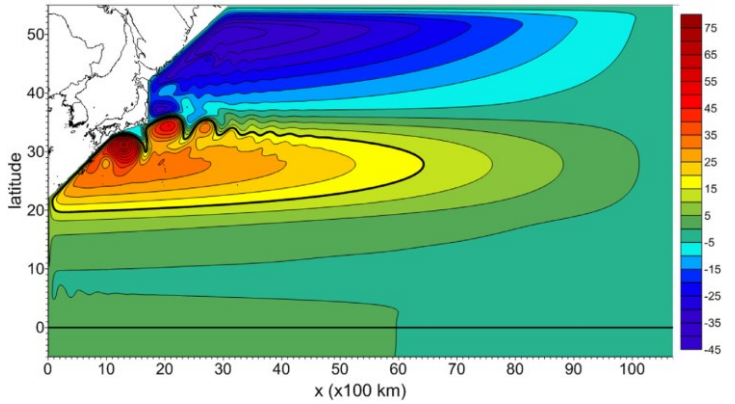

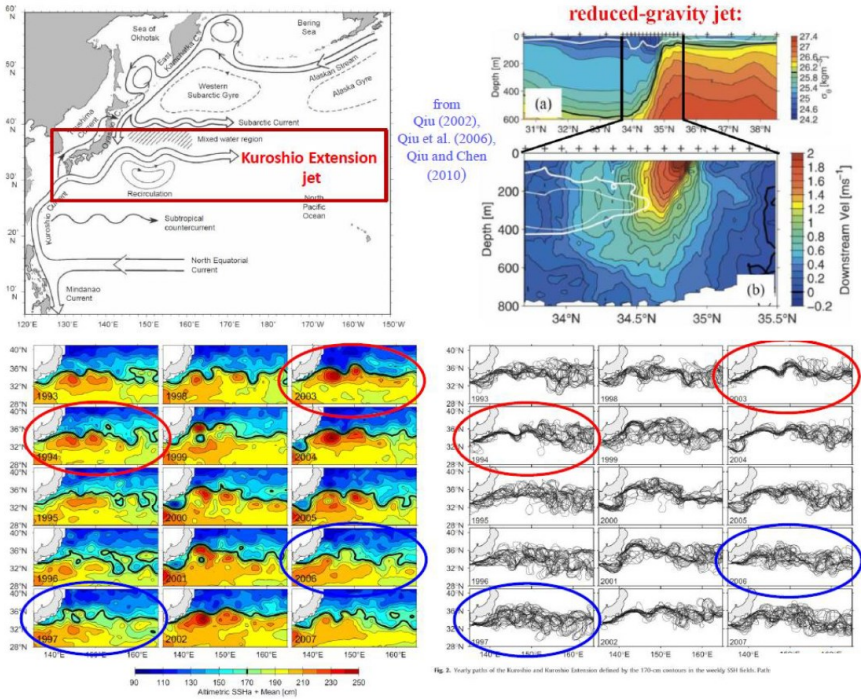

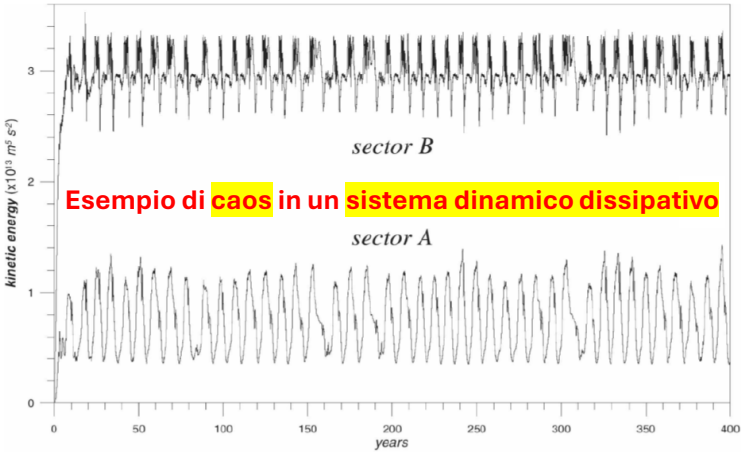

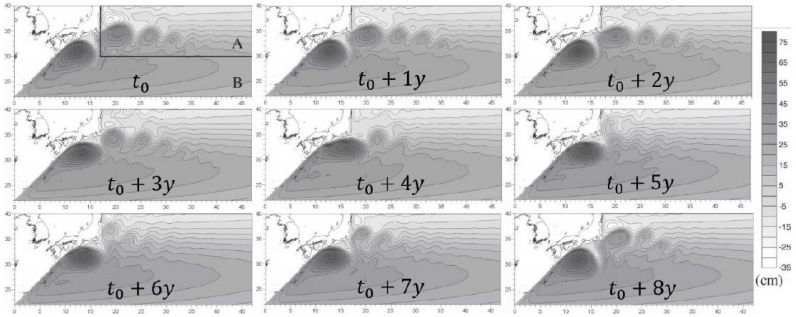

$t_0 = 143\ y$

oscillazioni di rilassamento autosostenute

Applicazioni della teoria dei sistemi dinamici nonlineari: **modelli alle equazioni primitive**

Pierini S., H. A. Dijkstra and A. Riccio, 2009: A nonlinear theory of the Kuroshio Extension bimodality. *Journal of Physical Oceanography*, **39**, 2212-2229.

Utrecht University

HPC-Europa

Prof. Henk Dijkstra

Francesco e Antonella

La parallelizzazione del modello (Prof. Angelo Riccio) ha permesso di effettuare *centinaia* di simulazioni con HPC facilities, dalle quali è stato possibile costruire il seguente

diagramma di biforcazione:

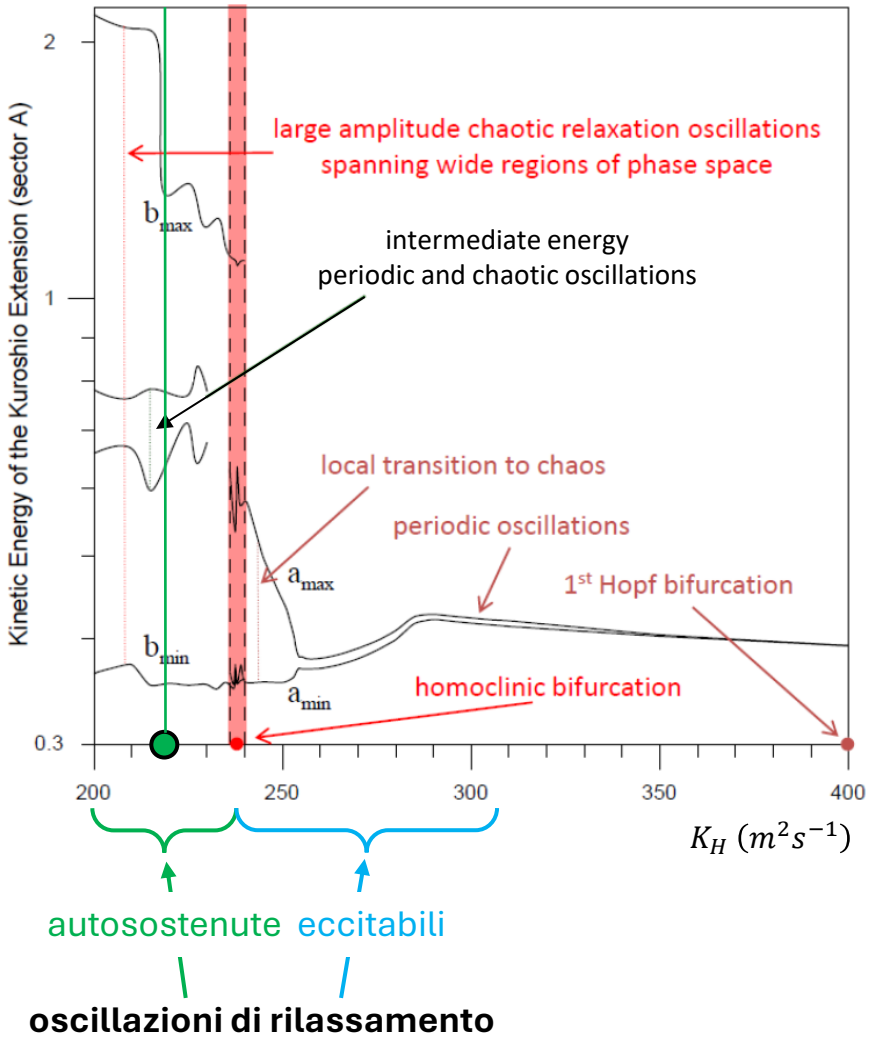

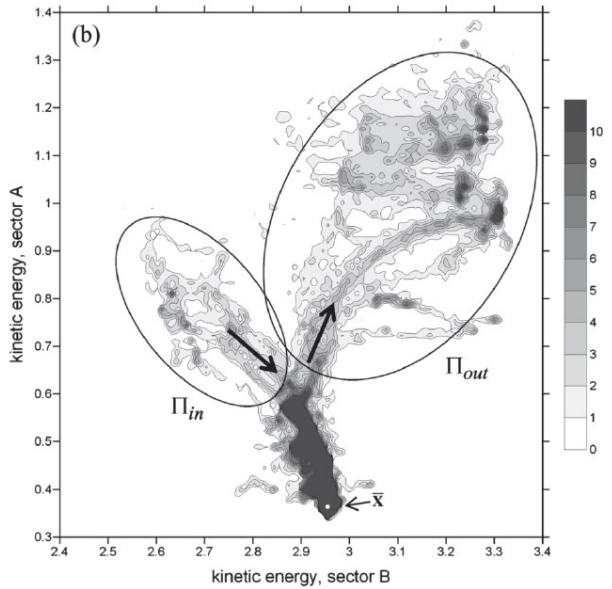

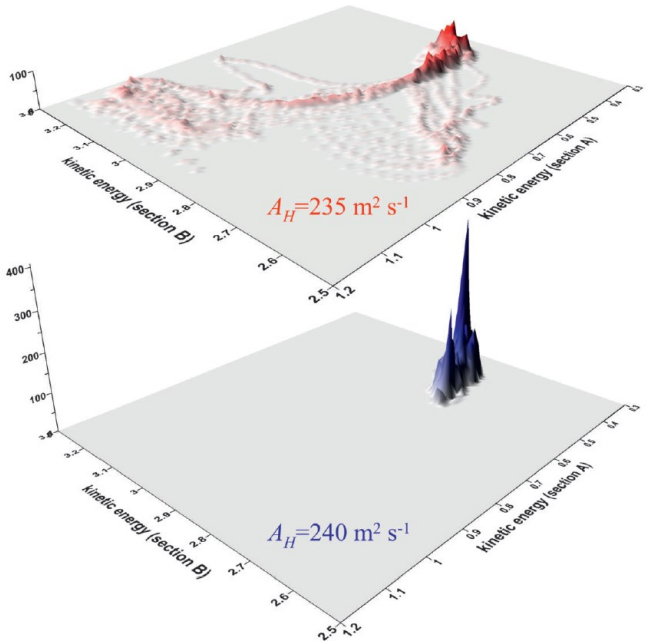

Applicazioni della teoria dei sistemi dinamici nonlineari: **modelli alle equazioni primitive**

Pierini S., 2014: Kuroshio Extension bimodality and the North Pacific Oscillation: a case of intrinsic variability paced by external forcing.
Journal of Climate, **27**, 448-454.

regime autosostenuto → regime eccitabile
forzante **costante** nel tempo → forzante **variabile** nel tempo

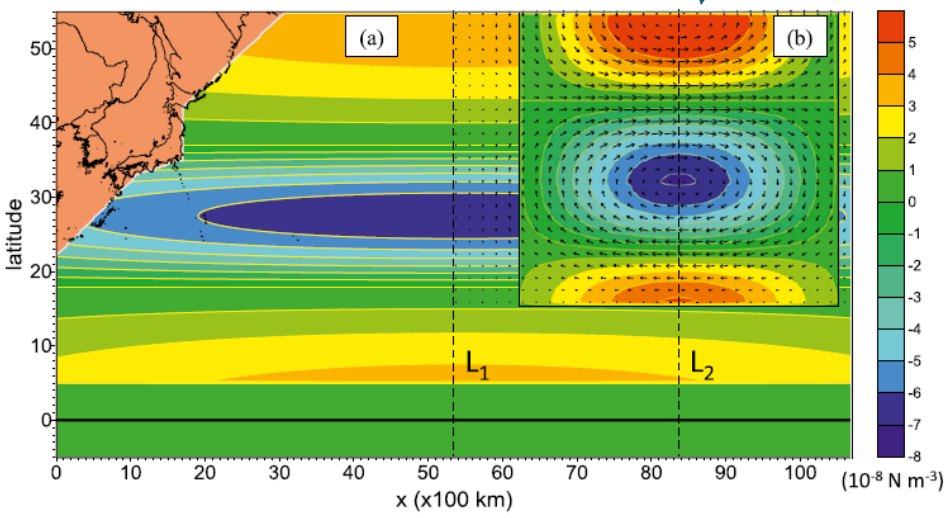

FIG. 1. (a) Curl of the climatological wind stress τ_0 (as in P06). (b) Curl of the spatial structure of the NPO wind stress τ_{NPO} (τ_{NPO} is shown by the arrows; for their amplitude see Fig. 2a).

Eccitazione deterministica (deterministic excitation)

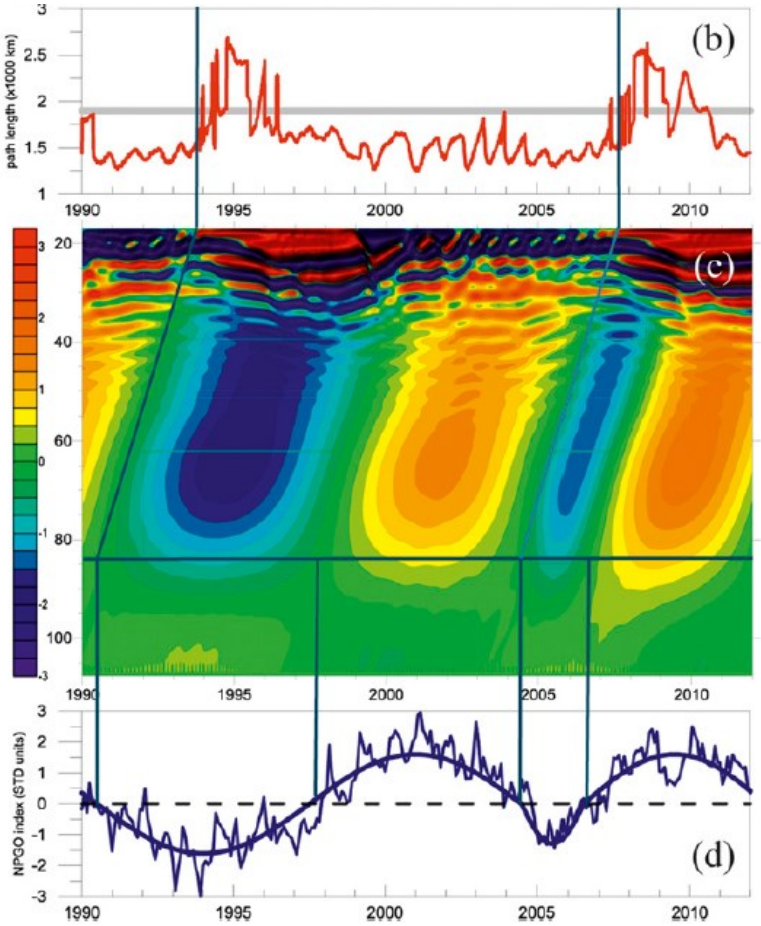

Applicazioni della teoria dei sistemi dinamici nonlineari: **modelli alle equazioni primitive**

Dottorandi

Quattrocchi G., S. Pierini and H. A. Dijkstra, 2012: Intrinsic low-frequency variability of the Gulf Stream. *Nonlinear Processes in Geophysics*, **19**, 155-164.

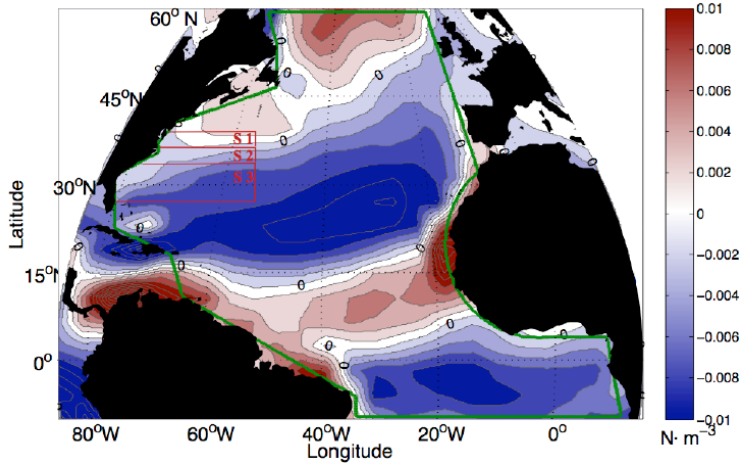

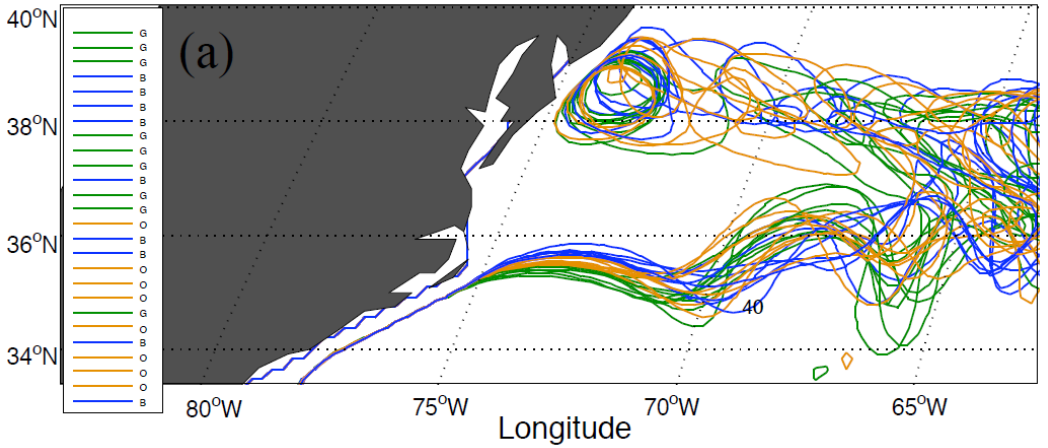

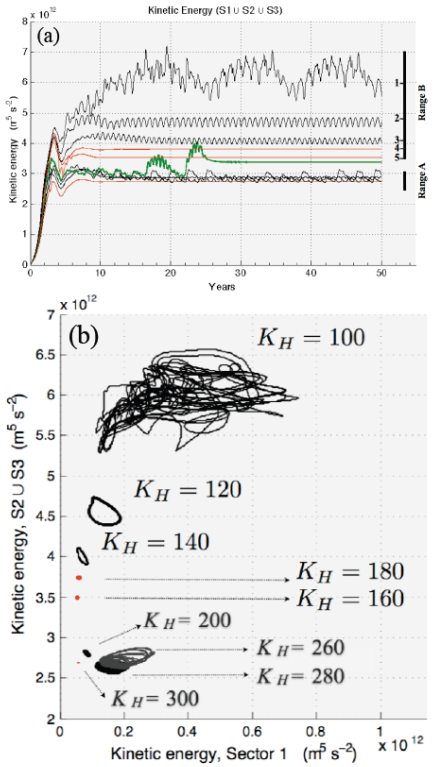

Fig. 9. **(a)** Time series of the kinetic energy integrated in sector S1∪S2∪S3 for different values of K_H: $K_H = 100$, 120, 140, 160, 180, 200, 220, 240, 260, 300 $m^2\,s^{-1}$, corresponding to lines 1,...,10, respectively. Two different energetic regimes (Range A and Range B) can be identified; the green line ($K_H = 200\,m^2\,s^{-1}$) marks the transition between them. The red lines identify steady states of the system. **(b)** Orbits projected onto the (kinetic energy)(S1) – (kinetic energy) (S2∪S3) plane for different values of K_H.

Applicazioni della teoria dei sistemi dinamici nonlineari: **modelli alle equazioni primitive**

Dottorandi

Sgubin G., S. Pierini and H. A. Dijkstra, 2014: Intrinsic variability of the Antarctic Circumpolar Current System: low- and high-frequency fluctuations of the Argentine Basin flow. *Ocean Science*, **10**, 201-2013.

THE PRINCETON OCEAN MODEL

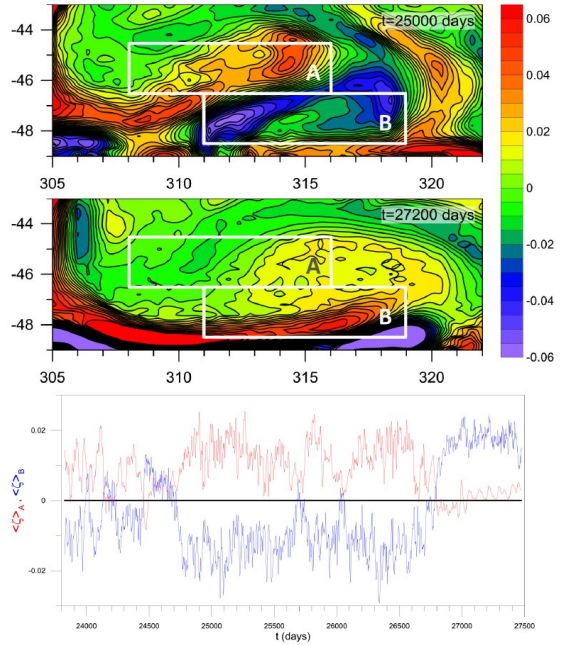

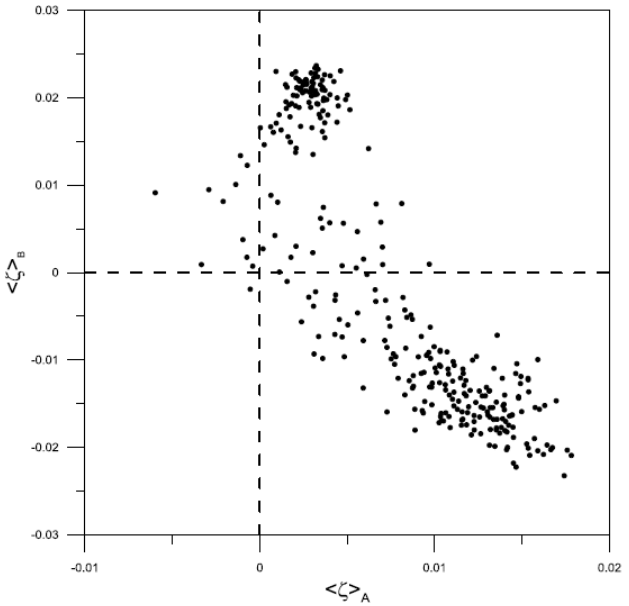

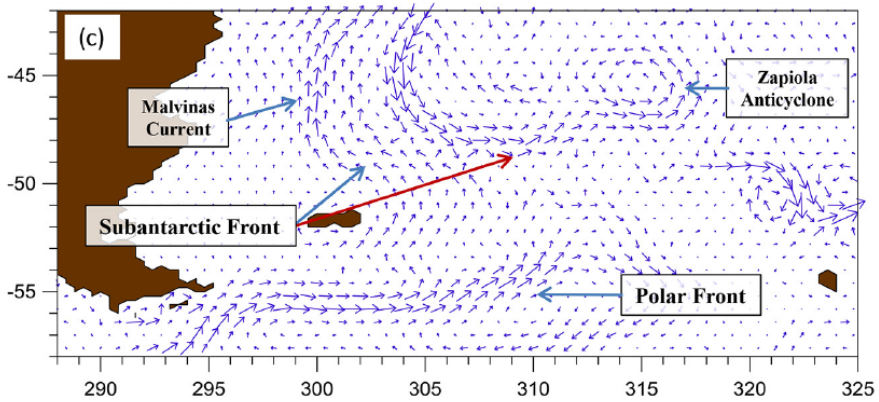

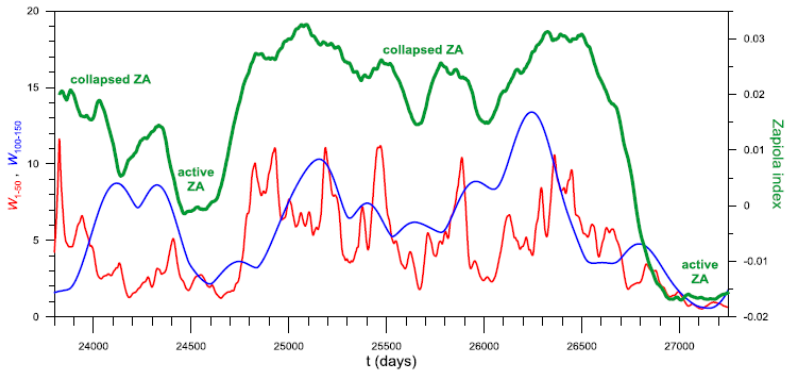

Fig. 15. Green line: Zapiola index. Red and blue lines: integrated wavelet amplitudes $W_{1,50}$ and $W_{100,150}$, respectively.

Applicazioni della teoria dei sistemi dinamici nonlineari: **modelli alle equazioni primitive**

Dottorandi

Gentile V., S. Pierini, P. de Ruggiero and L. Pietranera, 2018: Ocean modelling and altimeter data reveal the possible occurrence of intrinsic low-frequency variability of the Kuroshio Extension.
Ocean Modelling, **131**, 24-39.

Pierini S., 2015: A comparative analysis of Kuroshio Extension indices from a modeling perspective.
Journal of Climate, **28**, 5873-5881.

modello

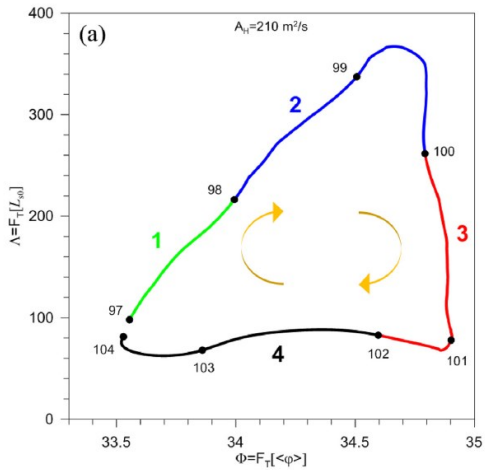

dati altimetrici

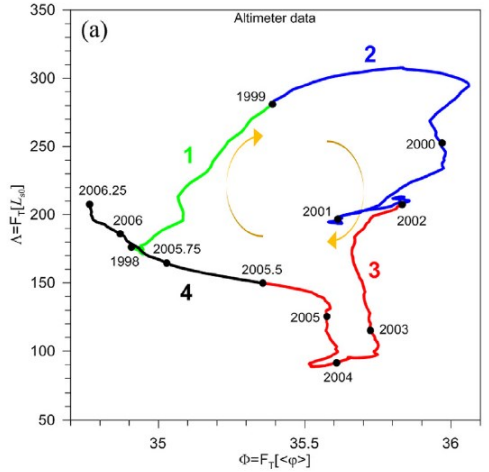

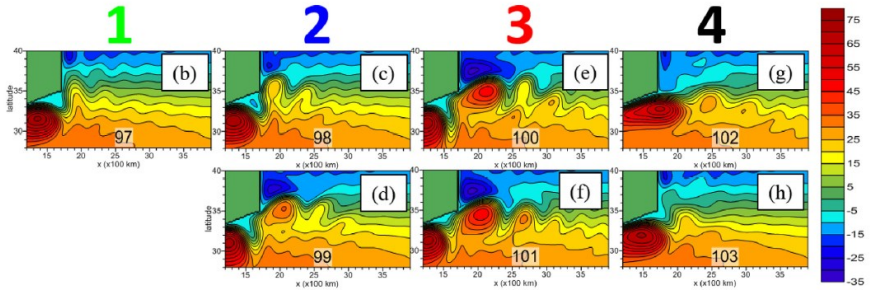

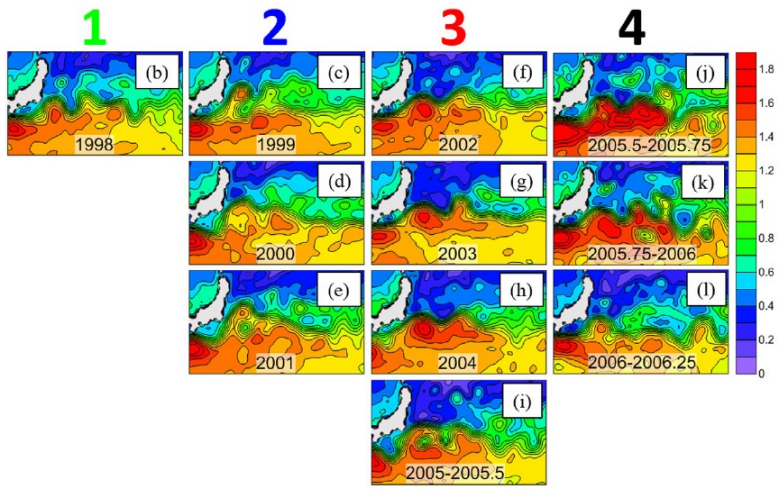

Applicazioni della teoria dei sistemi dinamici nonlineari: **modelli alle equazioni primitive**

Dottorandi

Fedele G., T. Penduff, S. Pierini, M. C. Alvarez-Castro, A. Bellucci and S. Masina, 2021: Interannual to decadal variability of the Kuroshio Extension: Analyzing an ensemble of global hindcasts from a dynamical system viewpoint.
Climate Dynamics, **57**, 975-992.

Dr. Thierry Penduff

OCCIPUT

OCCITENS: 1/4° global model dataset,
consisting in an ensemble of 50 ocean–sea ice hindcasts performed over the period 1960–2015

OCCICLIM: a one-member 330-year climatological simulation

Penduff et al. (2014), etc.

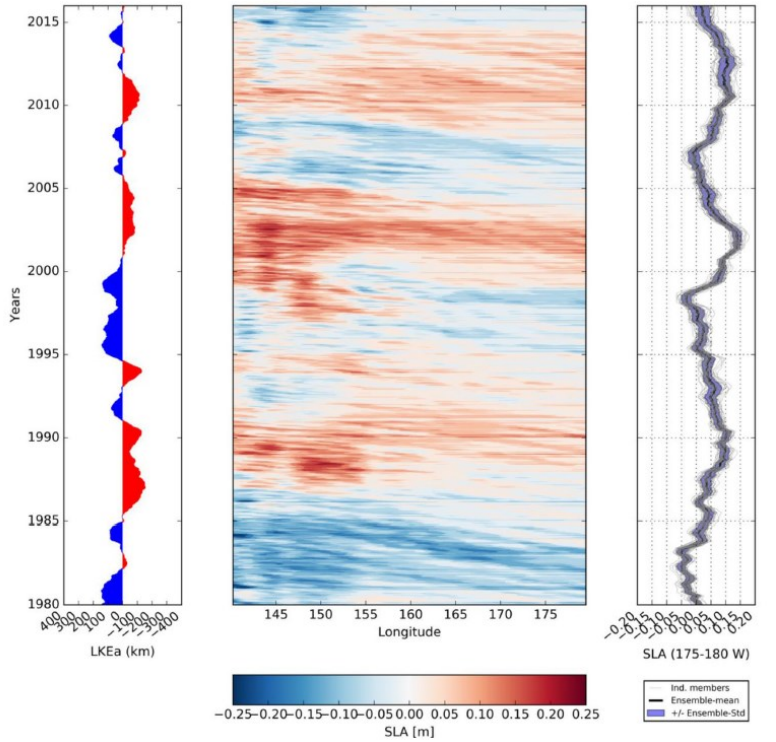

Fig. 4 Left: ensemble mean LKE anomaly (LKEa) (negative values in red, positive values in blue). Center: Hovmöller diagram of the ensemble mean SLA averaged over 32–34° N. Right: Low pass filtered SLA averaged between 32–34° N—175–180° W for the 50 ensemble members (thin gray lines) and for the ensemble mean (thick black line); the ensemble standard deviation is shaded

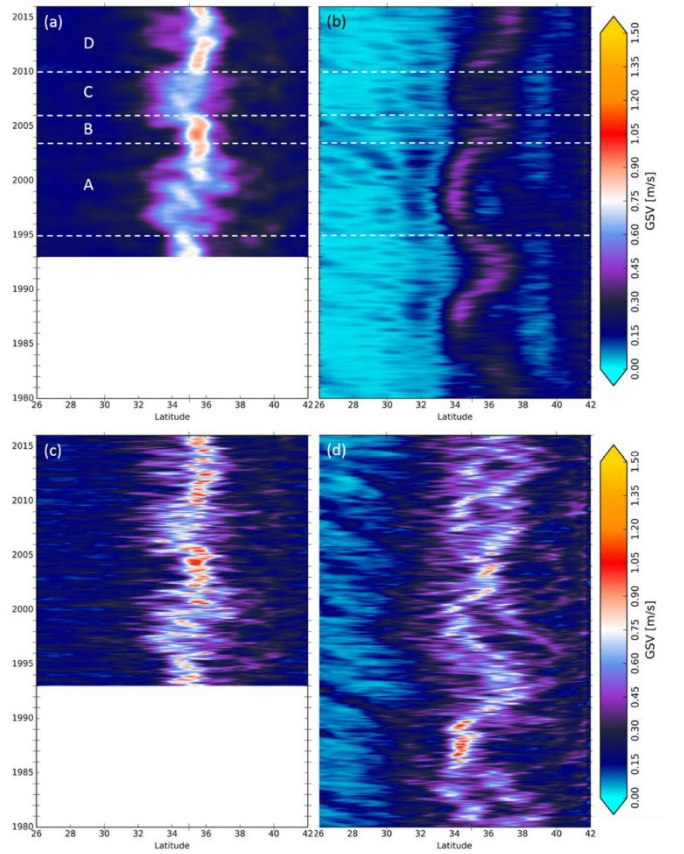

Fig. 6 Hovmöller diagram of the GSV in the latitude-time domain averaged in the upstream KE region. **a** Yearly averaged AVISO data. **b** OCCITENS ensemble mean. **c** AVISO data. **d** First OCCITENS ensemble member

Rotture di simmetria,
Stabilità di flussi

Modellistica di
onde nonlineari

Aspetti lineari della circolazione
indotta dal vento (Rossby waves)

Applicazioni della teoria
dei sistemi dinamici nonlineari:
modelli alle equazioni primitive

Applicazioni della teoria
dei sistemi dinamici nonlineari:
modelli di bassa dimensionalità

Predicibilità dei processi di
transizione dell'Estensione
del Kuroshio

Modellistica di circolazione
del Mar Mediterraneo

Modellistica Antartica

Simulazioni di laboratorio di
flussi oceanografici

Applicazioni della teoria dei sistemi dinamici nonlineari: **modelli di bassa dimensionalità**

Necessità di **simulazioni di *ensemble*** per sistemi dinamici **nonautonomi caotici**:

It has recently been recognized that the **correct description of a changing climate** subjected to both natural and anthropogenic forcing requires the knowledge of the time-dependent probability distributions associated with the system's ***snapshot/pullback attractor*** (PBA) (e.g., Romeiras et al. 1990; Ghil et al 2008; Chekroun et al, 2011; Bódai et al. 2011a,b; Drótos et al 2015, 2017)

The PBA is a mathematical tool which provides the **extension to a nonautonomous system of the classical concept of attractor of a nonlinear dissipative autonomous dynamical system**. If the external forcing and/or some parameter depend on time, the PBA is the subset $A(t)$ of phase space which, together with the probability measure supported on this set, is invariant under the governing equations and is such that any trajectory initialized in the remote past converges to it

Le **simulazioni di ensemble** appropriate per stimare il PBA richiedono **integrazioni più lunghe del tempo di predicibilità**, in modo che la memoria dell'inizializzazione venga persa grazie alla caoticità del sistema

L'**ensemble spread** è collegato alla variabilità intrinseca del sistema ed è, quindi, una **proprietà irriducibile del sistema climatico**

In questo caso, i membri dell'ensemble possono essere visti come **realizzazioni climatiche parallele** indipendenti, soggette tutte alle stesse equazioni di evoluzione, condizioni al contorno e forzante esterno, ma ciascuna emergente da una diversa condizione iniziale e caratterizzata da una data probabilità di accadimento

In questo contesto, **modelli di bassa dimensionalità** possono risultare utilissimi per delineare proprietà dei sistemi reali **caotici**, offrendo uno

strumento matematico estremamente agile col quale è, quindi, possibile effettuare **simulazioni di ensemble** con limitato costo computazionale

Applicazioni della teoria dei sistemi dinamici nonlineari: **modelli di bassa dimensionalità**

Pierini S., 2011: Low-frequency variability, coherence resonance and phase selection in a low-order model of the wind-driven ocean circulation.
Journal of Physical Oceanography, **41**, 1585-1604.

The model is based on the evolution equation of potential vorticity in the QG reduced-gravity approximation,

$$\frac{\partial}{\partial \bar{t}}\left(\bar{\nabla}^2\bar{\psi}-\frac{\bar{\psi}}{L_R^2}\right)+\bar{J}(\bar{\psi},\bar{\nabla}^2\bar{\psi})+\beta\bar{\psi}_{\bar{x}}=-r\bar{\nabla}^2\bar{\psi}+\frac{curl_{\bar{z}}\bar{\boldsymbol{\tau}}}{\rho H}$$

that can be adimensionalized as follows:

$$\frac{\partial}{\partial t}\left(\nabla_\lambda^2\psi-F\psi\right)+\gamma J\left(\psi,\nabla_\lambda^2\psi\right)+\psi_x=-R\nabla_\lambda^2\psi-T\tau_y$$

The truncated spectral model is obtained by expanding the stremfunction ψ as:

$$\psi(\mathbf{x},t)=\sum_{i=1}^{4}\Psi_i(t)|i\rangle$$

$$|1\rangle=e^{-\alpha x}sinx\,siny \qquad |3\rangle=e^{-\alpha x}sin2x\,siny$$
$$|2\rangle=e^{-\alpha x}sinx\,sin2y \qquad |4\rangle=e^{-\alpha x}sin2x\,sin2y$$

This choice follows that of Jiang et al. (1995), who adopted $|i\rangle$, i=1,2 in their 2D model. In the Hilbert space endowed with the inner product

$$\langle f|g\rangle=\frac{4}{\pi^2}\int_0^\pi\int_0^\pi e^{2\alpha x}\,fg\,dxdy$$

the basis is orthonormal: $\langle i|j\rangle=\delta_{ij}$.

The system reduces to a set of four coupled nonlinear ODEs:

$$\begin{cases}\dot{\Psi}_1+p\Psi_1+q\Psi_3+N_1=W_1\\ \dot{\Psi}_2+u\Psi_2+v\Psi_4+N_2=W_2\\ \dot{\Psi}_3+m\Psi_3+o\Psi_1+N_3=W_3\\ \dot{\Psi}_4+s\Psi_4+t\Psi_2+N_4=W_4\end{cases}$$

The nonlinear terms N_i are given by

$$N_i=\sum_{j,k=1}^{4}\Psi_jJ_{ijk}\Psi_k$$

so that the system can be written in compact form as follows:

$$\frac{d\boldsymbol{\Psi}}{dt}+\boldsymbol{\Psi}\mathbf{J}\boldsymbol{\Psi}+\mathbf{L}\boldsymbol{\Psi}=\mathbf{W}$$

W=G(t)w

The rank-3 tensor **J** is given by:

$$J_{1jk}=\frac{c_1Z_{1jk}-h_1Z_{3jk}}{h_1^2+a_1c_1},\quad J_{2jk}=\frac{d_1Z_{2jk}-h_1Z_{4jk}}{h_1^2+b_1d_1}$$
$$J_{3jk}=\frac{h_1Z_{1jk}+a_1Z_{3jk}}{h_1^2+a_1c_1},\quad J_{4jk}=\frac{h_1Z_{2jk}+b_1Z_{4jk}}{h_1^2+b_1d_1}$$

where

$$Z_{ijk}\equiv\langle i|Q_{jk}\rangle$$

and where **Q** is the symmetric tensor:

$$|Q_{jk}\rangle=\frac{\gamma}{2}\left[|j\rangle_x\left(|k\rangle_{xxy}+\lambda|k\rangle_{yyy}\right)+|k\rangle_x\left(|j\rangle_{xxy}+\lambda|j\rangle_{yyy}\right)\right.$$
$$\left.-|j\rangle_y\left(|k\rangle_{xxx}+\lambda|k\rangle_{yyx}\right)-|k\rangle_y\left(|j\rangle_{xxx}+\lambda|j\rangle_{yyx}\right)\right]$$

...

Applicazioni della teoria dei sistemi dinamici nonlineari: **modelli di bassa dimensionalità**

Pierini S., 2011: Low-frequency variability, coherence resonance and phase selection in a low-order model of the wind-driven ocean circulation.
Journal of Physical Oceanography, **41**, 1585-1604.

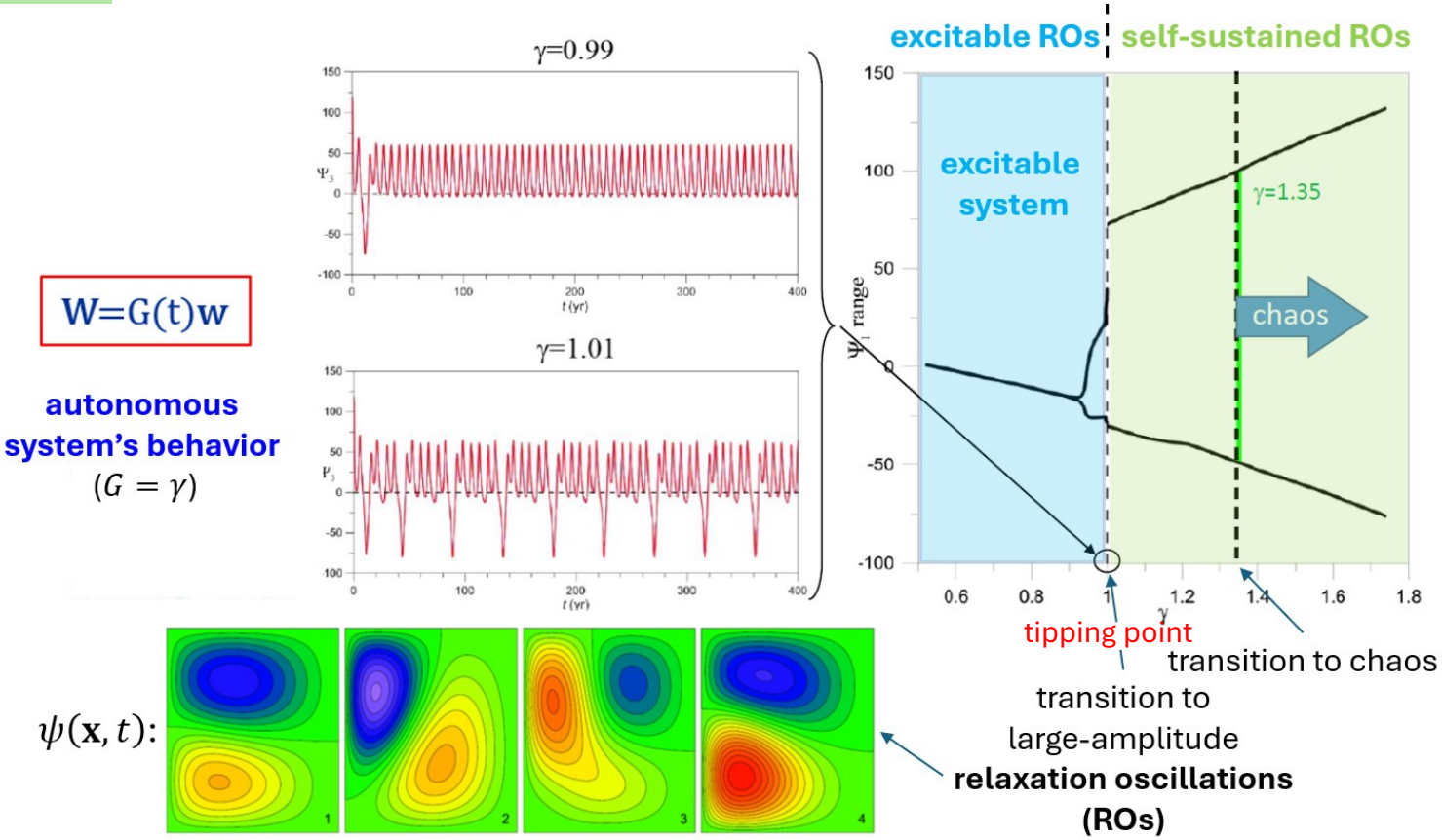

Applicazioni della teoria dei sistemi dinamici nonlineari: **modelli di bassa dimensionalità**

Pierini S., 2011: Low-frequency variability, coherence resonance and phase selection in a low-order model of the wind-driven ocean circulation.
Journal of Physical Oceanography, **41**, 1585-1604.

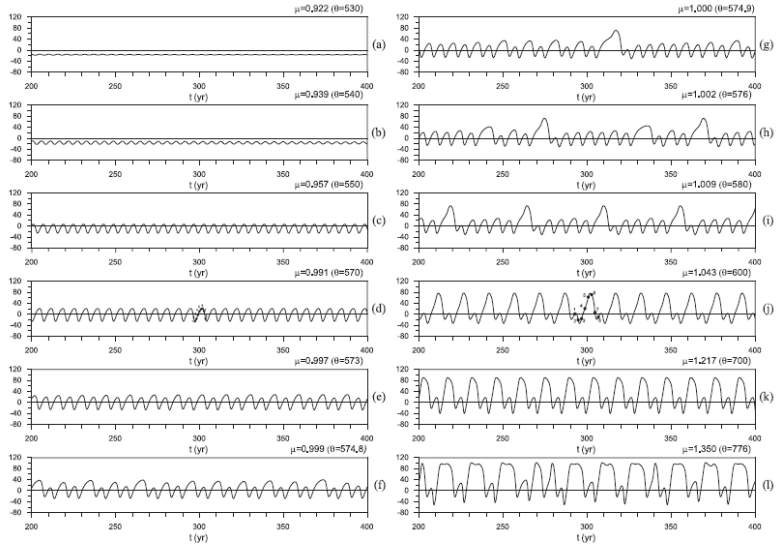

FIG. 3. Time series of Ψ_1 (scaled with 10^{-5}) obtained for several values of μ.

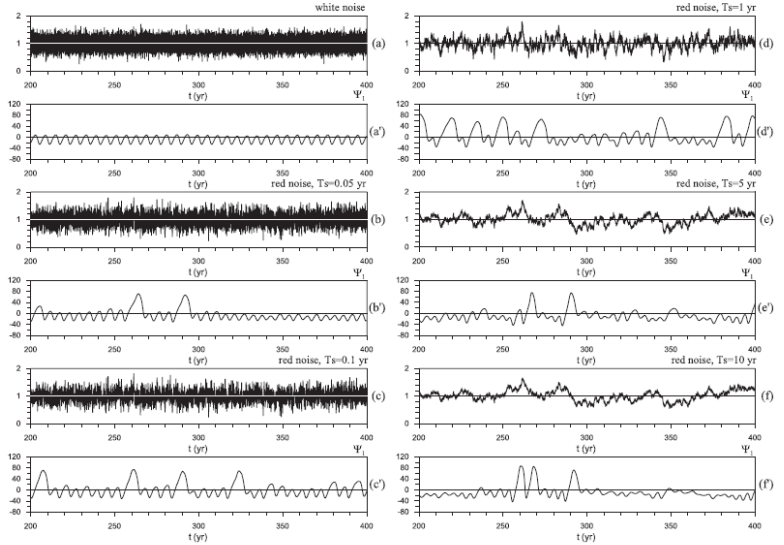

FIG. 8. Temporal dependence $G(t)$ of the wind stress curl forcing with $\varepsilon_1 = 0.2$ and $\varepsilon_2 = 0$: (a) for a white noise and a red noise with T_s = (b) 0.05, (c) 0.1, (d) 1.0, (e) 5.0 , and (f) 10 yr. (a′)–(f′) Corresponding model response of Ψ_1 (scaled with 10^{-5}) with $\mu = 0.957$.

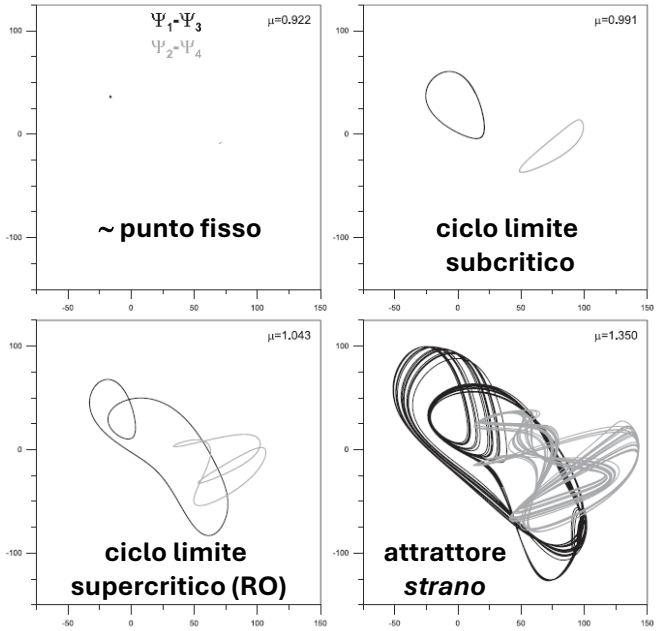

FIG. 4. Orbits in the Ψ_1–Ψ_3 (black lines) and Ψ_2–Ψ_4 (gray lines) planes for four different values of μ (reported in each graph).

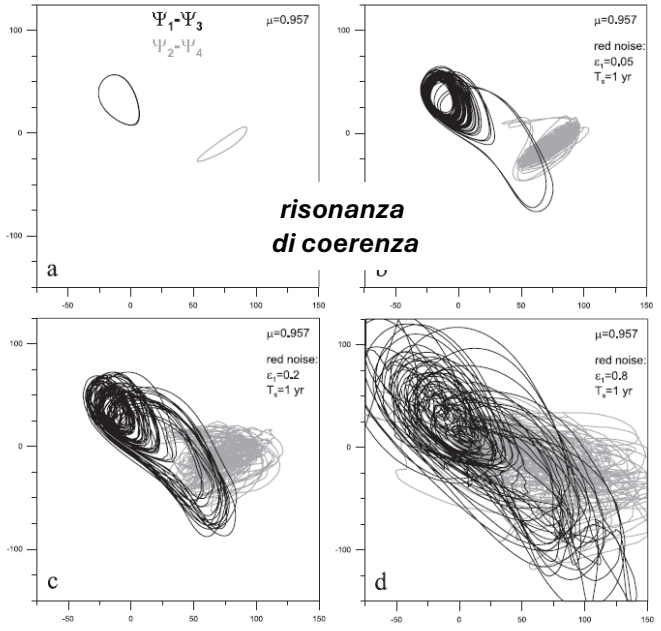

FIG. 10. Orbits in the Ψ–Ψ_3 (black lines) and Ψ_2–Ψ_4 (gray lines) planes for $\mu = 0.957$ (a) under steady forcing and under stochastic forcing with $\varepsilon_2 = 0$; $T_s = 1$ yr; and (b) $\varepsilon_1 = 0.05$, (c) $\varepsilon_1 = 0.2$, and (d) $\varepsilon_1 = 0.8$.

Applicazioni della teoria dei sistemi dinamici nonlineari: **modelli di bassa dimensionalità**

Pierini S., 2012: Stochastic tipping points in climate dynamics.
Physical Review E, **85**, 027101.

Definizione operativa di **tipping point *stocastico***

A crucial question recently raised in climate dynamics concerns abrupt climate transitions: Are they due to a tipping point (TP) being exceeded, or is fast noisy dynamics the cause of their excitation? In this respect, a case study based on a low-order ocean model is developed to show that in an excitable dynamical system perturbed by noise (a possible climate condition) the TPs may have limited physical meaning, with the coherence resonance mechanism being predominant. The analysis is based on an operational definition of stochastic TP, which accounts for the effect of noise and reconciles formally the TP and coherence resonance views.

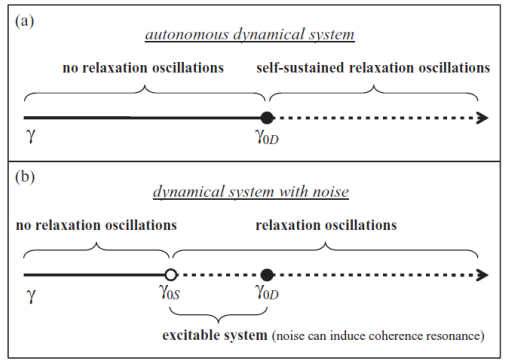

FIG. 1. (a) Definition of deterministic TP $\gamma_{0D}(g,T)$ in an autonomous DS with ROs. (b) Definition of STP $\Gamma_{0S}(g,S,T)$ in the same DS with noise; $\gamma_{0S}(g,S,T)$ denotes a generic realization of Γ_{0S}.

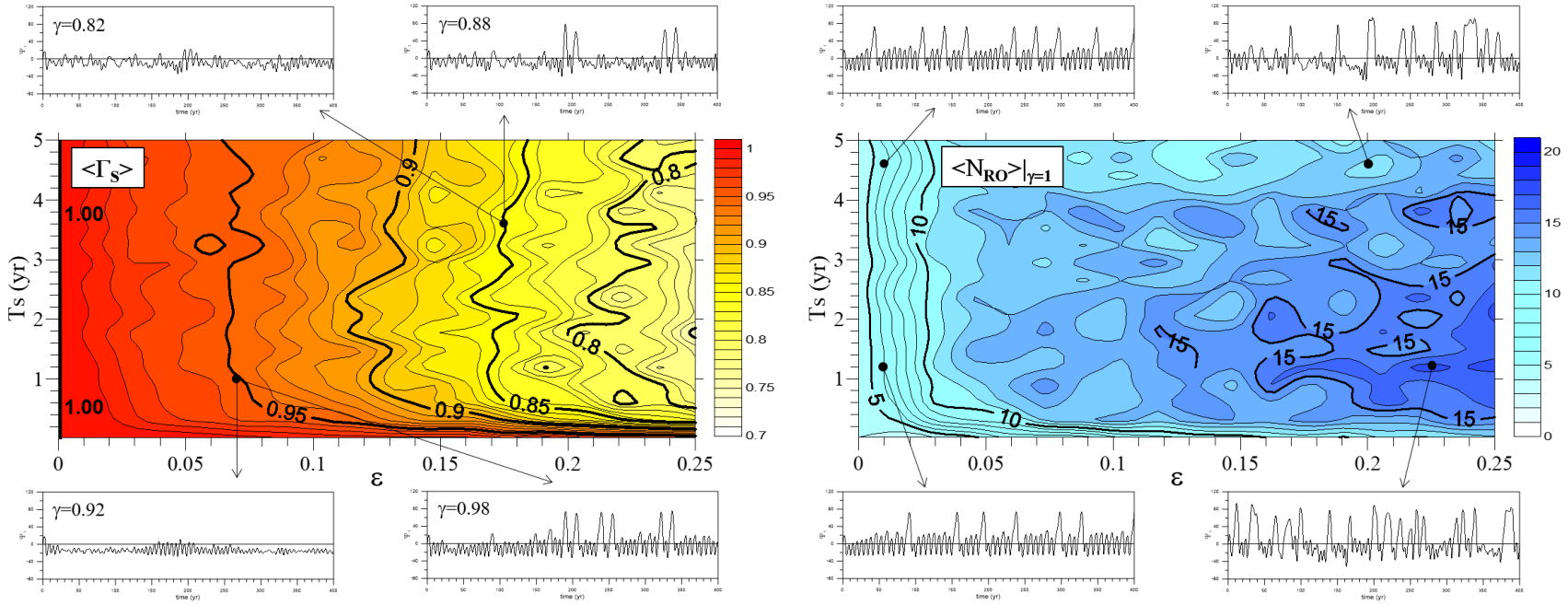

Applicazioni della teoria dei sistemi dinamici nonlineari: **modelli di bassa dimensionalità**

Pierini S., 2014: Ensemble simulations and pullback attractors of a periodically forced double-gyre system. *Journal of Physical Oceanography*, **44**, 3245-3254.

Pierini S., 2020: Statistical significance of small ensembles of simulations and detection of the internal climate variability: An excitable ocean system case study. *Journal of Statistical Physics*, **179**, 1475-1495

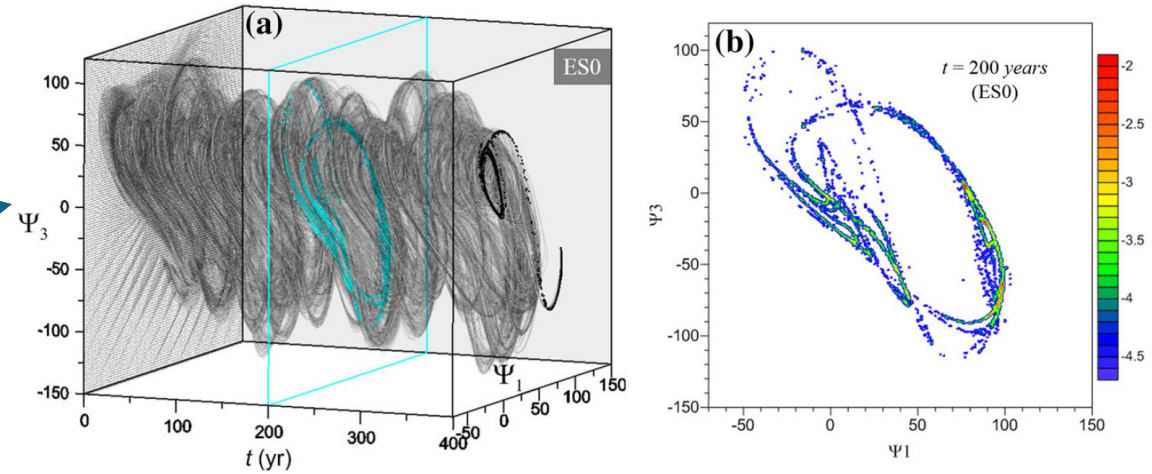

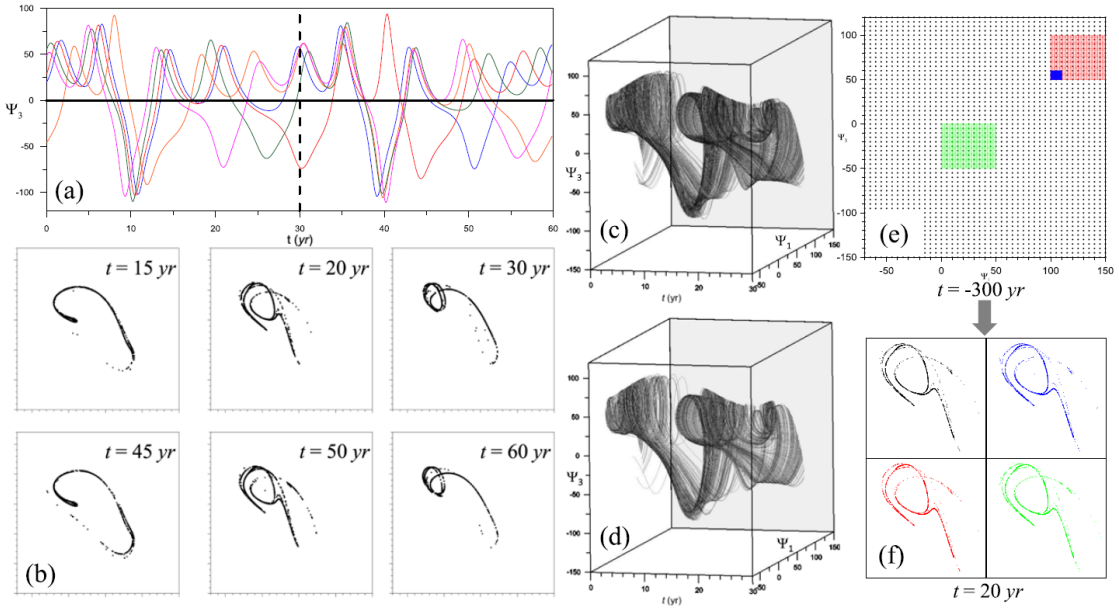

FIG. 3. (a) Projection of some of the aperiodic trajectories of Fig. 2 onto the $t - \Psi_3$ plane. (b) Intersection of 2475 trajectories of the PBA of Fig. 2 with the $\Psi_1 - \Psi_3$ plane at the times indicated in the panels [the axes correspond to those of panels (c),(d)]; the patterns separated by a 30-yr cycle are identical (periodic PBA). (c) One cycle of the PBA of Fig. 2 obtained with 1800 trajectories. (d) Superposition of 1800 successive 30-yr intervals of a single trajectory (with the parameters of Fig. 2), whose initial times are all shifted back to $t = 0$. (f) Intersection of the PBA of Fig. 2 with the $\Psi_1 - \Psi_3$ plane at $t = 20$ yr for the four sets of ICs shown in panel (e).

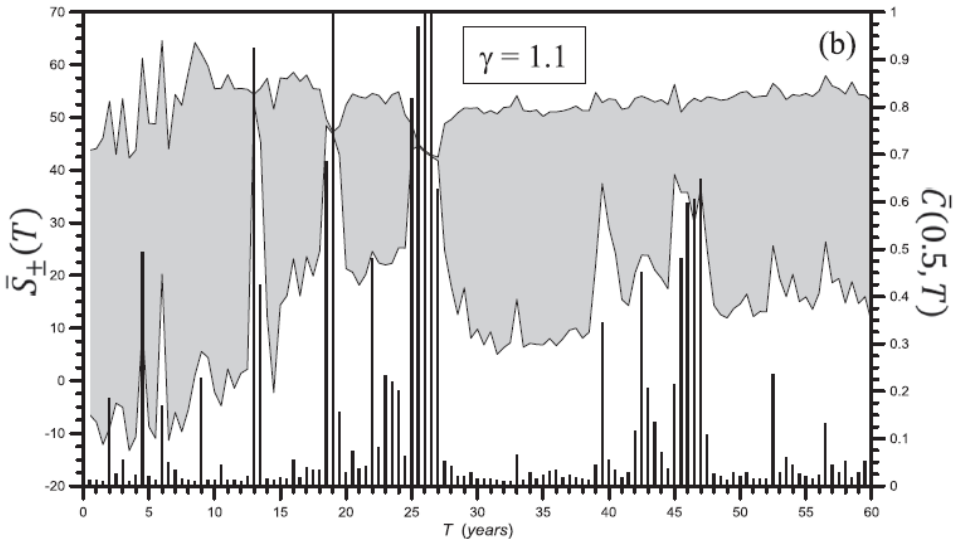

FIG. 4. (a) Diagram showing $\bar{S}_{\pm}(T)$ (lines, left scale) and $\bar{C}(0.5, T)$ (bars, right scale) defined in (4) and (5) for $\varepsilon = 0.2$ and $\gamma = 0.96$. (b) As in (a), but with $\gamma = 1.1$. The examples of cases (i)–(iv) indicated in (a) are explained in the text.

Applicazioni della teoria dei sistemi dinamici nonlineari: **modelli di bassa dimensionalità**

Pierini S., M. Ghil and M. D. Chekroun, 2016: Exploring the pullback attractors of a low-order quasigeostrophic ocean model: the deterministic case.
Journal of Climate, **29**, 4185-4202.

Pierini S., M. D. Chekroun and M. Ghil, 2018: The onset of chaos in nonautonomous dissipative dynamical systems: A low-order ocean–model case study.
Nonlinear Processes in Geophysics, **25**, 671-692

Pierini S. and M. Ghil, 2021**:** Tipping points induced by parameter drift in an excitable ocean model.
Scientific Reports, **11**, 11126.

September 10-12, 2024

Sorbonne Université,
Campus Pierre et Marie Curie of Sorbonne University,
4 place Jussieu, Paris.

With a series of lectures on Mathematics and Climate Dynamics in celebration of **Michael Ghil's 80th birthday.**

Applicazioni della teoria dei sistemi dinamici nonlineari: **modelli di bassa dimensionalità**

Pierini S., M. Ghil and M. D. Chekroun, 2016: Exploring the pullback attractors of a low-order quasigeostrophic ocean model: the deterministic case.
Journal of Climate, **29**, 4185-4202.

Pierini S., M. D. Chekroun and M. Ghil, 2018: The onset of chaos in nonautonomous dissipative dynamical systems: A low-order ocean–model case study.
Nonlinear Processes in Geophysics, **25**, 671-692

Pierini S. and M. Ghil, 2021**:** Tipping points induced by parameter drift in an excitable ocean model.
Scientific Reports, **11**, 11126.

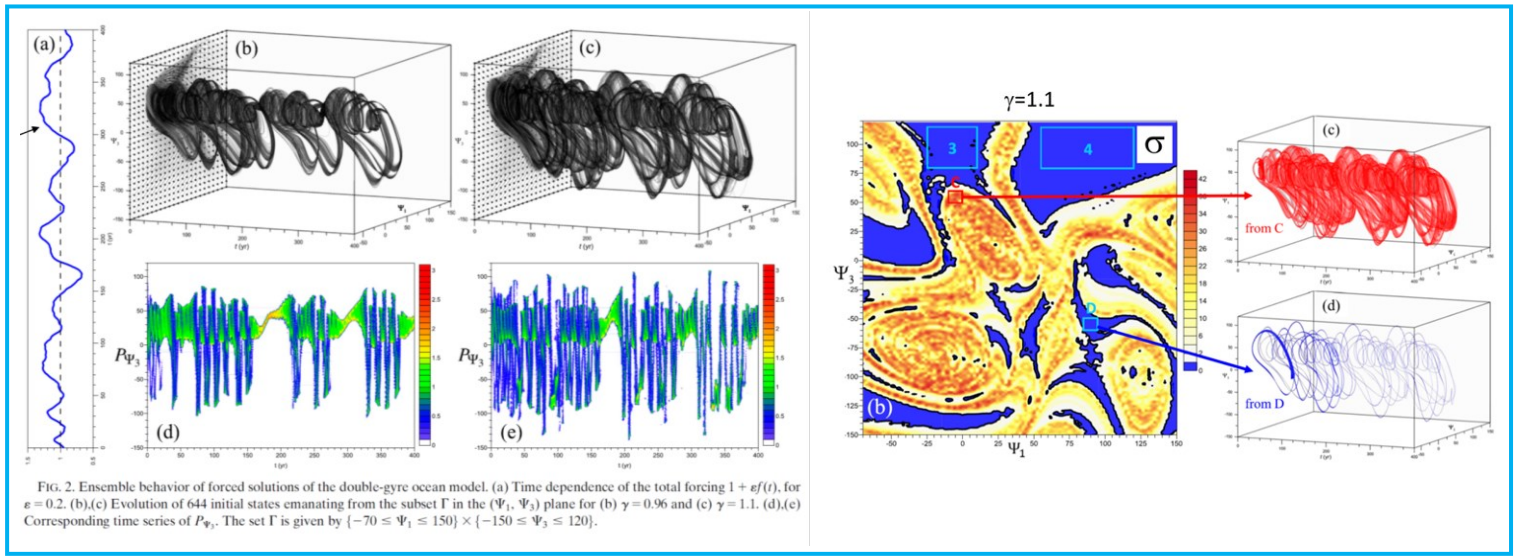

FIG. 2. Ensemble behavior of forced solutions of the double-gyre ocean model. (a) Time dependence of the total forcing $1 + \varepsilon f(t)$, for $\varepsilon = 0.2$. (b),(c) Evolution of 644 initial states emanating from the subset Γ in the (Ψ_1, Ψ_3) plane for (b) $\gamma = 0.96$ and (c) $\gamma = 1.1$. (d),(e) Corresponding time series of P_{Ψ_3}. The set Γ is given by $\{-70 \le \Psi_1 \le 150\} \times \{-150 \le \Psi_3 \le 120\}$.

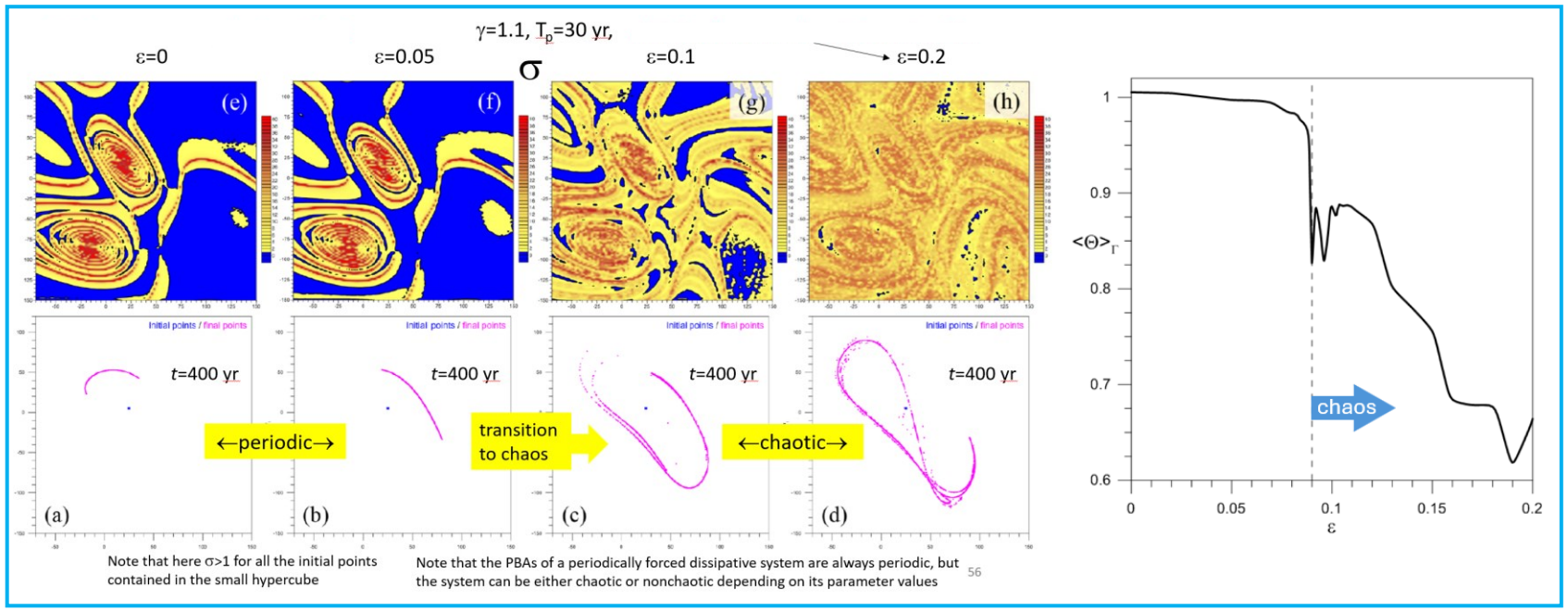

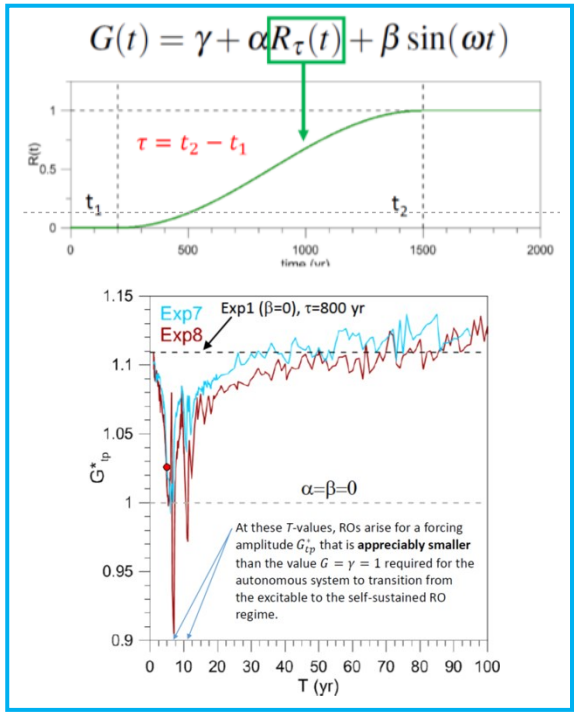

Applicazioni della teoria dei sistemi dinamici nonlineari: **modelli di bassa dimensionalità**

Pierini S., 2023**:** The deterministic excitation paradigm and the late Pleistocene glacial terminations.
Chaos, **33**, 033108.

deterministic excitation *vs*

stochastic resonance

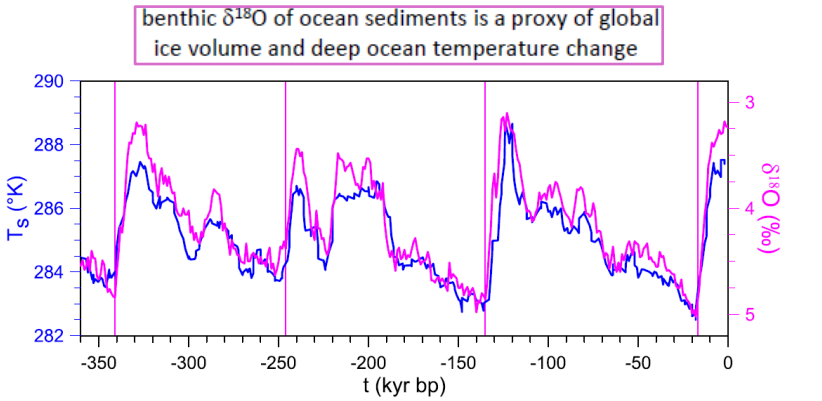

FIG. 1. Magenta line: LR04 benthic δ^{18}O stack constructed by the graphic correlation of 57 globally distributed benthic δ^{18}O records. Reproduced with permission from L. E. Lisiecki and M. E. Raymo, Paleoceanogr. **20**, PA1003 (2005). Copyright 2005 American Geophysical Union.[1] The magenta vertical lines mark the onset of the abrupt glacial–interglacial transitions. Blue line: global surface temperature estimate. Reproduced with permission from Hansen *et al.*, Phil. Trans. R. Soc. A **371**, 20120294 (2013). Copyright 2013 The Royal Society Publishing.[4]

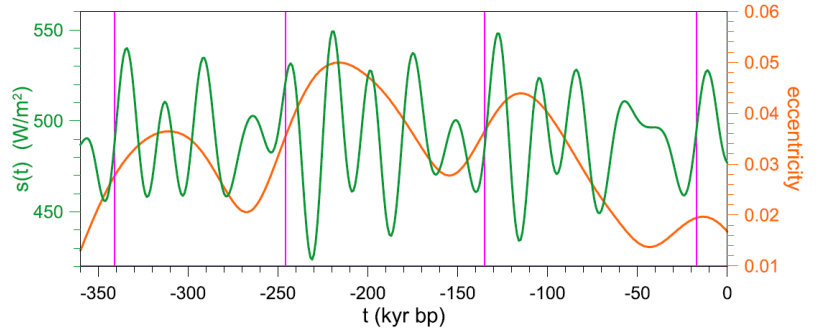

FIG. 3. Mean daily insolation at 65°N on summer solstice (green line) and Earth's eccentricity (orange line). Both lines are obtained from Laskar *et al.*[55,56] (data available at https://biocycle.atmos.colostate.edu/shiny/Milankovitch/). For the definition of the magenta vertical lines, see Fig. 1.

Thus, in the simulations, the prognostic variable will be the Earth's surface temperature $\zeta \equiv T_s$, and the following energy-balance model will be used:

$$C_s \frac{dT_s}{dt} = \frac{S(t)}{4}\left[1 - \alpha\left(T_s\right)\right] - \tilde{\epsilon}\sigma T_s^4, \qquad (2)$$

where S is the solar irradiance, α is the Earth's albedo, $\tilde{\epsilon} = 1 - \epsilon/2$ is the bulk emissivity that takes into account the greenhouse effect (where ϵ is the average emissivity of the atmosphere in the infrared), σ is the Stefan–Boltzmann constant, and C_s is the heat capacity of the Earth. The derivation of Eq. (2) and a bifurcation analysis of the corresponding autonomous system are reported in the Appendix.

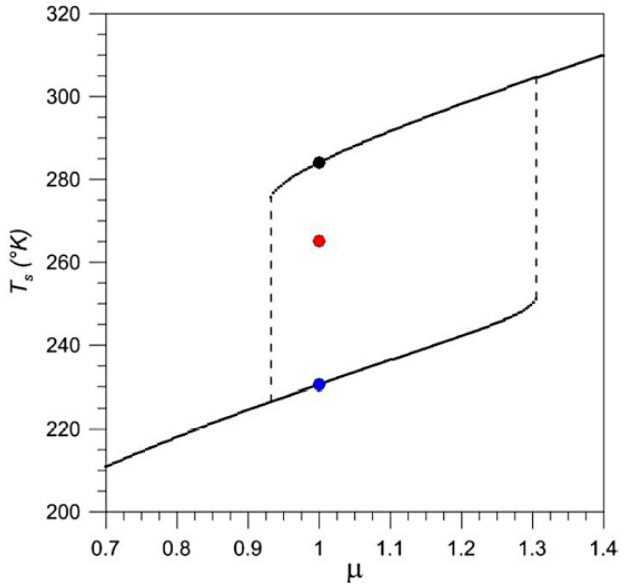

FIG. 9. Bifurcation diagram with T_s as a function of $\mu = S/S_0$ in the autonomous case. Small black dots: asymptotic state of 40 000 points in the (T_s, μ) plane initially and uniformly distributed in the intervals T_s : [200°K, 300°K]; μ : [0.7, 1.4]. Big black dot: stable fixed point ($\mu = 1$, $T_s = 284.1$°K) corresponding to the glacial state of the reference simulation. Big blue dot: stable fixed point ($\mu = 1$, $T_s = 230.6$°K) corresponding to a snowball Earth state. Big red dot: unstable fixed point ($\mu = 1$, $T_s = 265$°K).

Applicazioni della teoria dei sistemi dinamici nonlineari: **modelli di bassa dimensionalità**

Pierini S., 2023**:** The deterministic excitation paradigm and the late Pleistocene glacial terminations. *Chaos,* **33**, 033108.

… The timing of the glacial terminations obtained in a reference simulation is found to be in **good agreement with proxy records**. A sensitivity analysis insures the **robustness** of the timing. …

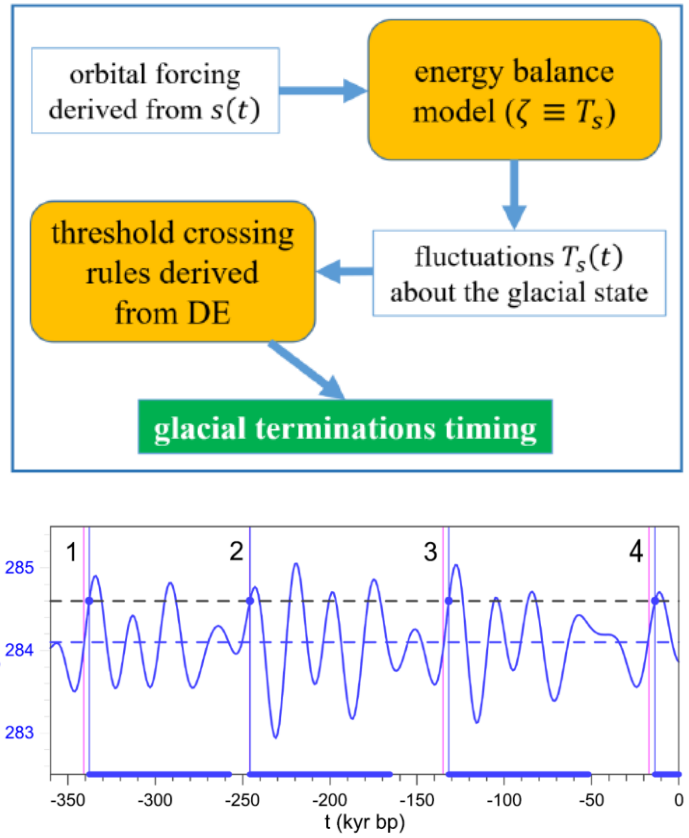

FIG. 4. Timing of the simulated glacial terminations vs timing derived from proxy data. Continuous blue line: $T_s(t)$. Dashed blue line: $T_{s(glacial)}$. Dashed black line: $\overline{T}_s$. The thick blue segments have a temporal length τ_{ro} and begin at $\hat{t}_{i(mod)}$, i.e., when a glacial termination is identified by the model; the same times are also indicated by a dot and a vertical blue line. The vertical magenta lines indicate the times $\hat{t}_{i(proxy)}$ at which the glacial terminations have occurred according to proxy data (see Fig. 1).

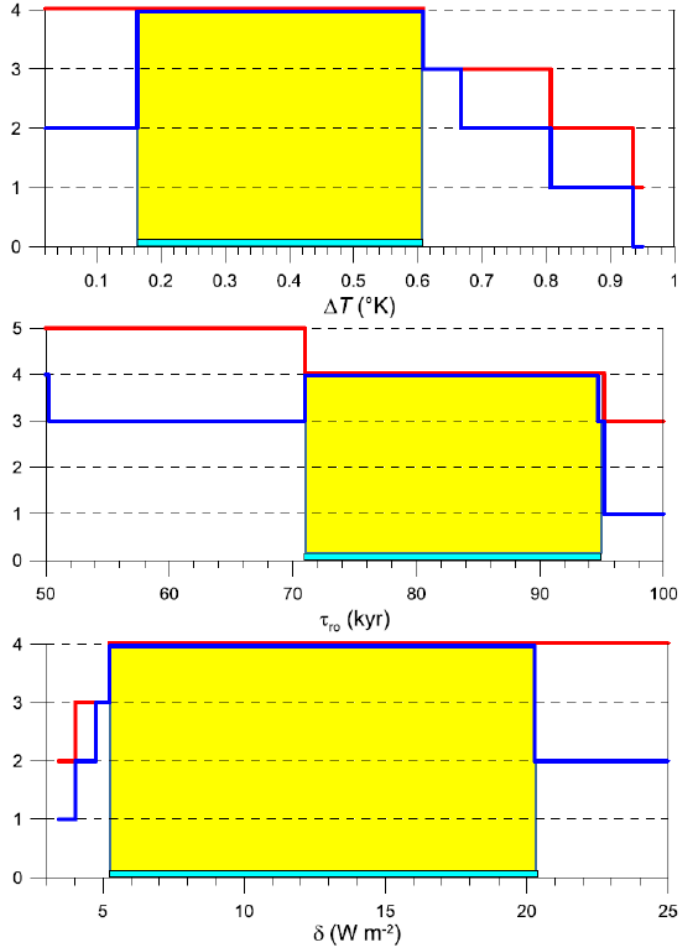

Applicazioni della teoria dei sistemi dinamici nonlineari: **modelli di bassa dimensionalità**

Pierini S., 2023**:** The deterministic excitation paradigm and the late Pleistocene glacial terminations.
Chaos, **33**, 033108.

МИЛАНКОВИЋЕВА ТЕОРИЈА КЛИМАТСКИХ ПРОМЕНА – СТО ГОДИНА ПОСЛЕ

MILANKOVIC'S THEORY OF CLIMATE CHANGES – HUNDRED YEARS AFTERWARDS

1924.2024.2124.

4-5 November 2024

Keynote Talk:

The deterministic excitation paradigm and the late Pleistocene glacial terminations

Stefano Pierini

Department of Science and Technology
Parthenope University of Naples (Italy)

website: http://dist.altervista.org/PIERINI/
stefano.pierini@uniparthenope.it
stefano.pierini@collaboratore.uniparthenope.it

Elegantly Modeling Earth's Abrupt Glacial Transitions

MARCH 7, 2023
CHAOS | NEWS

SHARE:

Simple and intuitive model illustrates how climate cycles are influenced by our planet's orbit.

From the Journal: Chaos

WASHINGTON, March 7, 2023 – Proxy data – indirect records of the Earth's climate found in unlikely places like coral, pollen, trees, and sediments – show interesting oscillations approximately every 100,000 years starting about 1 million years ago. Strong changes in global ice volume, sea level, carbon dioxide concentration, and surface temperature indicate cycles of a long, slow transition to a glacial period and an abrupt switch to a warm and short interglacial period.

The Laurentide Ice Sheet covered most of northern North America during glacial periods. Credit: NOAA Great Lakes Environmental Research Laboratory, jan.ucc.nau.edu/~rcb7/nam.html. Permission to re-use. https://www.flickr.com/photos/noaa_glerl/8740576431

Milutin Milankovitch hypothesized that the timing of these cycles was controlled by the orbital parameters of the Earth, including the shape of its path around the sun and the tilt of the planet. A slightly closer orbit or more tilted planet could create a small increase in solar radiation and a feedback loop that leads to massive changes in climate. This idea suggests that there may be some predictability in the climate, a notoriously complex system.

In Chaos, by AIP Publishing, Stefano Pierini of Parthenope University of Naples proposed a new paradigm to simplify the verification of the Milankovitch hypothesis.

"The main motivation behind this study was the wish to characterize and illustrate the Milankovitch hypothesis in a simple, elegant, and intuitive way," Pierini said.

Many models suggest that Milankovitch is correct; however, such methods are often detailed and study specific. They incorporate climate feedback loops – for example, increased ice cover reflects more radiation back into space, leading to further cooling and more ice cover – as threshold crossing rules. This means that an abrupt jump in climate only occurs once a parameter reaches a given tipping point.

Pierini's "deterministic excitation paradigm" combines the physics concepts of relaxation oscillation and excitability to link Earth's orbital parameters and the glacial cycles in a more generic way. The relaxation oscillation component describes how the climate slowly returns to its original glacier state after it is disturbed. At that point, the excitability piece of the model captures the external orbital changes and triggers the next glacial cycle.

By using his own threshold crossing rules and adopting a classical energy-balance model, Pierini obtained correct and robust timing of the most recent glacial cycles.

"The application of the deterministic excitation paradigm in the present basic formulation can explain the timing of the last four glacial terminations," he said. "Extending the same analysis to the whole Pleistocene will be the subject of a future investigation."

Pierini believes similar methods could be used in other fields of nonlinear science and in connection with other climate phenomena.

###

Article Title	Authors	Author Affiliations
The deterministic excitation paradigm and the late Pleistocene glacial terminations	Stefano Pierini	Parthenope University of Naples

Rotture di simmetria,
Stabilità di flussi

Modellistica di
onde nonlineari

Aspetti lineari della circolazione
indotta dal vento (Rossby waves)

Applicazioni della teoria
dei sistemi dinamici nonlineari:
modelli alle equazioni primitive

Applicazioni della teoria
dei sistemi dinamici nonlineari:
modelli di bassa dimensionalità

Predicibilità dei processi di
transizione dell'Estensione
del Kuroshio

Modellistica di circolazione
del Mar Mediterraneo

Modellistica Antartica

Simulazioni di laboratorio di
flussi oceanografici

Predicibilità dei processi di transizione dell'Estensione del Kuroshio

Zhang X., M. Mu, Q. Wang and S. Pierini, 2017: Optimal precursors triggering the Kuroshio Extension state transition obtained by the Conditional Nonlinear Optimal Perturbation approach.
Advances in Atmospheric Sciences, **34**, 685–699.

Wang Q., Y. Tang, S. Pierini and M. Mu, 2017: Effects of singular vector-type initial errors on the short-range prediction of Kuroshio Extension transition processes.
Journal of Climate, **30**, 5961-5983.

Wang Q., S. Pierini and Y. Tang, 2019: Parameter sensitivity analysis of the short-range prediction of Kuroshio Extension transition processes using an optimization approach.
Theoretical and Applied Climatology, **138**, 1481-1492.

Wang Q., M. Mu and S. Pierini, 2020: The fastest growing initial error in prediction of the Kuroshio Extension state transition processes and its growth.
Climate Dynamics, **54**, 1953-1971.

Wang Q. and S. Pierini, 2020: On the role of the Kuroshio Extension bimodality in modulating the surface eddy kinetic energy seasonal variability.
Geophysical Research Letters, **47**, e2019GL086308.

Wang Q. and S. Pierini, 2023: Causal forcing analysis on the low-frequency variations of eddy kinetic energy in the Kuroshio Extension region.
Journal of Climate, **36**, 1-32.

Geng Y., Q. Wang, H-L. Ren, B. Dan, S. Pierini and H. Zhang, 2024: Observing array designed for improving the short-term prediction of Kuroshio Extension state transition processes.
Earth and Space Science, 11, e2024EA003881.

- **Conditional Nonlinear Optimal Perturbation** (CNOP)
- **Singular Vector** (SV)
- **Optimization Parameter Sensitivity Analysis** (OPSA)
- **Convergent Cross Mapping** (CCM)

Given the essential implications of Kuroshio Extension (KE) bimodality on oceanic dynamical environment and climate, the present study investigates the targeted observation schemes, based on the conditional nonlinear optimal perturbation (CNOP) method and a reduced-gravity shallow-water model, to improve the forecast skills of transition processes of KE bimodal states.

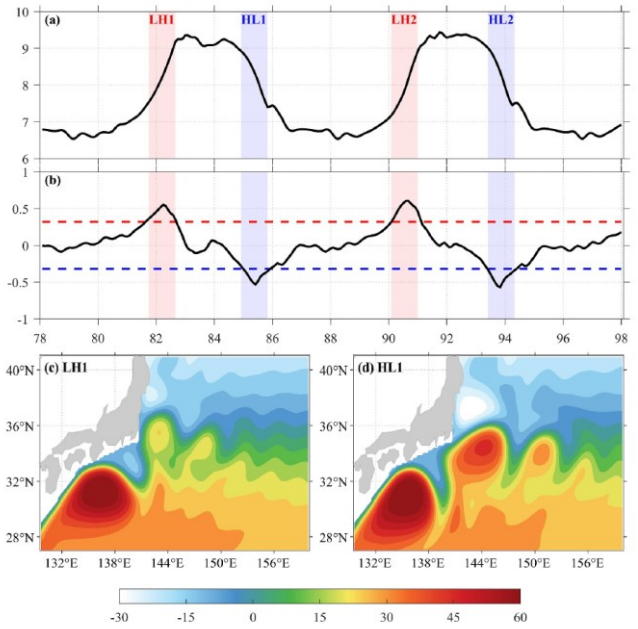

Figure 2. (a) Time series of the enlargement of total potential energy (TPE) (units: 10^{13} m^5 s^{-2}) integrated over the region *S* during the model years 78–98. (b) Same as panel (a), but for the tendency of TPE (black line; units: 10^6 m^5 s^{-3}). The red (blue) dashed line denotes the 1.2 times positive (negative) standard deviation of TPE tendency. The pink (purple) bands in panels (a) and (b) represent the cases of LH1 and LH2 (HL1 and HL2). Spatial distributions of sea surface height (units: cm) at the start time of panels (c) LH1 and (d) HL1 cases.

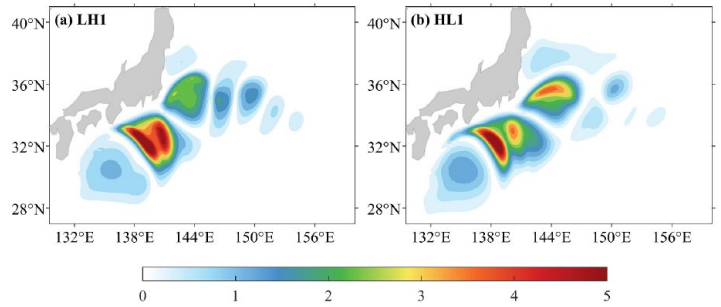

Figure 3. Spatial distributions of the conditional nonlinear optimal perturbation for panels (a) LH1 and (b) HL1 cases.

Predicibilità dei processi di transizione dell'Estensione del Kuroshio

Kramer W., H. A. Dijkstra, S. Pierini and P. J. Van Leeuwen, 2012: Measuring the impact of observations on the predictability of the Kuroshio Extension in a shallow-water model.
Journal of Physical Oceanography, **42**, 3-17.

Sequential importance sampling is used to assess the impact of observations on an ensemble prediction for the decadal path transitions of the Kuroshio Extension. This **particle-filtering approach** gives access to the probability density of the state vector, which allows the predictive power —an entropy-based measure— of the ensemble prediction to be determined.

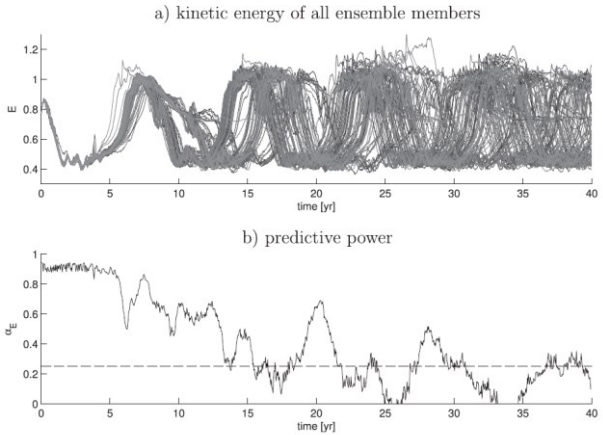

FIG. 2. Ensemble forecast for the KE with a stochastic forced shallow-water model starting from a single initial state. (a) Evolution of the kinetic energy E of the KE for the 96 ensemble realizations and (b) PP α_E for the kinetic energy signal of the forecast.

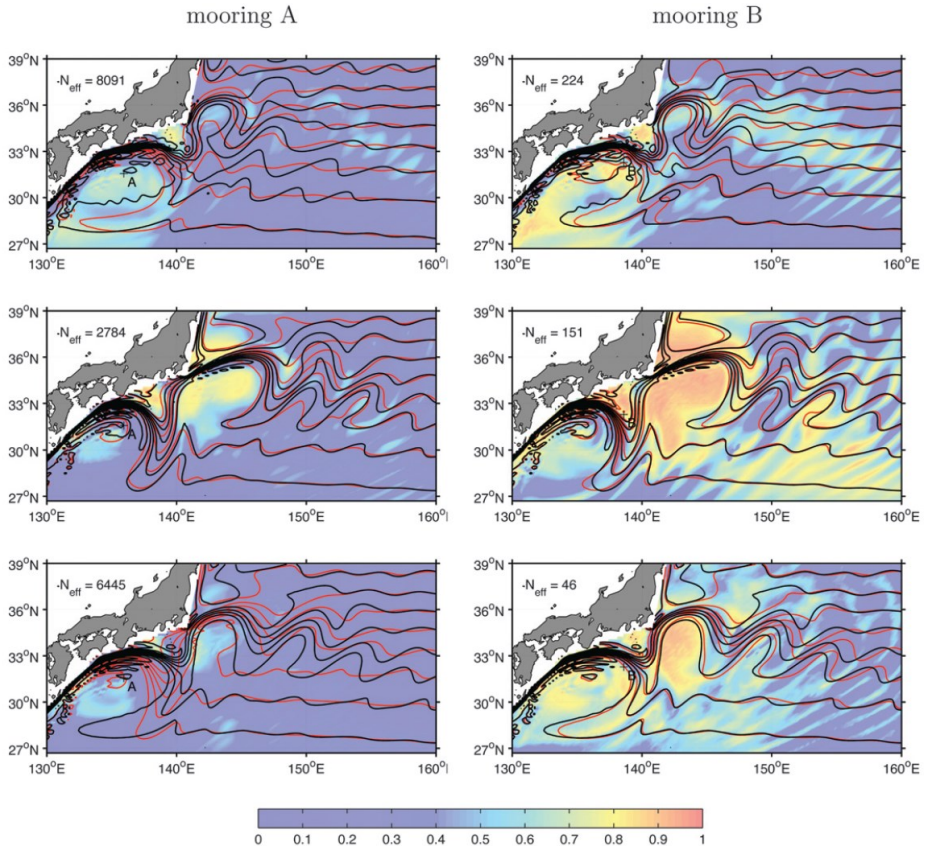

FIG. 9. One-year increase in the PP $\alpha_Q(\mathbf{x}, t)$. Velocity observations from mooring (left)–(right) A, B, C, and D are assimilated during one year, starting at years (top)–(bottom) 4, 8, and 12. Red contour lines depict the PV mean from the analysis. Black lines give the PV field from the synthetic truth. For each analysis, the effective number of particles is given in the top-left corner.

Rotture di simmetria,
Stabilità di flussi

Modellistica di
onde nonlineari

Aspetti lineari della circolazione
indotta dal vento (Rossby waves)

Applicazioni della teoria
dei sistemi dinamici nonlineari:
modelli alle equazioni primitive

Applicazioni della teoria
dei sistemi dinamici nonlineari:
modelli di bassa dimensionalità

Predicibilità dei processi di
transizione dell'Estensione
del Kuroshio

Modellistica di circolazione
del Mar Mediterraneo

Modellistica Antartica

Simulazioni di laboratorio di
flussi oceanografici

Modellistica di circolazione del Mar Mediterraneo

Pierini, S., Simioli, A., 1998: A wind-driven circulation model of the Tyrrhenian Sea area.
Journal of Marine Systems , **18**, 161-178.

MTP I
MERMAIDS-II

Prof.ssa Nadia Pinardi

$$\begin{cases} \boldsymbol{u}_t + (\boldsymbol{u}\cdot\nabla)\boldsymbol{u} + f\boldsymbol{k}\times\boldsymbol{u} = -g\nabla\eta + \dfrac{(\tau_w - \tau_b)}{\rho_o H} + A_H\nabla^2\boldsymbol{u} \\ \eta_t + \nabla(H\boldsymbol{u}) = O \end{cases}$$

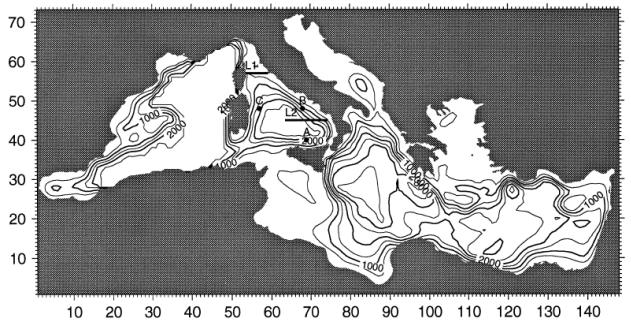

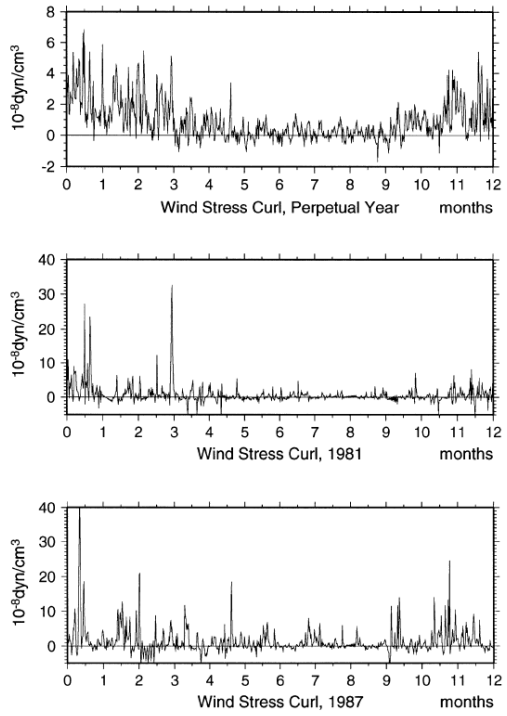

Fig. 2. Wind stress curl in a point in the middle of the Tyrrhenian Sea for the perpetual year and for the test years 1981 and 1987.

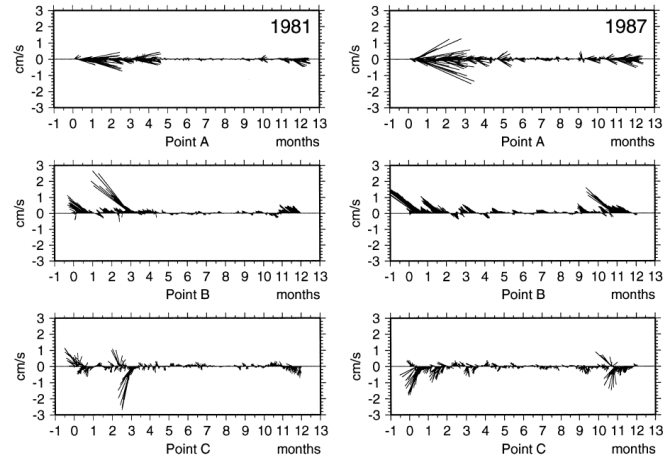

Fig. 9. Stick-diagrams of the instantaneous 1981 and 1987 currents in points A, B and C of Fig. 1.

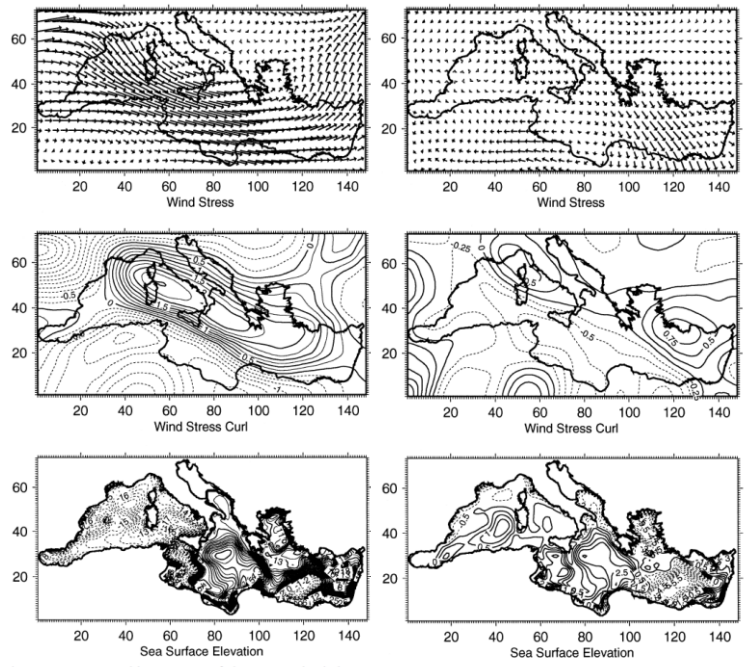

Fig. 3. January monthly averages of the perpetual wind stres wind stress curl and induced sea surface elevation.

Fig. 4. June monthly averages of the perpetual wind stress, wind stress curl and induced sea surface elevation.

Modellistica di circolazione del Mar Mediterraneo

Pierini, S., 1996: Topographic Rossby modes in the Strait of Sicily.
Journal of Geophysical Research, **101**, 6429-6440.

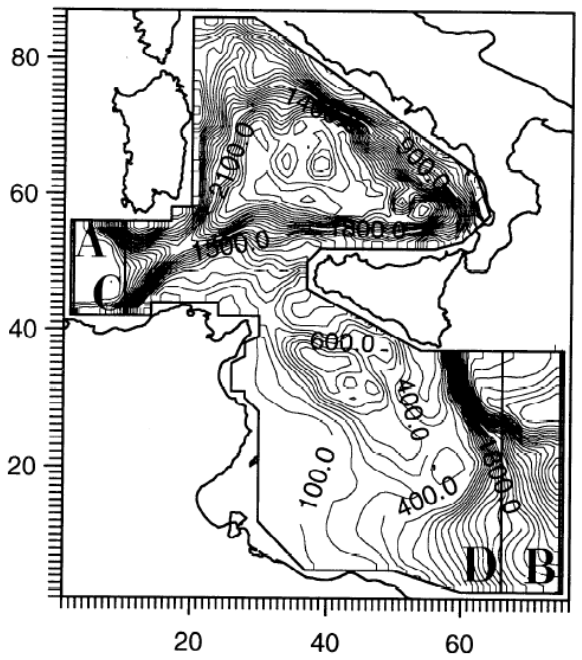

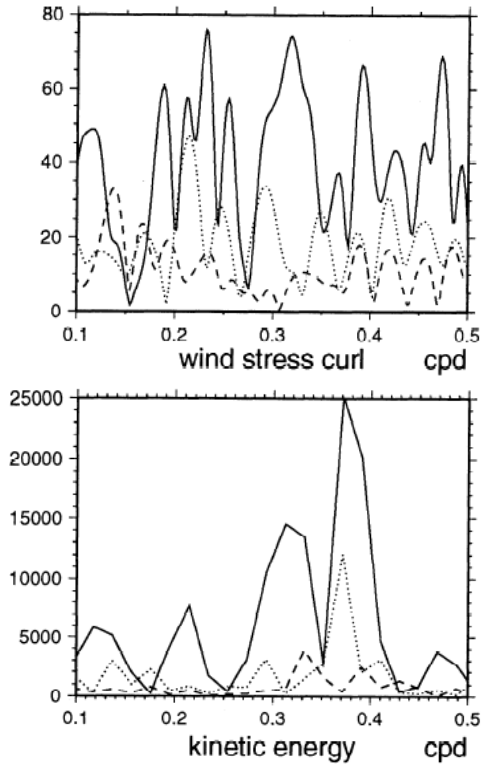

Figure 11. Spectra of the 1980 National Meteorological Center (top) wind stress curl in the Strait of Sicily and (bottom) of the kinetic energy of the flow at point P3 for the periods January-February (solid lines), June-July (dashed lines), and October-November (dotted lines).

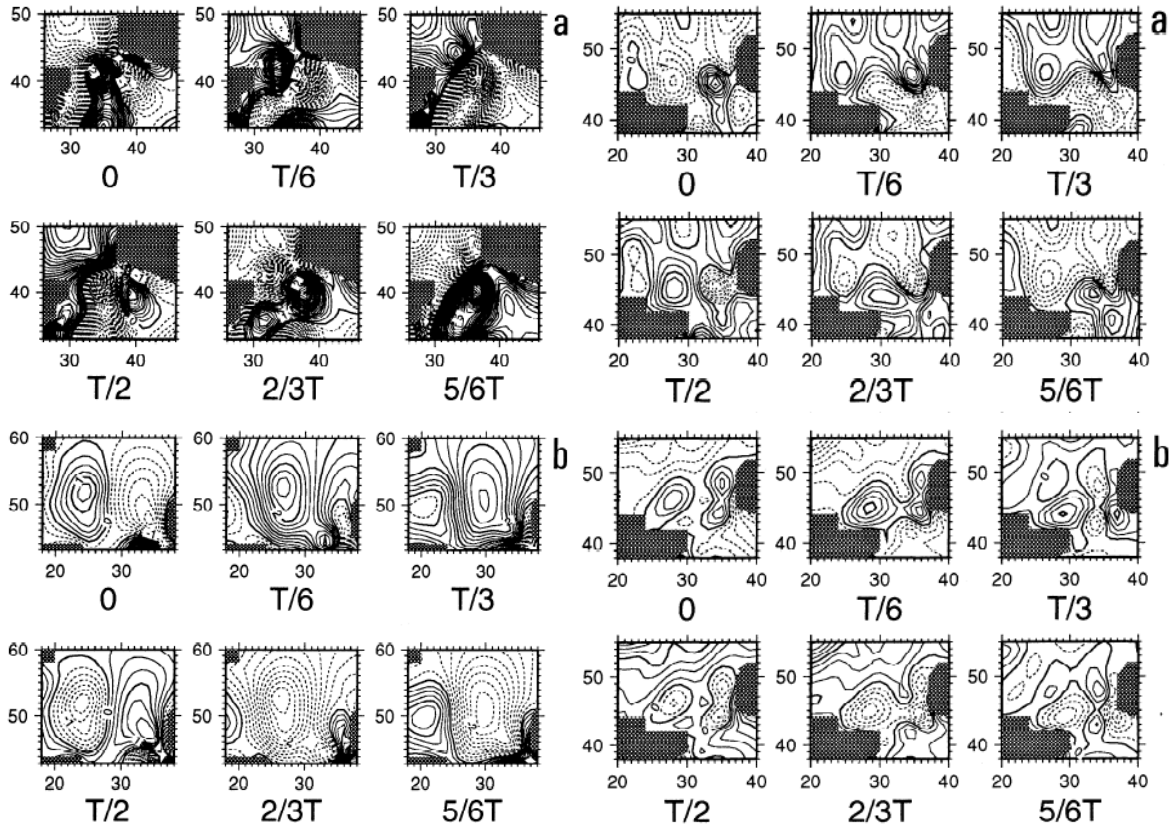

Modellistica di circolazione del Mar Mediterraneo

Pierini, S., Rubino, A., 2001: Modeling the oceanic circulation in the area of the Strait of Sicily: the remotely-forced dynamics.
Journal of Physical Oceanography, **31**, 1397-1412.

Prof. Angelo Rubino

MTP II-MATER

Universität Hamburg

Rubino (1994)

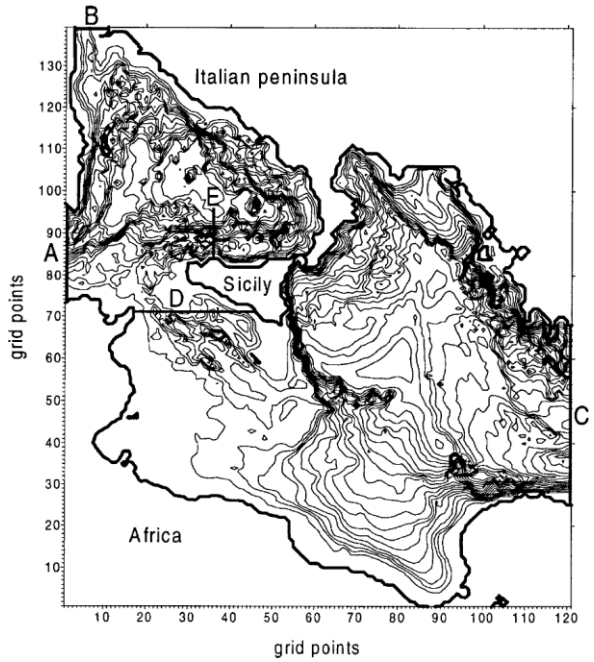

$$\frac{\partial \mathbf{U}_1}{\partial t} + \nabla \cdot (\mathbf{u}_1 \times \mathbf{U}_1) + \mathbf{F} \cdot \mathbf{U}_1 = -gh_1 \nabla \eta_1 - \frac{\kappa_1}{\rho_1}(\mathbf{u}_1 - \mathbf{u}_2)|\mathbf{u}_1 - \mathbf{u}_2| + A_h h_1 \nabla_h^2 \mathbf{u}_1, \quad (1)$$

$$\frac{\partial h_1}{\partial t} + \nabla \cdot \mathbf{U}_1 = 0, \quad (2)$$

for the intermediate layer they read:

$$\frac{\partial \mathbf{U}_2}{\partial t} + \nabla \cdot (\mathbf{u}_2 \times \mathbf{U}_2) + \mathbf{F} \cdot \mathbf{U}_2 = -g\frac{\rho_1}{\rho_2}h_2 \nabla \eta_1 - g\frac{\rho_2 - \rho_1}{\rho_2}h_2 \nabla \eta_2 + \frac{\kappa_1}{\rho_2}(\mathbf{u}_1 - \mathbf{u}_2)|\mathbf{u}_1 - \mathbf{u}_2| - \frac{\kappa_2}{\rho_2}(\mathbf{u}_2 - \mathbf{u}_3)|\mathbf{u}_2 - \mathbf{u}_3| + A_h h_2 \nabla_h^2 \mathbf{u}_2, \quad (3)$$

$$\frac{\partial h_2}{\partial t} + \nabla \cdot \mathbf{U}_2 = 0, \quad (4)$$

and for the bottom layer they read:

$$\frac{\partial \mathbf{U}_3}{\partial t} + \nabla \cdot (\mathbf{u}_3 \times \mathbf{U}_3) + \mathbf{F} \cdot \mathbf{U}_3 = -g\frac{\rho_1}{\rho_3}h_3 \nabla \eta_1 - g\frac{\rho_2 - \rho_1}{\rho_3}h_3 \nabla \eta_2 - g\frac{\rho_3 - \rho_2}{\rho_3}h_3 \nabla \eta_3 + \frac{\kappa_2}{\rho_3}(\mathbf{u}_2 - \mathbf{u}_3)|\mathbf{u}_2 - \mathbf{u}_3| - \frac{\kappa_3}{\rho_3}\mathbf{u}_3|\mathbf{u}_3| + A_h h_3 \nabla_h^2 \mathbf{u}_3, \quad (5)$$

$$\frac{\partial h_3}{\partial t} + \nabla \cdot \mathbf{U}_3 = 0, \quad (6)$$

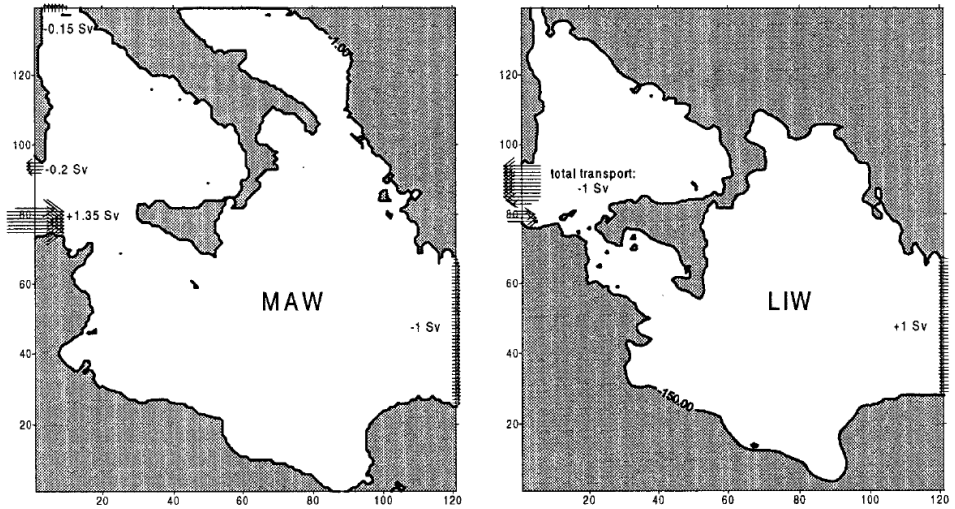

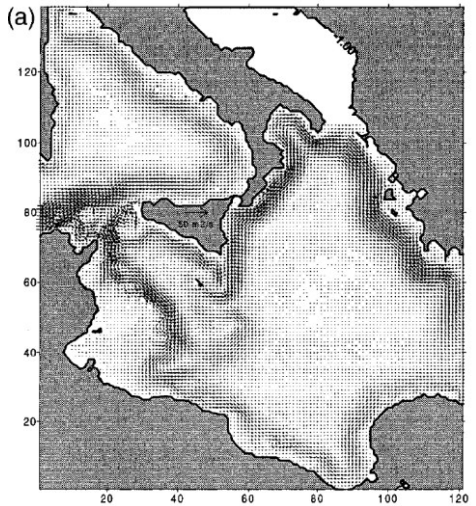

$$R_{maw} = \frac{\text{MAW transport entering the Tyrrhenian}}{\text{MAW transport crossing the strait}}$$

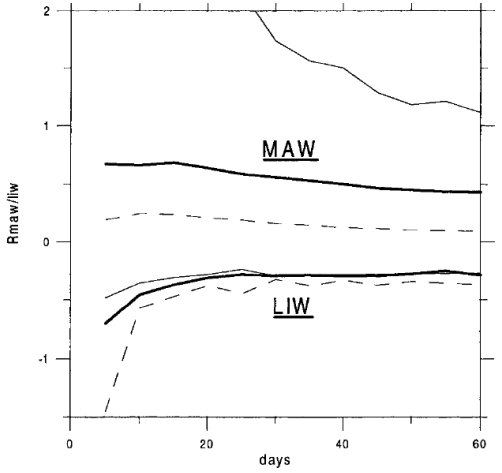

Modellistica di circolazione del Mar Mediterraneo

Rubino A., S. Pierini, S. Rubinetti, M. Gnesotto and D. Zanchettin, 2023: The skeleton of the Mediterranean Sea. *Journal of Marine Science and Engineering*, **11**, 2098.

Gnesotto M., S. Pierini, D. Zanchettin, S. Rubinetti and A. Rubino, 2024: Influence of intrinsic oceanic variability induced by a steady flow on the Mediterranean sea level variability. *Journal of Marine Science and Engineering*, **12**, 1356.

P.R.I.N. **INVMED**
(partirà nel Febbraio 2025)

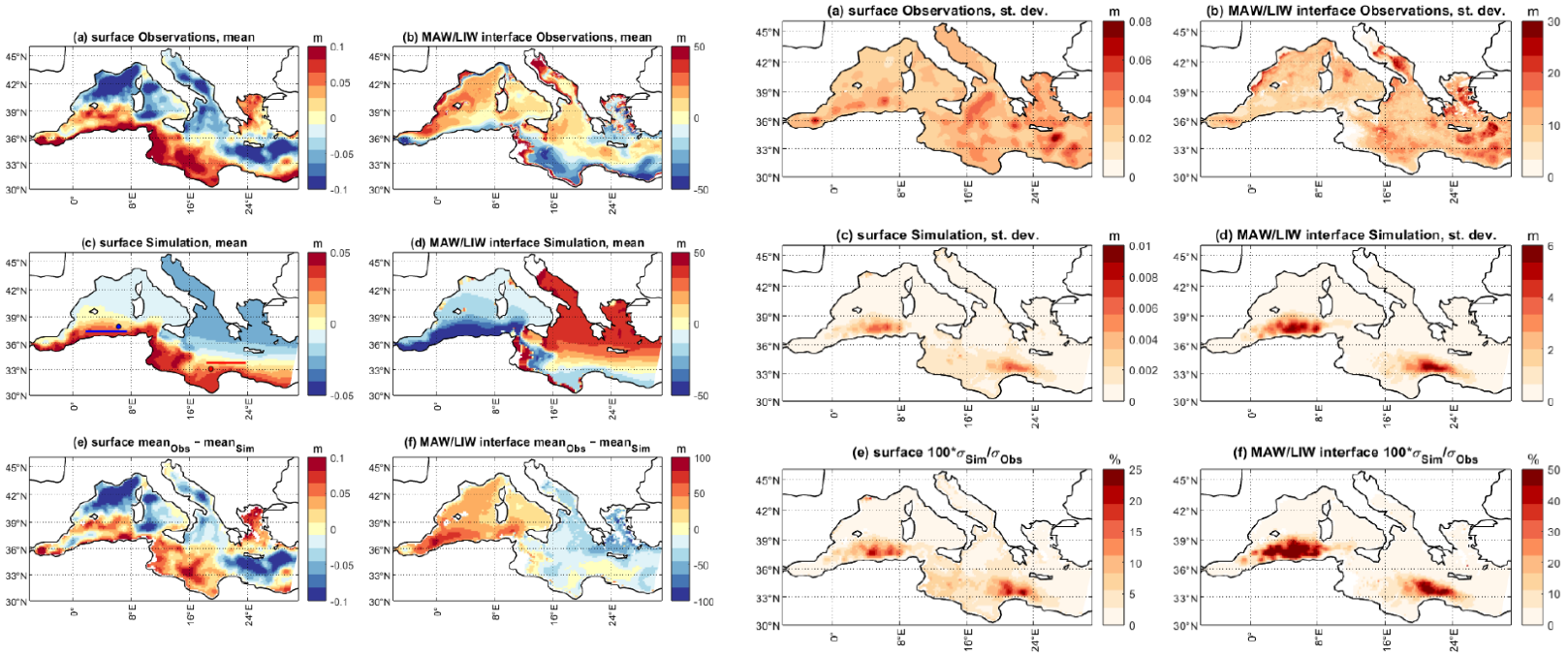

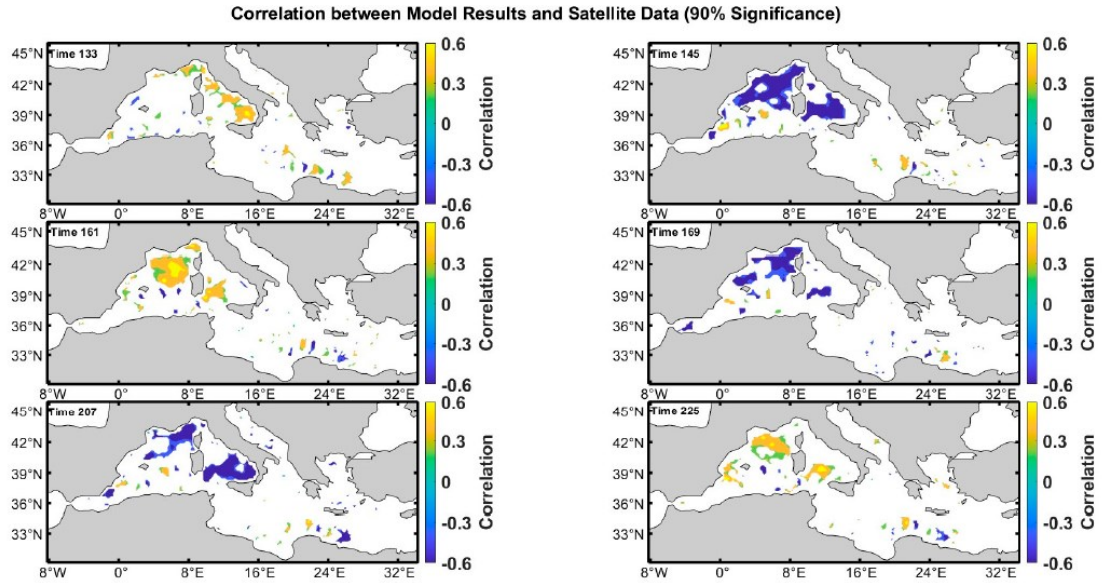

Modellistica di circolazione del Mar Mediterraneo

Gravili, D., Napolitano, E., Pierini, S., 2001: Barotropic aspects of the dynamics of the Gulf of Naples (Tyrrhenian Sea).
Continental Shelf Research, **21**, 455-471.

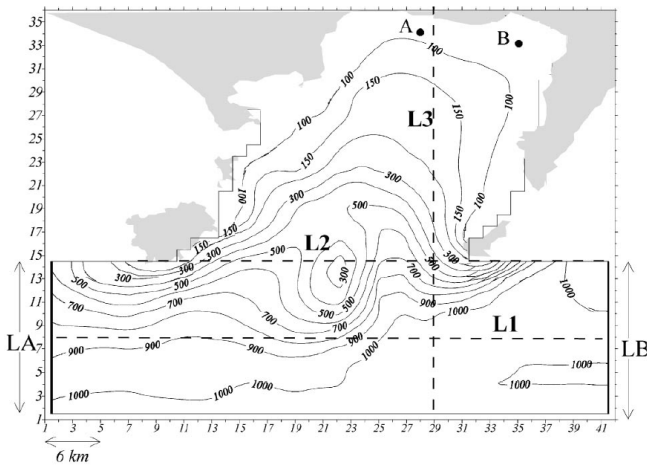

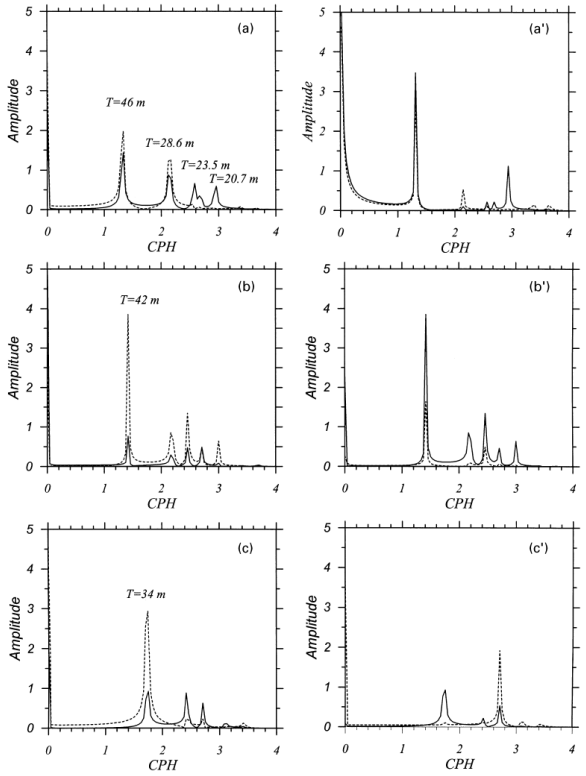

Fig. 3. Spectra of the sea-surface elevation computed after the relaxation of the wind setup taken at points A (solid line) and B (dashed line), for south-easterly (left column) and south-westerly (right column) winds. (a,a′) refer to the complete domain, (b,b′) to the domain delimited by line L_1 of Fig. 1 and (c, c′) to the domain delimited by line L_2 of Fig. 1.

Table 1
The eigenperiods of the seiches observed by Caloi and Marcelli (1949) (left column) and the eigenperiods identified by the analysis of Section 3 (right column)

Experimental data	Numerical simulations
$T = 58–59$ min	—
$T = 48$ min	$T_1 = 46$ min
—	$T_2 = 28$ min
$T = 22$ min	$T_3 = 23$ min
$T = 17.8$ min	$T_4 = 20$ min

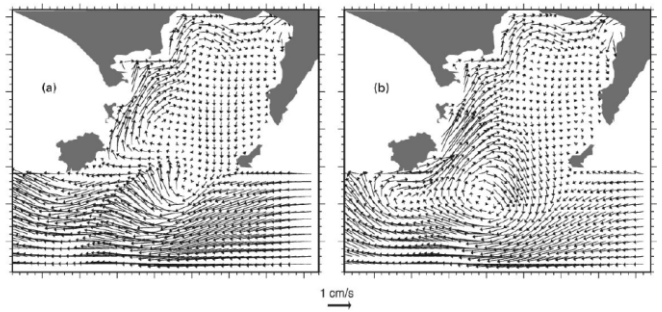

Fig. 9. Depth-averaged currents corresponding to the forcing shown in Fig. 7b at times indicated by A, B, C, D.

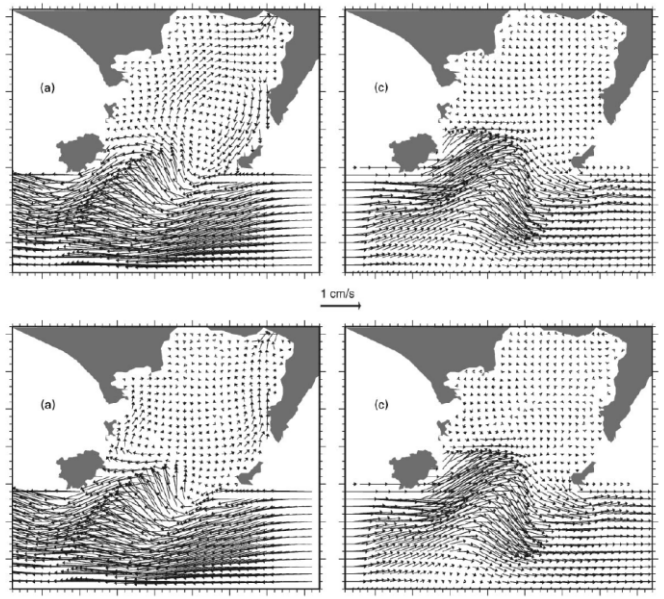

Fig. 10. Upper panels: depth-averaged currents corresponding to the forcing shown in Fig. 7b (with the wind flowing along y) at times indicated by A and C. Lower panels: depth-averaged currents corresponding to the forcing shown in Fig. 7a (with the wind flowing along y) at times indicated by A and C.

Modellistica di circolazione del Mar Mediterraneo

De Ruggiero P., E. Napolitano, R. Iacono and S. Pierini, 2016: A high-resolution modelling study of the circulation along the Campania coastal system, with a special focus on the Gulf of Naples.
Continental Shelf Research, **122**, 85-101.

* **C**ampania **R**egional **O**cean **M**odel

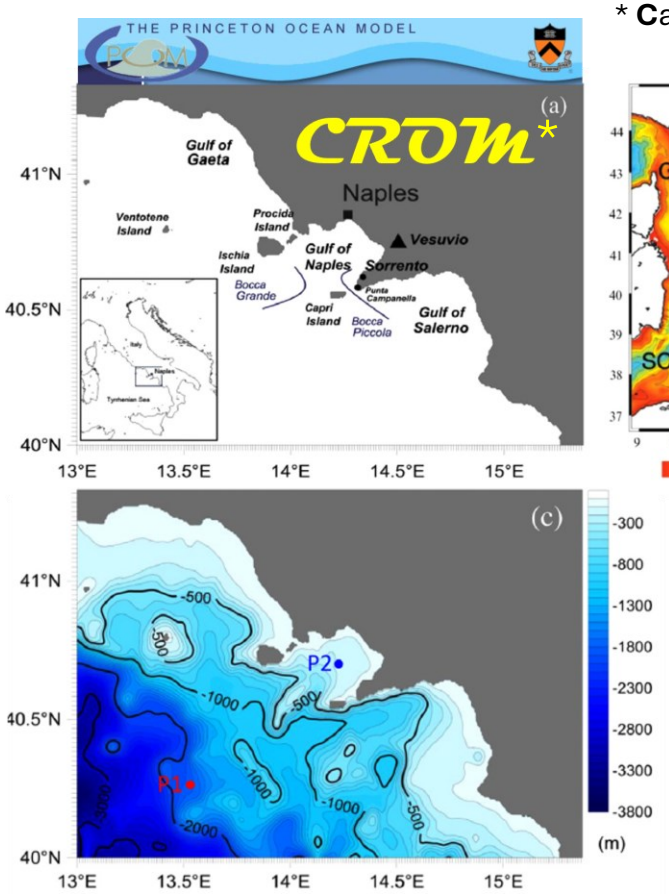

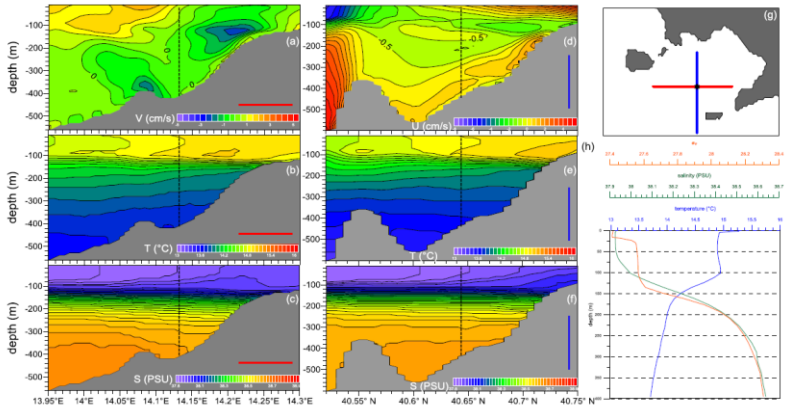

Fig. 6. First column: transects averaged over the winter period of v (a), T (b) and S (c) along the red transect shown in map (g). Second column: transects averaged over the winter period of u (d), T (e) and S (f) along the blue transect shown in map (g). (h): vertical profiles of σ_t, S and T at the intersection of the two transects.

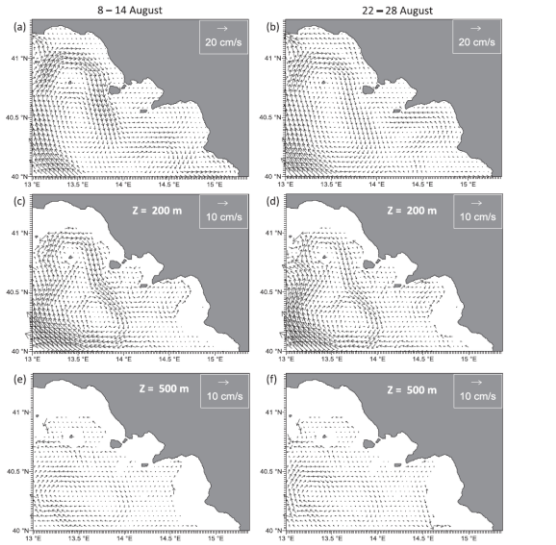

Fig. 7. First column: maps of current velocities simulated by CROM averaged over the week 8–14 August 2009 at the surface (a) and at z=200 m (c) and z=500 m (e). Right column: same quantities averaged over the week 22–28 August 2009.

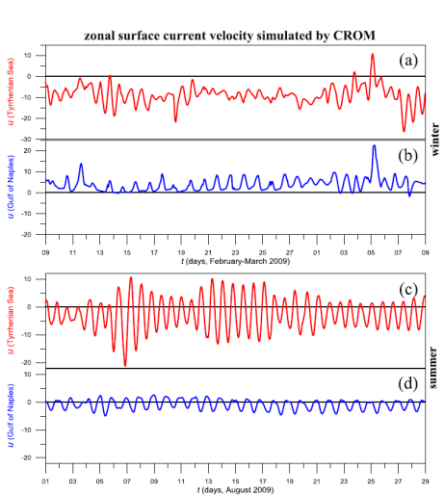

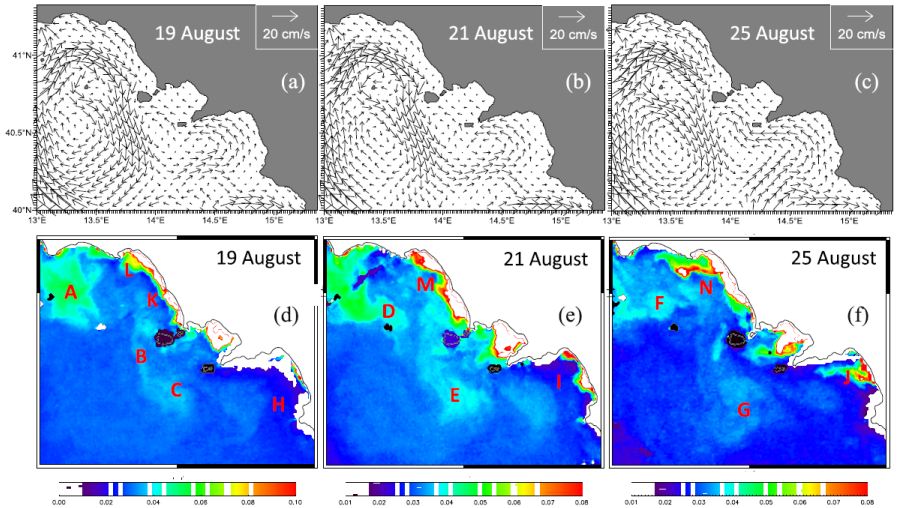

Fig. 15. Upper panels: daily averages of the surface currents simulated by CROM for 19 (a), 21 (b) and 25 (c) August 2009. Lower panels: maps of the diffuse attenuation coefficient (K490) in the same days (for the explanation of the letters A-N see the text).

Modellistica di circolazione del Mar Mediterraneo

CROM

Montuori A., P. de Ruggiero, M. Migliaccio, S. Pierini and G. Spezie, 2013: X-band COSMO-SkyMed wind field retrieval, with application to coastal circulation modeling. *Ocean Science*, **9**, 121-132.

De Ruggiero P., E. Napolitano, R. Iacono, S. Pierini and G. Spezie, 2018: A baroclinic coastal trapped wave event in the Gulf of Naples (Tyrrhenian Sea). *Ocean Dynamics*, **68**, 1683-1694.

Castagno P., P. De Ruggiero, S. Pierini, E. Zambianchi, A. De Alteris, M. De Stefano and G. Budillon, 2020: Hydrographic and dynamical characterization of the Bagnoli-Coroglio Bay (Gulf of Naples, Tyrrhenian Sea). *Chemistry and Ecology*, **36**, 598-618.

De Ruggiero P., G. Esposito, E. Napolitano, R. Iacono, S. Pierini and E. Zambianchi, 2020: Modelling the marine circulation of the Campania Coastal System (Tyrrhenian Sea) for the year 2016: Analysis of the dynamics. *Journal of Marine Systems*, **210**, 103388.

Saviano S., G. Esposito, R. Di Lemma, P. de Ruggiero, E. Zambianchi, S. Pierini, P. Falco, B. Buonocore, D. Cianelli and M. Uttieri, 2021: Wind direction data from a coastal HF radar system in the Gulf of Naples (Central Mediterranean Sea). *Remote Sensing*, **13**, 1333

Gifuni L., P. de Ruggiero, D. Cianelli, E. Zambianchi and S. Pierini S., 2022**:** Hydrology and dynamics in the Gulf of Naples during spring of 2016: In situ and model data. *Journal of Marine Science and Engineering*, **10**, 1776.

Gifuni L., P. de Ruggiero, D. Cianelli, S. Pierini and E. Zambianchi, 2023**:** Numerical investigation of the three-dimensional paths of plastic polymers in the Gulf of Naples. *Marine Pollution Bulletin*, **193**, 115259.

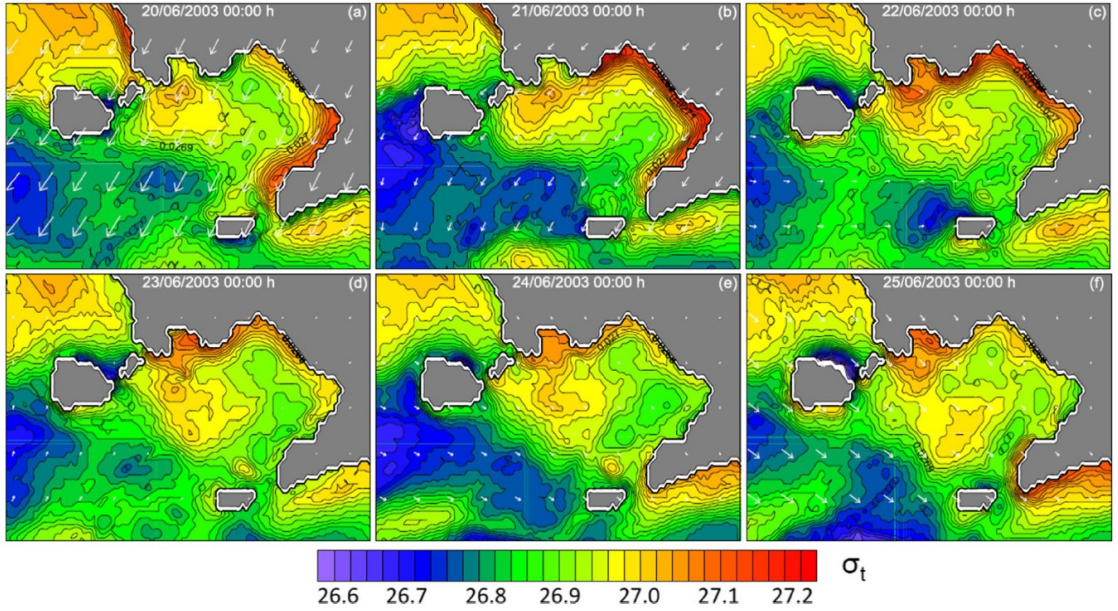

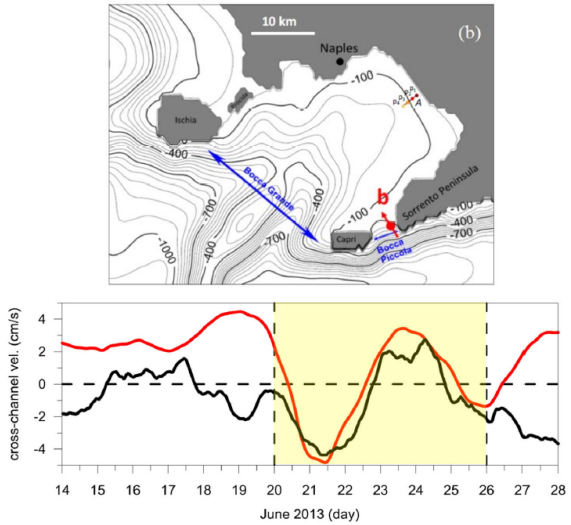

Fig. 9 Low-pass filter (24 h) time series of the along-channel current velocity at $z = -25$ m in point b of Fig. 1b: current meter data (black line) and CROM data (red line)

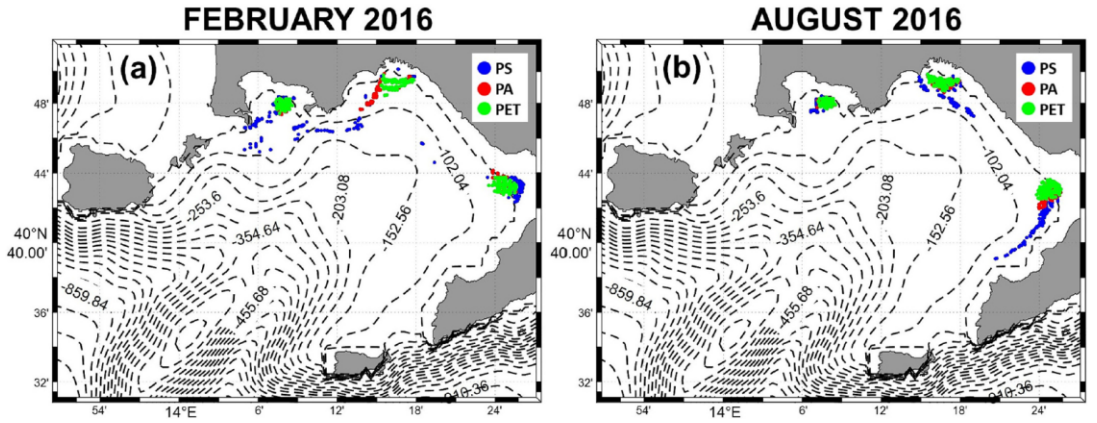

Rotture di simmetria,
Stabilità di flussi

Modellistica di
onde nonlineari

Aspetti lineari della circolazione
indotta dal vento (Rossby waves)

Applicazioni della teoria
dei sistemi dinamici nonlineari:
modelli alle equazioni primitive

Applicazioni della teoria
dei sistemi dinamici nonlineari:
modelli di bassa dimensionalità

Predicibilità dei processi di
transizione dell'Estensione
del Kuroshio

Modellistica di circolazione
del Mar Mediterraneo

Modellistica Antartica

Simulazioni di laboratorio di
flussi oceanografici

Oceanografia fisica in Antartide

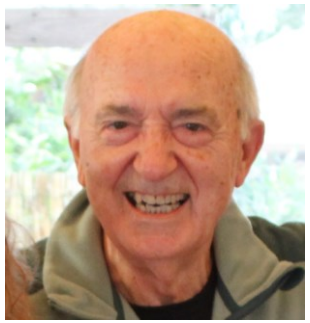

Prof.

Giancarlo Spezie
Giorgio Budillon
Enrico Zambianchi
Pierpaolo Falco
Giannetta Fusco
Yuri Cotroneo
Pasquale Castagno
Giuseppe Aulicino
etc.

Deep–Sea Research II 218 (2024) 105429

Contents lists available at ScienceDirect

Deep-Sea Research Part II

journal homepage: www.elsevier.com/locate/dsr2

Ocean-atmosphere-ice processes in the Ross Sea: A review

Pierpaolo Falco [a,b], Giuseppe Aulicino [c], Pasquale Castagno [b,d], Vincenzo Capozzi [c], Paola de Ruggiero [c], Angela Garzia [a,e], Antonino Ian Ferola [c], Yuri Cotroneo [b,c], Alessio Colella [c], Giannetta Fusco [b,c], Stefano Pierini [b,c], Giorgio Budillon [b,c], Enrico Zambianchi [b,c,*], Giancarlo Spezie [c]

[a] Dipartimento di Scienze della Vita e dell'Ambiente, Università Politecnica delle Marche, 60131, Ancona, Italy
[b] CoNISMa (Consorzio Nazionale Universitario per le Scienze del Mare), 00196, Roma, Italy
[c] Dipartimento di Scienze e Tecnologie, Università degli Studi di Napoli "Parthenope", 80143, Napoli, Italy
[d] Dipartimento di Scienze Matematiche e Informatiche, Scienze Fisiche e Scienze della Terra, Universita degli Studi di Messina, 98166, Messina, Italy
[e] Dipartimento di Ingegneria Civile, Edile e Ambientale, Università degli Studi di Roma "Sapienza", 00184, Roma, Italy

ARTICLE INFO

Handling Editor: Dr W Smith

Keywords:
Ross sea
Antarctic waters
Water masses
Ocean variability
Polynyas
Sea ice

ABSTRACT

The Ross Sea has been the site of extensive investigations since the earliest days of polar exploration. The International Geophysical Year of 1957-58 enhanced research activities with the establishment of scientific stations and the collection of oceanographic observations in the area. While many features of its oceanography, ecology, physics, glaciology, geology, and biogeochemistry are known, recent advances provide new insights into its structure and function, as well as into its relationship to global climate. We present a comprehensive review of the advances of understanding the main processes occurring in the area, such as the formation of dense shelf water and the production of Antarctic Bottom Water (AABW), as well as the main drivers (at both large and local scales) of local dynamics and water mass variability. We also summarize the main modeling applications, which are still limited and need to be improved using high-resolution models and, locally, limited-area models to explain processes driven mainly by thermodynamics and water-mass transformations. The Ross Sea forms the most saline AABW due to the activity of two polynyas in the western sector. A salinity gradient occurs on the shelf, with fresh Low Salinity Shelf Waters concentrated in the eastern Ross Sea, which is influenced by the inflow of fresh water from the Amundsen and Bellingshausen Seas. This freshwater inflow was thought to be the cause of a multi-decadal freshening of the High Salinity Shelf Water, precursor to the AABW, although a rebound in salinity in the Ross Sea has been observed since 2014. The increase in salinity has also affected the production of AABW, with the respective rebound occurring almost simultaneously.

Modellistica Antartica

Commodari, V., Pierini, S., 1999: A wind and boundary driven circulation model of the Ross Sea. In: *"Oceanography of the Ross Sea (Antarctica)"*, G. Spezie and G.M.R. Manzella (Editors). Springer-Verlag (ISBN: 88-470-0039-4), 135-144.

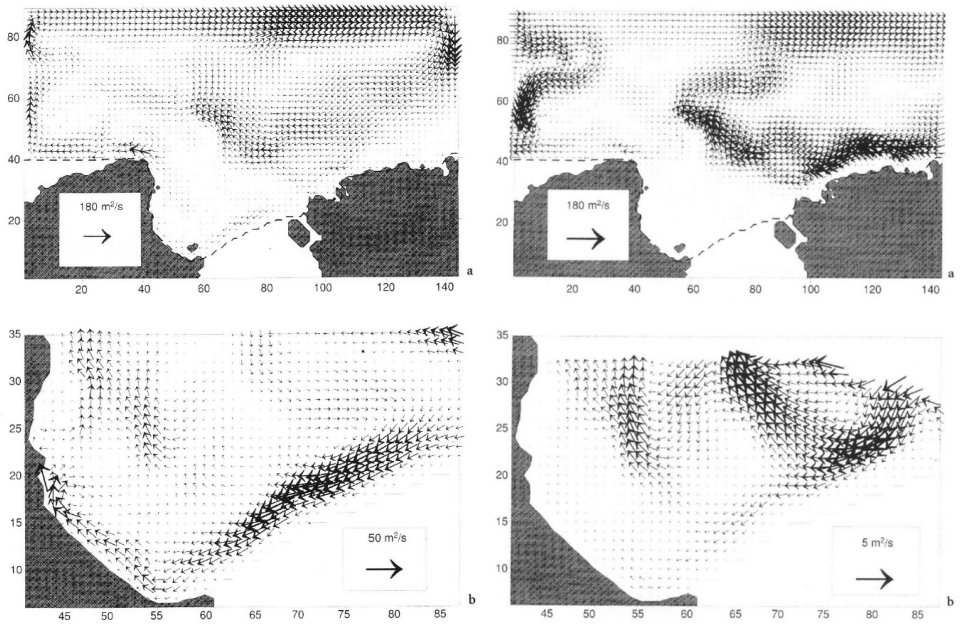

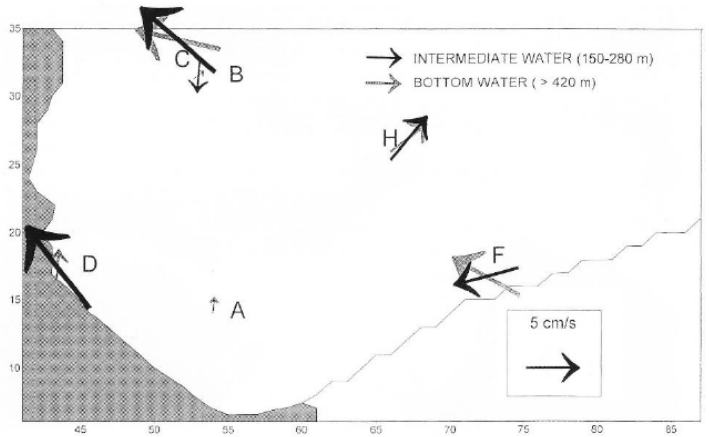

Fig. 5. Intermediate (*black arrows*) and bottom (*gray arrows*) currents measured in the framework of the Italian PNRA averaged over summer 1994-1995. (Courtesy of P. Picco; see [13])

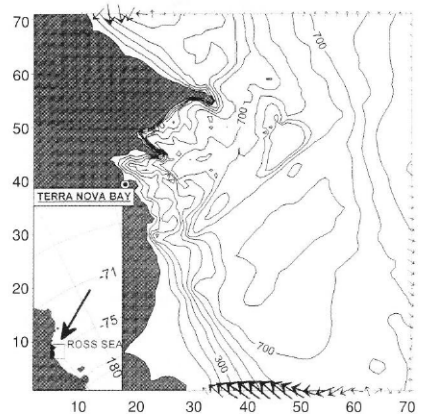

Fig. 6. Domain of integration of the high resolution model of the Terra Nova Bay area. Boundary forcing defined by *lateral arrows* derives from the wind-driven numerical experiment of the Ross Sea

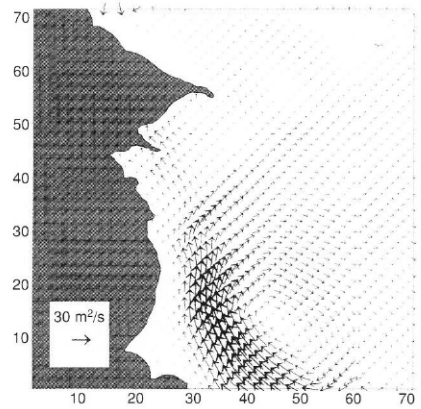

Fig. 7. Vertically integrated transport induced by boundary forcing and by easterly winds

Modellistica Antartica

Rubino, A., Budillon, G., Pierini, S., Spezie, G., 2003: A model for the spreading and sinking of the Deep Ice Shelf Water in the Ross Sea.
Antarctic Science, **15**, 25-30.

Sgubin G., S. Pierini and H. A. Dijkstra, 2014: Intrinsic variability of the Antarctic Circumpolar Current System: low- and high-frequency fluctuations of the Argentine Basin flow.
Ocean Science, **10**, 201-2013.

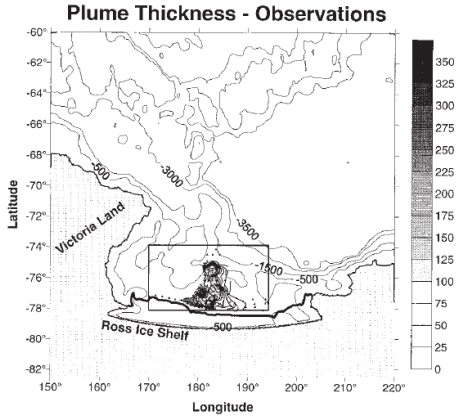

Fig. 2. Thickness of the DISW as measured during summer 1994/95. The values indicate the thickness of the water column where the measured potential temperature is colder than the corresponding freezing point at the sea surface. Triangles mark the locations wher hydrographical measurements used to trace the DISW vein were performed.

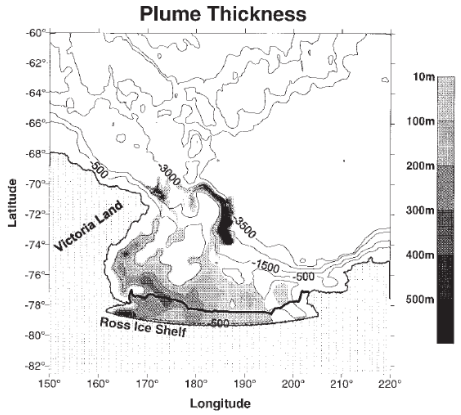

Fig. 3. Thickness of the DISW plume (after 20 years of integration) as a result of the numerical simulation carried out using an idealized ambient density.

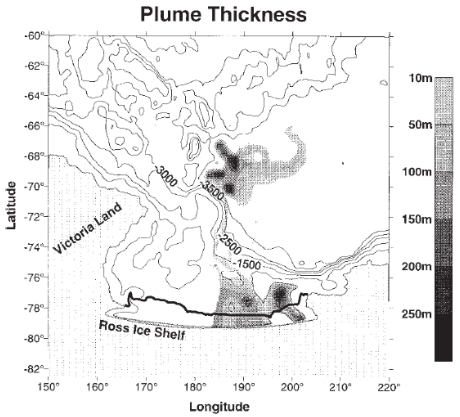

Fig. 4. Thickness of the DISW plume (after 20 years of integration) as a result of the numerical simulation carried out using a realistic ambient density.

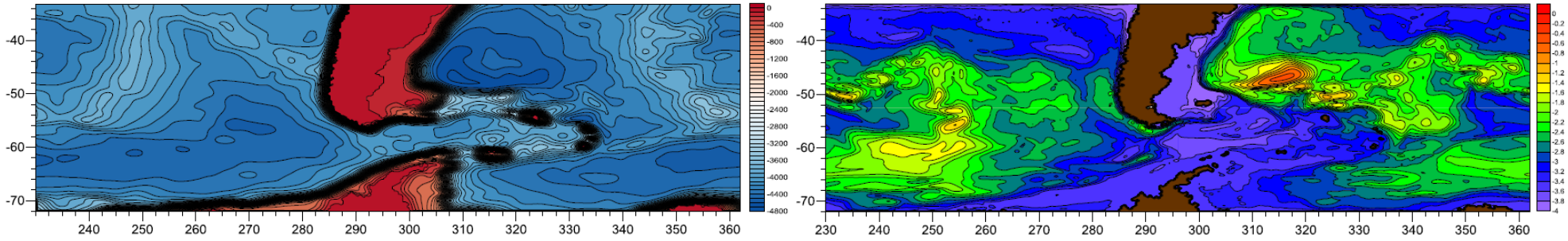

Fig. 6. Logarithm of the rms of the low-frequency SSH signal.

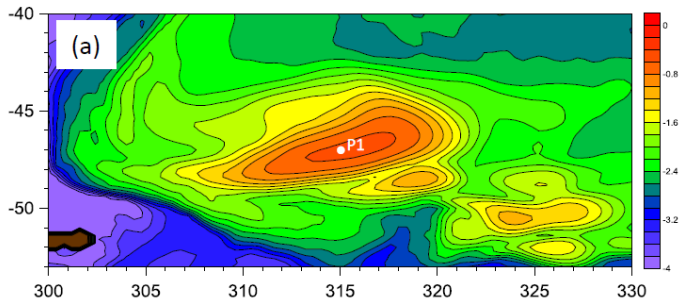

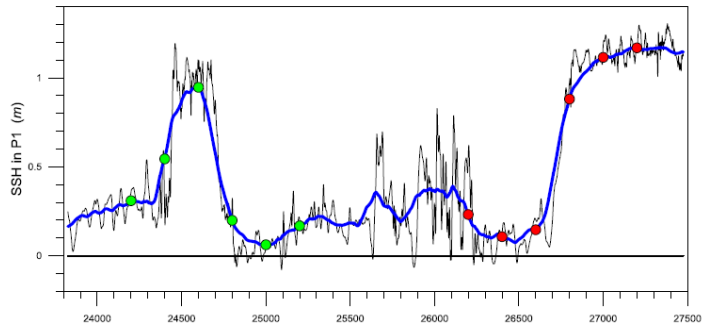

Modellistica Antartica

* **PAR**thenope **S**outhern **O**cean **M**odel

PARSOM*

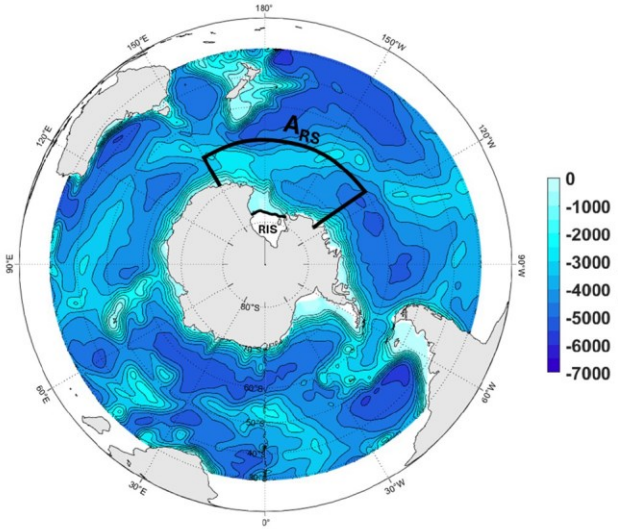

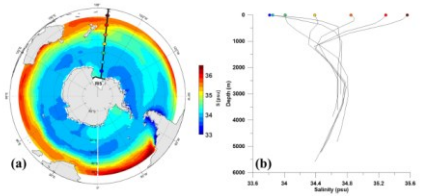

Figure 4.8: *Salinity field used for model initialization. (a) Map of the surface salinity. (b) Vertical salinity profiles in selected points located along a meridional transect.*

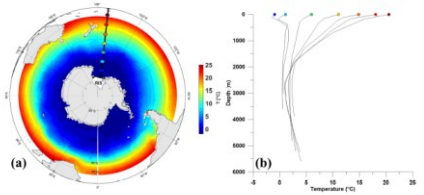

Figure 4.9: *Temperature field used for model initialization. (a) Map of the surface temperature. (b) Vertical temperature profiles in selected points located along a meridional transect.*

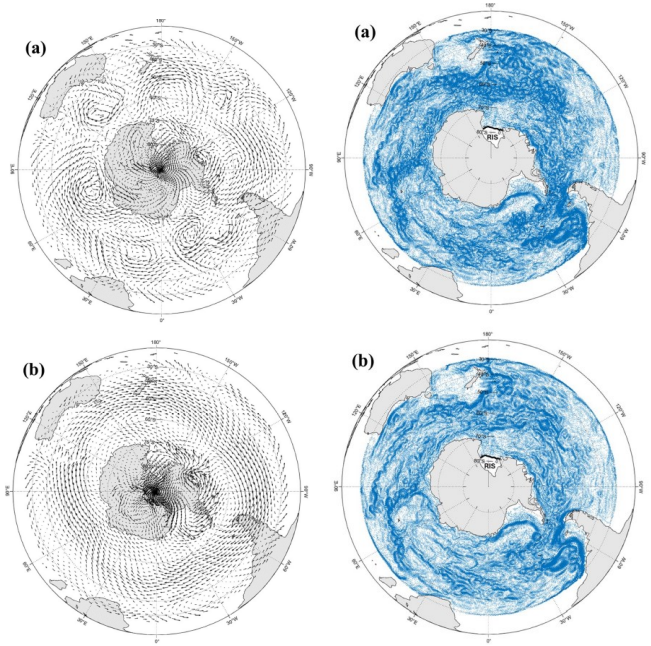

Colella, A., de Ruggiero, P., Pierini, S., 2025: Analysis of the intrinsic variability of the Ross Sea summer circulation with a model of the dynamics of the Southern Ocean. In preparation.

Colella, A., de Ruggiero, P., Pierini, S., 2025: Intrinsic variability of the Antarctic Circumpolar Current studied with a model of the dynamics of the Southern Ocean. In preparation.

Spinup dell'ensemble

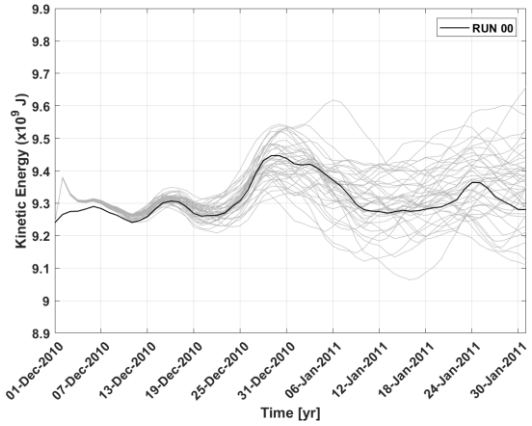

SSH mediato sulle stagioni estive degli anni 2010-20

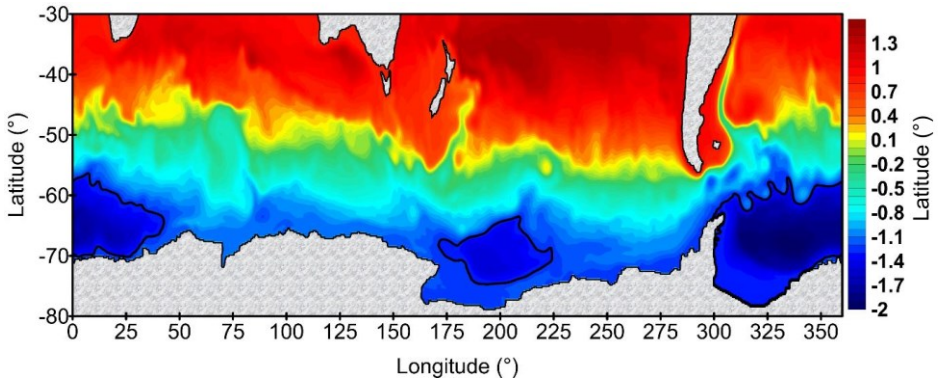

Variabilità intrinseca (ensemble spread)

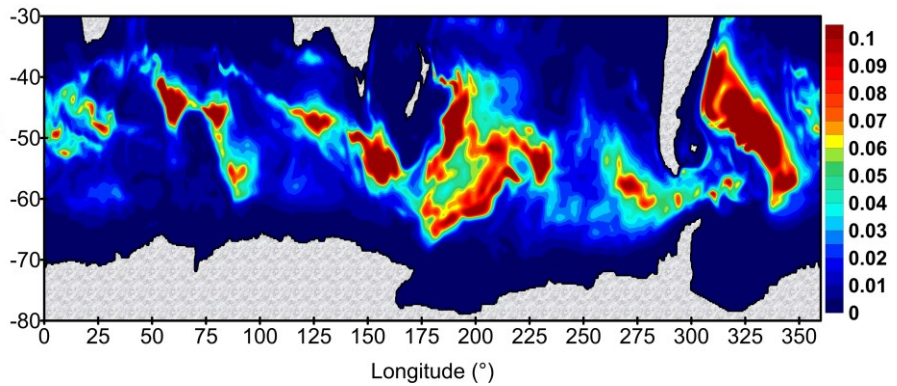

L'alto grado di realismo di questo modello consentirà una forte
sinergia tra studi sperimentali e modellistici nel DiST nell'ambito del PNRA

Rotture di simmetria,
Stabilità di flussi

Modellistica di
onde nonlineari

Aspetti lineari della circolazione
indotta dal vento (Rossby waves)

Applicazioni della teoria
dei sistemi dinamici nonlineari:
modelli alle equazioni primitive

Applicazioni della teoria
dei sistemi dinamici nonlineari:
modelli di bassa dimensionalità

Predicibilità dei processi di
transizione dell'Estensione
del Kuroshio

Modellistica di circolazione
del Mar Mediterraneo

Modellistica Antartica

Simulazioni di laboratorio di
flussi oceanografici

Simulazioni di laboratorio di flussi oceanografici

Pierini, S., Fincham, A., Renouard, D., D'Ambrosio, R., Didelle, H., 2002: Laboratory modeling of topographic Rossby normal modes.
Dynamics of Atmospheres and Oceans, **35**, 205-225.

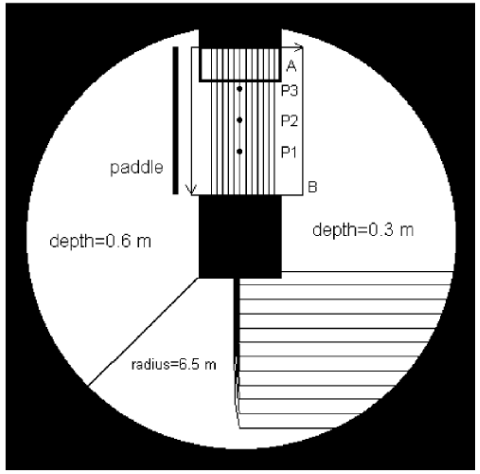

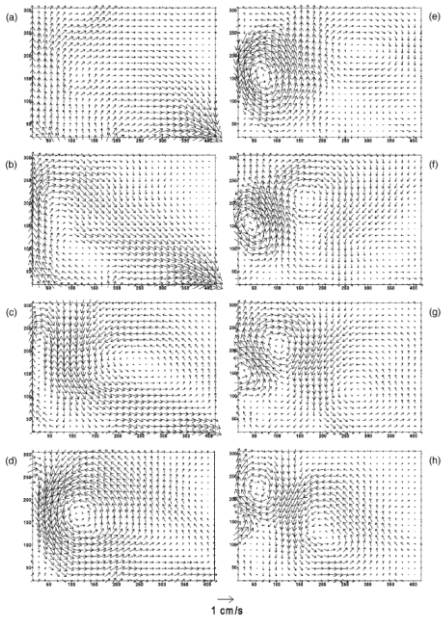

Fig. 2. Velocities measured by the CIV for exp. A. Parts a–h correspond to $t = 0.5, 1, \ldots, 4$ min. Axis units are in cm, with orientation as shown in Fig. 1a (the paddle is situated below the long (x) axis).

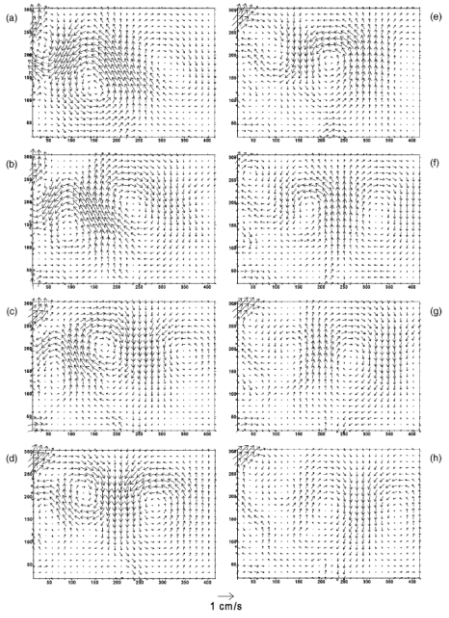

Fig. 3. Velocities measured by the CIV for exp. A. Parts a–h correspond to $t = 4.5, 5, \ldots, 8$ min. Axis units are in cm.

Pierini S., V. Malvestuto, G. Siena, T. A. McClimans and S. M. Løvås, 2008: A laboratory study of the zonal structure of western boundary currents.
Journal of Physical Oceanography, **38**, 1073-1090.

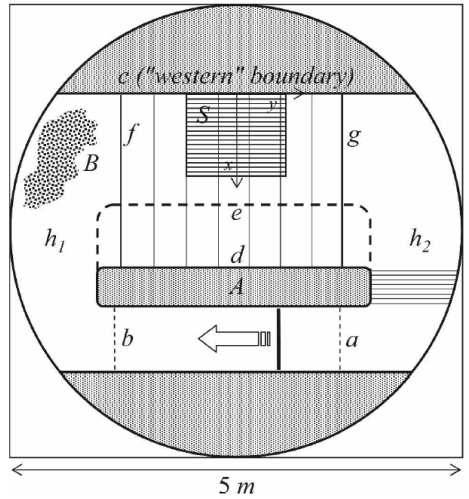

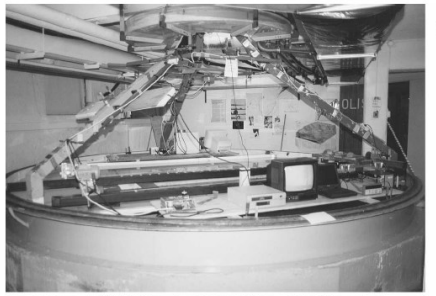

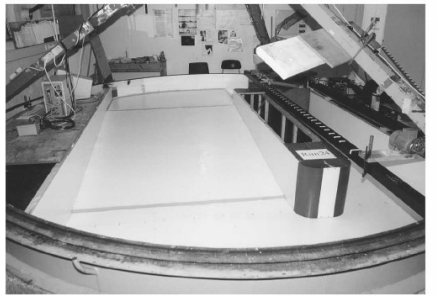

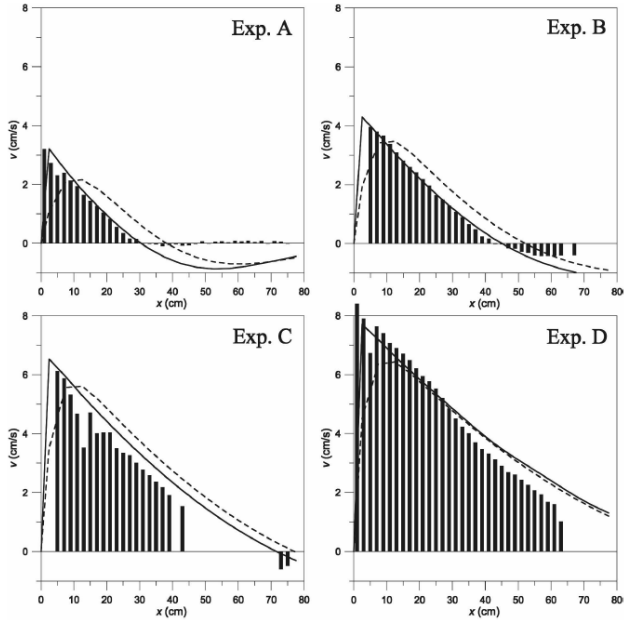

Simulazioni di laboratorio di flussi oceanografici

Pierini S., P. Falco, G. Zambardino, T. A. McClimans, and I. Ellingsen, 2011: A laboratory study of nonlinear western boundary currents, with application to the Gulf Stream separation due to inertial overshooting. *Journal of Physical Oceanography,* **41**, 2063-2079.

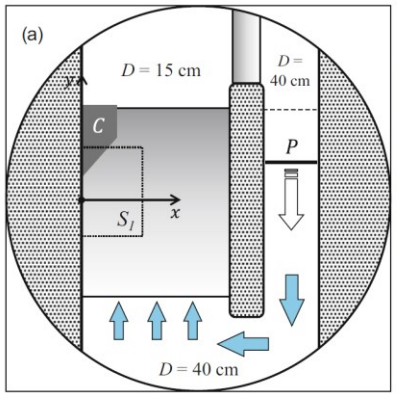

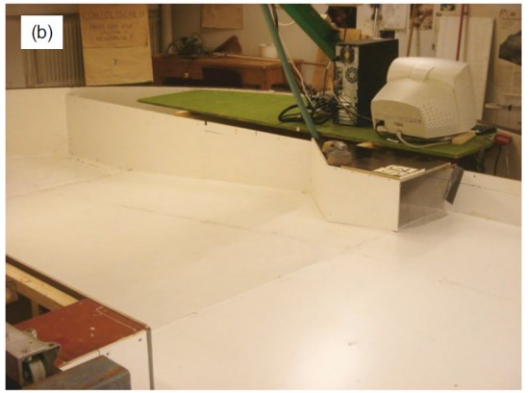

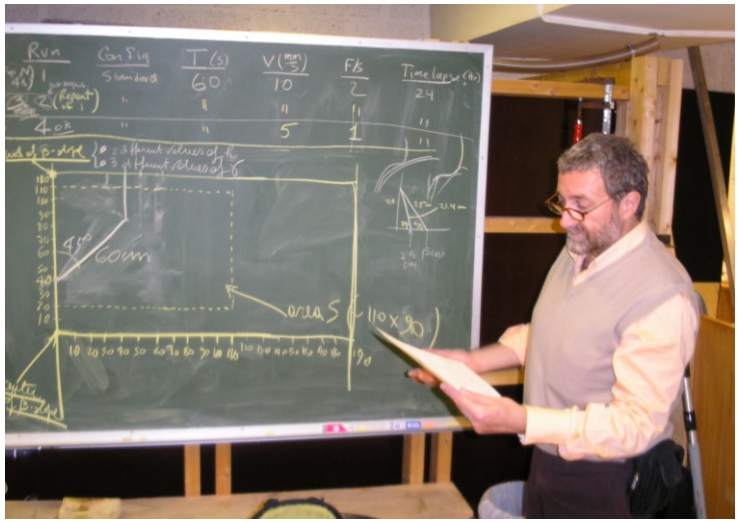

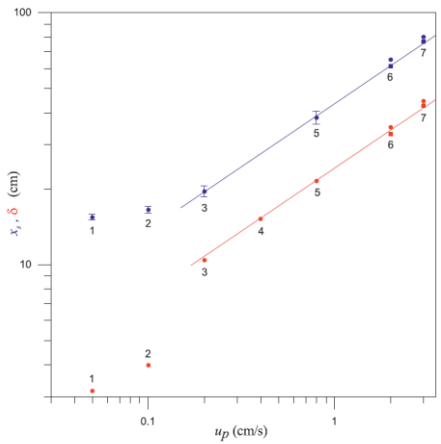

FIG. 5. Blue dots: zonal location of the stagnation point x_s of the solid lines of Fig. 4a vs u_p. Red dots: *e*-folding length scale δ of the dashed lines (exponential fits) of Fig. 4a vs u_p (see text). Red and blue squares: corrected values obtained by taking into account the small difference in β between these experiments and those of PEA08 (see text). The numbers refer to the profiles of Fig. 4a, and the lines denote the power law u_p^{α} with $\alpha = ½$.

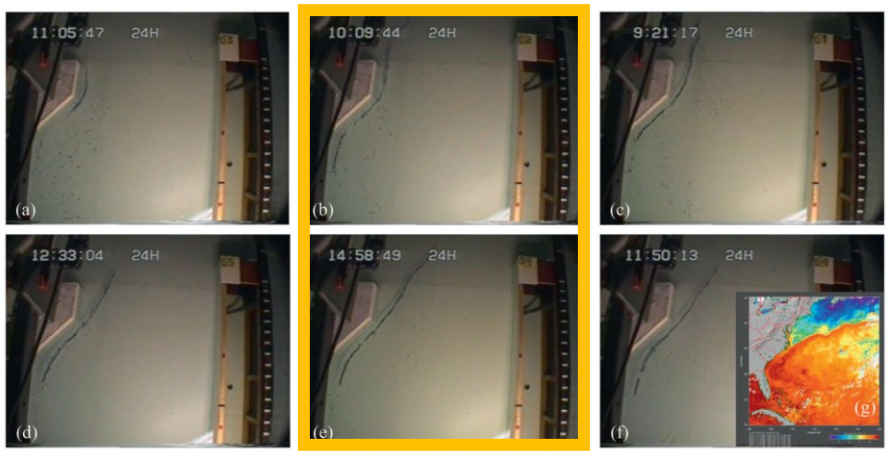

FIG. 9. Paths of the WBC evidenced by a dye stream and recorded by a wide-angle video camera in the experiments with a wedge-shaped continent with the inclined boundary forming an angle of 43° with the *y* direction, in cases with $T = 30$ s and u_p = (a) 2.5, (b) 5, (c) 10, (d) 15, (e) 20, and (f) 30 mm s^{-1}. (g) Satellite thermal image of the GS obtained by Advanced Very High Resolution Radiometer (AVHRR) multiple-pass data (courtesy of the Ocean Remote Sensing Group of the Johns Hopkins University).

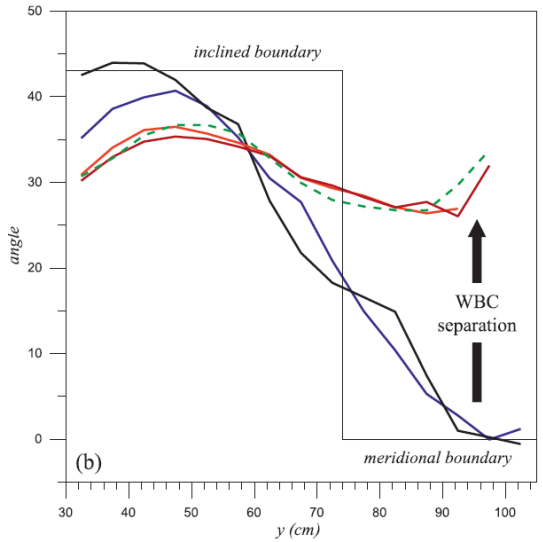

Simulazioni di laboratorio di flussi oceanografici

Pierini S., P. de Ruggiero, M. E. Negretti, I. Schiller-Weiss, J. Weiffenbach, S. Viboud, T. Valran, H. A. Dijkstra and J. Sommeria, 2022**:** Laboratory experiments reveal intrinsic self-sustained oscillations in ocean relevant rotating fluid flows.
Scientific Reports, **12**, 1375.

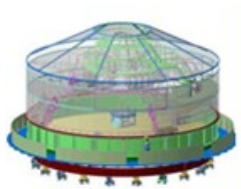

hydralab+
Adaptation for Climate Change

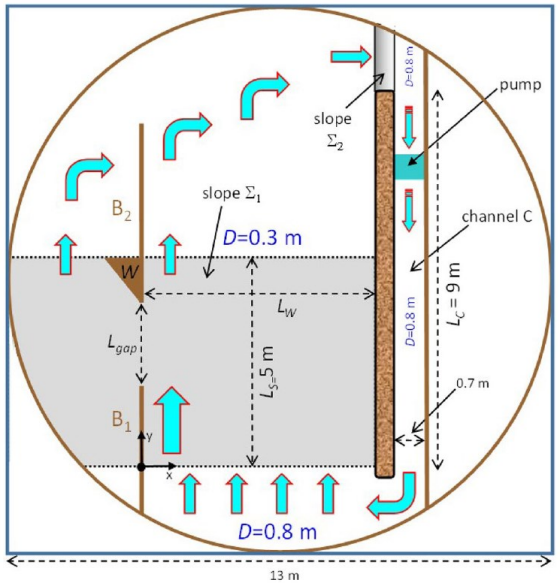

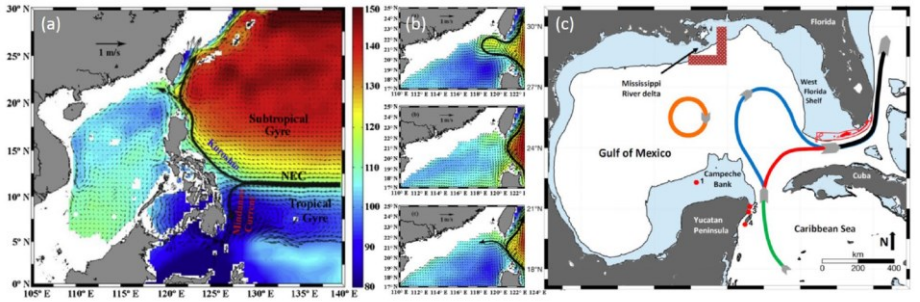

Figure 1. (**a**) Map of the Kuroshio intrusion into the South China Sea through the Luzon Strait (NEC stands for North Equatorial Current). (**b**) Sketch of the three types of Kuroshio intrusion, from top to bottom: looping, leaping and leaking path. (**c**) Sketch of the different states of the GoM Loop Current. Panels (**a**,**b**) are adapted from[5], panel (**c**) is adapted from[6].

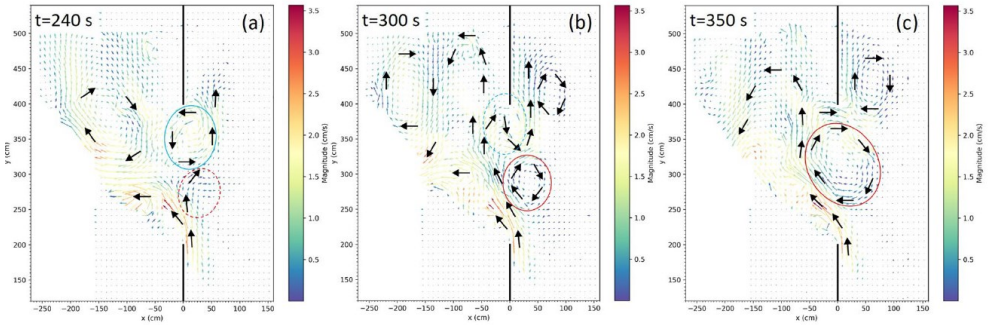

Figure 7. Snapshots of the current velocity field (in $cm\ s^{-1}$) at $t = 240$ s (**a**), $t = 300$ s (**b**) and $t = 350$ s (**c**) for $Q = 2$ and a rotation period $T = 60$ s (see the black dots in Fig. 5a, the u—field along black the dashed lines in Fig. 6b and Supplementary Figure S6 for the u—profiles along the gap).

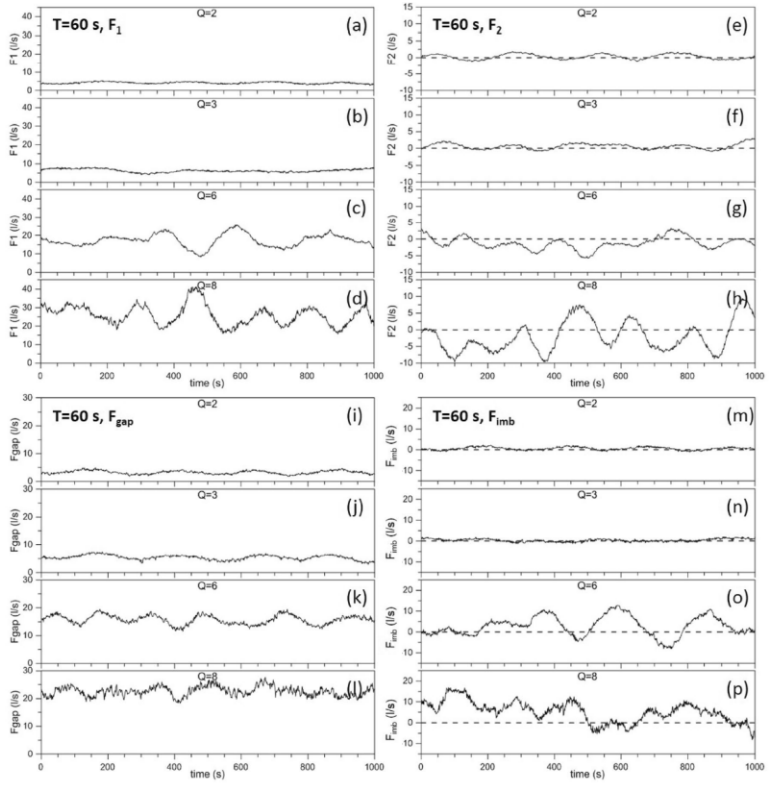

RICERCA

DIDATTICA

ISTITUTO UNIVERSITARIO NAVALE - NAPOLI

l'inizio ...

ANNO ACCADEMICO 1983 - 1984

L'Istituto Universitario Navale è costituito dalle seguenti Facoltà:

a) SCIENZE NAUTICHE - conferisce la LAUREA IN DISCIPLINE NAUTICHE

b) ECONOMIA MARITTIMA - conferisce la LAUREA IN SCIENZE ECONOMICO-MARITTIME

FACOLTA' DI SCIENZE NAUTICHE

In conformità col D.P.R. n. 261 dell'1-4-1980 pubblicato sulla G.U. n. 170 del 23-6-80 la Facoltà di Scienze Nautiche conferisce la Laurea in Discipline Nautiche, articolata in tre distinti indirizzi:
— AMBIENTE MARINO FISICO — GEODETICO — NAVIGAZIONE RADIOELETTRONICA
La durata del corso di studi per il conseguimento della laurea è di cinque anni.

Sono insegnamenti fondamentali per tutti e tre gli indirizzi:

1) ANALISI MATEMATICA I
2) ANALISI MATEMATICA II
3) CALCOLO NUMERICO E PROGRAMMAZIONE
4) CHIMICA
5) COMPLEMENTI DI MATEMATICA PER LE APPLICAZIONI
6) FISICA I
7) FISICA II
8) GEOMETRIA ANALITICA CON ELEMENTI DI PROIETTIVA
9) ISTITUZIONI DI ELETTROMAGNETISMO
10) ISTITUZIONI DI NAVIGAZIONE
11) MECCANICA RAZIONALE
12) TEORIA DEI SISTEMI
13) COMUNICAZIONI ELETTRICHE

Sono insegnamenti fondamentali per i singoli indirizzi:

a) INDIRIZZO AMBIENTE MARINO FISICO

14) ELETTRONICA APPLICATA
15) GEOLOGIA MARINA APPLICATA
16) MECCANICA DEI FLUIDI
17) METEOROLOGIA
18) MISURE ELETTRICHE
19) OCEANOGRAFIA
20) PROTEZIONE DELL'AMBIENTE MARINO

b) INDIRIZZO GEODETICO:

14) ASTRONOMIA GENERALE E SFERICA
15) ASTRONOMIA NAUTICA
16) GEODESIA E IDROGRAFIA
17) METEOROLOGIA E OCEANOGRAFIA
18) NAVIGAZIONE
19) TEORIA E MANOVRA DELLA NAVE
20) TOPOGRAFIA

c) INDIRIZZO NAVIGAZIONE RADIOELETTRONICA:

14) APPLICAZIONI DI ELETTRONICA
15) MISURE ELETTRICHE E RADIOELETTRICHE
16) NAVIGAZIONE
17) NAVIGAZIONE AEREA
18) RADIOTECNICA
19) RADAR E RADIOAIUTI ALLA NAVIGAZIONE
20) TEORIA E TECNICA DELLE ONDE ELETTROMAGNETICHE

Sono insegnamenti complementari per tutti e tre gli indirizzi:

1) AEROFOTOGRAMMETRIA
2) AERONAUTICA GENERALE
3) ANTENNE E PROPAGAZIONE
4) ARTE NAVALE
5) ASSISTENZA AL VOLO E CONTROLLO DEL TRAFFICO AEREO
6) CHIMICA MARINA
7) COSTRUZIONI MARITTIME
8) DISEGNO
9) ECONOMIA E POLITICA DELL'AMBIENTE
10) ELETTROACUSTICA SUBACQUEA
11) ELETTROTECNICA
12) EPISTEMOLOGIA
13) GEOFISICA MARINA
14) GEOTECNICA MARINA
15) LINGUA INGLESE (laboratorio) biennale con esame unico
16) METEOROLOGIA SINOTTICA E PREVISIONI DEL TEMPO
17) METODI DI OSSERVAZIONE E MISURA
18) MISURE ASTROGEODETICHE
19) MISURE OCEANOGRAFICHE
20) NAVIGAZIONE SPAZIALE
21) NAVI SPECIALI
22) OCEANOGRAFIA COSTIERA
23) SCIENZA DELL'EDUCAZIONE
24) SICUREZZA DELLA NAVE
25) STATISTICA APPLICATA
26) TECNICA CATASTALE
27) TECNICA ED ECONOMIA AZIENDALE
28) TECNICHE AERONAUTICHE
29) TECNICHE OPERATIVE IN NAVIGAZIONE AEREA
30) TELEDIAGNOSTICA AMBIENTALE

Per essere ammesso all'esame di laurea lo studente deve aver superato gli esami relativi a ventisei insegnamenti (venti fondamentali e sei complementari) secondo uno dei piani consigliati dalla Facoltà, ferme restando le norme vigenti relative alla liberalizzazione dei piani di studio.

Per gli studenti attualmente iscritti alla Facoltà e per quelli provenienti da altre Facoltà o da altre Università (anche straniere) le autorità accademiche prenderanno, caso per caso, i provvedimenti relativi alla loro carriera scolastica.

Corsi da me tenuti:

Istituto Universitario Navale:
Oceanografia (*SN*)
Meccanica dei Fluidi (*SN*)

Università dell'Aquila:
Climatologia e Meteorologia (*SA*)
Metodi Matematici della Fisica (*Fisica*)

Università di Napoli Parthenope:

Statistica e Processi Stocastici (*SA*)
Geofluidodinamica (*SNA*)
Modellistica Oceanografica (*STN*)
Fluidodinamica (*SNAMO*)
Modellistica Meteo-Oceanografica e Climatologica (*STN*)
Applications of Chaos Theory to Climate Dynamics (*Dottorato FERIA*)

Università del Salento –
Università di Napoli Parthenope:

Fluidodinamica dell'Atmosfera e dell'Oceano
(*Master di II Livello in Meteorologia e Oceanografia Fisica*)

20 miei laureandi/dottorandi sono attivi nell'ambito della ricerca di base e applicata:

Università Parthenope, Venezia Ca' Foscari, Bologna, Palermo
ISMAR-CNR
IAS-CNR
ENEA
CMCC
NEXTGEO
e-GEOS
Centri Meteorologici
Los Alamos National Laboratory

in rosso: attività didattica corrente

UNITEXT_for_Physics

https://link.springer.com/book/10.1007/978-3-031-71129-9

2025, *Springer Nature*,
ISBN: 978-3-031-71128-2

https://link.springer.com/book/10.1007/978-3-031-77991-6

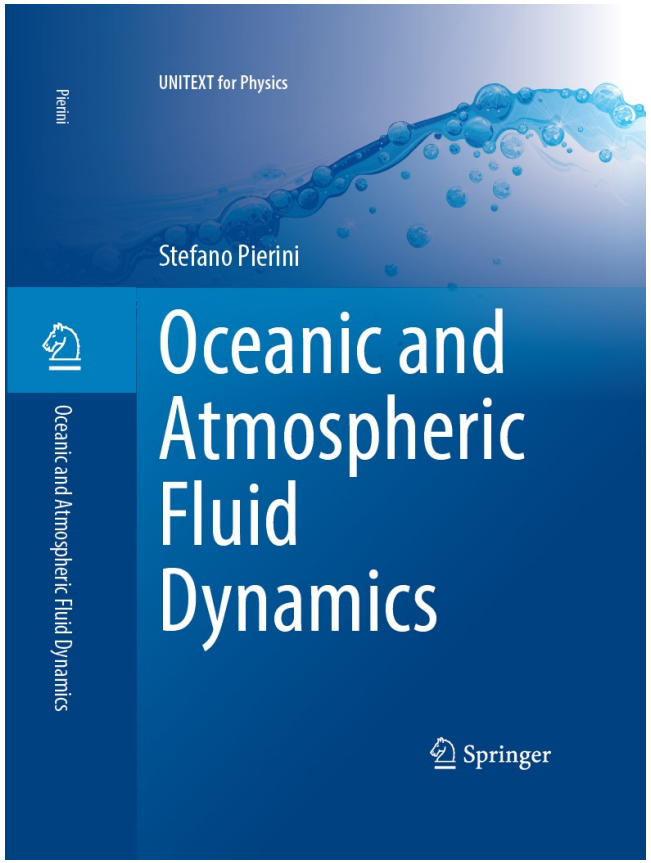

2025, *Springer Nature*,
ISBN: 978-3-031-77990-9

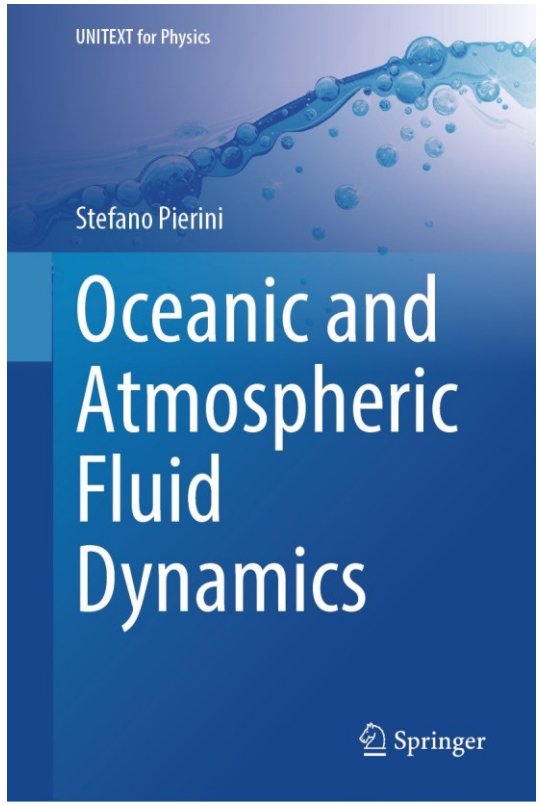

Contents

Vi ringrazio per la vostra attenzione!

Foto di gruppo dell’evento: